EUROPEAN ORGANIZATION FOR NUCLEAR RESEARCH

CERN-EP/89-103
15 August 1989

A MEASUREMENT OF DIFFERENTIAL CROSS-SECTIONS AND NUCLEON STRUCTURE FUNCTIONS IN CHARGED-CURRENT NEUTRINO INTERACTIONS ON IRON

P. Berge[1], H. Burkhardt, F. Dydak, R. Hagelberg, M.W. Krasny, H.J. Meyer, P. Palazzi, F. Ranjard, J. Rothberg[2], J. Steinberger, H. Taureg, H. Wahl, R.W. Williams[2] and J. Wotschack

CERN, Geneva, Switzerland

H. Blümer[3], H.D. Brummel[3], P. Buchholz[4], J. Duda, F. Eisele, B. Kampschulte, K. Kleinknecht[3], J. Knobloch[3], E. Müller[3], B. Pszola and B. Renk[3]

Institut für Physik der Universität, Dortmund, Fed. Rep. Germany*)

T. Alvarez[5], R. Belusevic, B. Falkenburg, R. Geiges, C. Geweniger, V. Hepp, H. Keilwerth and K. Tittel

Institut für Hochenergiephysik der Universität, Heidelberg, Fed. Rep. Germany*)

P. Debu, C. Guyot, J.P. Merlo, A. Para[6], P. Perez, F. Perrier, B. Peyaud, J.P. Schuller, R. Turlay and B. Vallage

DPhPE, CEN-Saclay, France

H. Abramowicz, J. Królikowski and A. Lipniacka

Institute of Experimental Physics, University of Warsaw, Poland**)

(Submitted to Zeitschrift für Physik)

---

1) Visiting from Fermilab, Batavia, Ill., USA.
2) Visiting from University of Washington, Seattle, Wash., USA.
3) Now at Universität Mainz, Fed. Rep. Germany.
4) Now at Temple University, Philadelphia, Pa., USA.
5) Visiting from Universidad Autónoma de Madrid, Spain.
6) Now at Fermilab, Batavia, Ill., USA.

*) Funded by the German Federal Ministry for Research and Technology (BMFT).
**) Supported by the Polish Ministry of Education under grant CPB01-06

ABSTRACT

A high-statistics measurement of the differential cross-sections for neutrino–iron scattering in the wide-band neutrino beam at the CERN SPS is presented. Nucleon structure functions are extracted and compared with the predictions of quantum chromodynamics.

1. INTRODUCTION

Deep-inelastic lepton–nucleon scattering is the primary tool for studies of the nucleon structure. Early experiments on inelastic electron scattering have provided evidence for the quark–parton picture and for scaling of the nucleon structure functions [1–3]. Later neutrino and muon experiments established deviations from scaling, consistent with the predictions of quantum chromodynamics (QCD) [4–10]. The comparison of results obtained from neutrino scattering with those using muon and electron beams gave further support to the quark model, including fractional quark charges. Precise measurements of nucleon structure functions provide an unambiguous test of QCD and permit a determination of the scale parameter Λ of strong interactions. They are essential for relating various hard scattering processes to each other, as well as for predicting expected yields of new particles at future accelerators.

Measurements of the nucleon structure functions made by this group, and their comparison with QCD predictions, have already been published [4, 11–15]. The motivation for an independent measurement was twofold:

- In certain kinematical domains the errors on structure functions were dominated by statistics. In particular, this was the case for xF_3 and for the longitudinal structure function F_L.
- The comparison of the published results with those of other neutrino experiments [16, 17] showed differences in certain regions of x and Q^2, outside the error bars. It was considered important to clarify the origin of these differences.

The upgraded CDHS detector, in conjunction with the high flux of the CERN wide-band neutrino beam, was used for this experiment. The results presented here are derived from about 640000 neutrino and 550000 antineutrino events, after cuts. In the analysis, new measurements of the total cross-sections from a separate narrow-band beam exposure [18] were used for normalization.

This paper is organized as follows. The beam and the experimental set-up are described in Sections 3 and 4, followed by details of the experimental procedure in Sections 5 to 9. The determination of the differential cross-sections and the extraction of the nucleon structure functions are presented in Sections 10 and 11. Section 12 is devoted to an analysis of the results within the framework of QCD. Finally, in Section 13 we compare the results with those of other deep-inelastic scattering experiments.

2. DEEP-INELASTIC SCATTERING FORMALISM

The charged-current neutrino–nucleon interaction is assumed to proceed through virtual $W^{\pm}$ vector-boson exchange, as shown in Fig. 1. The following definitions are used for the kinematic variables:

$q = k - k'$ is the four-momentum transfer.

$Q^2 = -q^2 = 4E_\nu E_\mu \sin^2(\theta/2)$, where θ is the laboratory scattering angle of the muon; E_ν and E_μ are the energies of the incoming neutrino and outgoing muon, respectively.

$\nu = (p \cdot q)/M$, where M is the nucleon mass, and ν is the energy transfer to the final-state hadronic system. This is equivalent to the total kinetic energy E_{had} of the hadronic final state in the laboratory system.

In addition, we use the Bjorken scaling variables:

$y = p \cdot q/p \cdot k = \nu/E_\nu$ is the fractional energy transfer, related to the scattering angle in the centre-of-mass system.

$x = Q^2/2(p \cdot q) = Q^2/2M\nu$ is the fraction of nucleon momentum carried by a struck parton in the infinite momentum frame.

Assuming a V – A current–current form of the interaction and neglecting terms proportional to $m_\mu{}^2/M^2$ (m_μ being the muon mass), the most general form of the differential cross-section is

$$\frac{d^2\sigma^{\nu,\bar{\nu}}}{dxdy} = \sigma_0 \left[\left(1 - y - \frac{Mxy}{2E_\nu}\right) F_2^{\nu,\bar{\nu}}(x,Q^2) + \frac{y^2}{2} 2xF_1^{\nu,\bar{\nu}}(x,Q^2) \pm \left(y - \frac{y^2}{2}\right) xF_3^{\nu,\bar{\nu}}(x,Q^2) \right] , \quad (2.1)$$

where, in terms of the Fermi coupling constant G_F and the mass m_W of the weak intermediate vector boson,

$$\sigma_0 = \frac{G_F^2 M E_\nu}{\pi} [1 + (Q^2/m_W^2)]^{-2} .$$

For simplicity, the dependence of the structure functions on x and Q^2 is not always written explicitly. The structure functions $2xF_1$, F_2, and xF_3 are related to the absorption cross-sections of left, right, transverse, and longitudinally polarized W bosons σ_+ , σ_- , σ_T, σ_L in the following way:

$$2xF_1^{\nu,\bar{\nu}} = \frac{2M\,x\,k}{\pi} \frac{1}{2}(\sigma_+ + \sigma_-)^{\nu,\bar{\nu}} = \frac{2M\,x\,k}{\pi} \sigma_T^{\nu,\bar{\nu}} , \quad (2.2)$$

$$F_2^{\nu,\bar{\nu}} = \frac{2M\,x\,k}{\pi} \frac{1}{1 + Q^2/\nu^2} (\sigma_T + \sigma_L)^{\nu,\bar{\nu}} , \quad (2.3)$$

$$xF_3^{\nu,\bar{\nu}} = \frac{2M\,x\,k}{\pi} \frac{1}{\sqrt{1 + Q^2/\nu^2}} \frac{1}{2} (\sigma_+ - \sigma_-)^{\nu,\bar{\nu}} , \quad (2.4)$$

where $k = (W^2 - M^2)/2M$ and W is the invariant mass of the hadronic final state.

The longitudinal structure function F_L is defined as

$$F_L^{\nu,\bar{\nu}} = F_2^{\nu,\bar{\nu}} \left(1 + \frac{4M^2x^2}{Q^2}\right) - 2xF_1^{\nu,\bar{\nu}} . \quad (2.5)$$

It is related to the quantity $R = \sigma_L/\sigma_T$ measured in charged-lepton scattering through $R(x,Q^2) = F_L(x,Q^2)/2xF_1(x,Q^2)$. This function is of particular interest as it measures the scalar component of the nucleon. It is also directly sensitive to the gluon structure function.

All structure functions can be *a priori* different for ν and $\bar{\nu}$ scattering on protons or neutrons, giving twelve independent functions. Assumptions such as discussed in the following are needed in order to reduce the number of independent functions. In this analysis, three structure functions are sufficient to describe the neutrino scattering off an isoscalar target.

In the quark-parton model the structure functions acquire a simple interpretation: σ_+ and σ_- are proportional to the momentum distributions of quarks and antiquarks. The momentum distributions q(x) and $\bar{q}(x)$ of all quarks and antiquarks in the nucleon are identified with the structure functions as follows:

$$\begin{aligned} 2xF_1^{\nu} &= 2xF_1^{\bar{\nu}} = q + \bar{q} , \\ xF_3^{\nu,\bar{\nu}} &= q - \bar{q} \pm 2x(s - c) , \end{aligned} \quad (2.6)$$

$$xF_3 = \frac{1}{2}(xF_3^{\nu} + xF_3^{\bar{\nu}}) = q - \bar{q} , \quad (2.7)$$

where $q = x(u + d + s + c)$, $\bar{q} = x(\bar{u} + \bar{d} + \bar{s} + \bar{c})$, and u, d, s, and c are the corresponding quark densities in the proton.

3. THE WIDE-BAND NEUTRINO BEAM

The neutrino and antineutrino beams resulted from decays of pions and kaons which were produced in the forward direction by a 400 GeV proton beam striking a beryllium target. A collimator, placed after the target, was used to absorb secondaries produced at angles exceeding 8 mrad. A magnetic horn [19], further downstream, focused secondaries of a selected sign into a 292 m long evacuated decay tunnel. Muons accompanying the neutrinos were absorbed in the 464 m long iron and earth shield. Typically, 10^{13} protons were extracted from the CERN Super Proton Synchrotron every 14.4 s in a bell-shaped spill with a 2 ms base, yielding about 70 neutrino or 30 antineutrino interactions in the detector.

The data reported here were collected in 1983. A total of 1.3×10^{18} protons were targeted during neutrino running, yielding 4.3×10^{6} triggers, whereas the antineutrino exposure with 2.5×10^{18} protons on target gave 5.4×10^{6} triggers.

The energy spectrum and the spatial distribution of the wide-band neutrino beams are not known with sufficient precision. They were derived from the observed event rates, assuming a total cross-section rising linearly with neutrino energy (see Section 9).

4. THE EXPERIMENTAL SET-UP

The CDHS detector [20] was upgraded for the purpose of this experiment [21]. It consisted of a large magnetized iron calorimeter, 3.75 m in diameter and about 21 m long, interspaced with drift chambers (see Fig. 2). The calorimeter served as the target and was used to measure the energy deposited by final-state hadrons. The muon momentum and angle were derived from the track reconstructed in the drift chambers. The energy of the incoming neutrino was taken as the sum of hadron energy and muon momentum.

The first ten calorimeter modules (Fig. 3) were of recent construction. Each module consisted of 20 plates of 2.45 cm thick iron, followed by a 0.5 cm thick scintillator plane. The scintillators were subdivided into 24 strips, 15 cm wide, and each strip was cut into two independent halves viewed by individual photomultipliers. A reflecting mirror was placed at the far end of each scintillator in order to reduce the light-attenuation effects. The pulse heights from both halves were summed; 10% of the sum was used for triggering purposes, the remainder was fed into analog-to-digital converters (ADCs). Five consecutive strips along the beam axis were combined onto a single phototube. The scintillator strips were alternately horizontal and vertical, thus permitting the localization of a neutrino interaction to about 3 cm in a plane perpendicular to the beam direction. The total length of a module was 59 cm, 49 cm of it being iron.

The front ten modules were followed by five modules with 5 cm sampling and six modules with 15 cm sampling which were employed in the previous set-up [20]. This part was used for the muon momentum measurement only. All modules were magnetized with a toroidal field of 1.65 T, on the average. The central hole for the magnetic coils in the front modules was reduced to a diameter of 10 cm, as compared with a 30 cm hole plugged with non-magnetic material in the other modules. The neutrino beam was directed 45 cm below the axis of the apparatus.

Triple-plane drift chambers were installed in the 31 cm wide gaps between the calorimeter modules. They measured the trajectory of an outgoing muon to a precision of about 1 mm. Drift velocities and the reference times for each chamber, as well as the relative alignments, were determined using muon tracks registered without magnetic field.

The field direction was chosen to focus negative muons in the neutrino beam and positive muons in the antineutrino beam. This focusing property resulted in a good muon acceptance over almost the entire phase space.

All electronics channels were equipped with 40-event-deep buffers, thus permitting several events to be registered per burst. The buffer size was the limiting factor of the data-taking rate.

To guard against the background of beam-related muons, an upstream plane consisting of 4×4 m^2 of scintillation counters was used in veto. All triggers occurring within 20 ns of an incoming muon were vetoed.

5. THE TRIGGER

The apparatus was triggered on the basis of the pulse-height information summed over individual calorimeter modules. Three parallel triggers were used in this analysis:

- *Low-threshold trigger:* Any three modules showing a pulse height exceeding ~ 1/3 of the pulse height of a minimum-ionizing particle. One of these modules was required to be in the front part of the detector. This was a low-threshold trigger, fully efficient above $E_\nu = 7$ GeV. It was prescaled by a factor of 16 for the neutrino case and of 4 for the antineutrino case. The sample of low-threshold triggers was used to determine the efficiency of other triggers.
- *Charged-current trigger:* The low-threshold trigger, with the additional requirement that the total 'visible' energy should exceed ~ 7 GeV—the total 'visible' energy being the linear sum of all pulse heights in the entire apparatus. For neutrino interactions originating in the front part of the detector, this trigger was fully efficient for $E_\nu > 12$ GeV (see Fig. 4a). During the neutrino running, this trigger was prescaled by a factor of 2.
- *Hard charged-current trigger:* As above, but the total 'visible' energy had to exceed ~ 15 GeV. This trigger was fully efficient for $E_{had} > 20$ GeV (see Fig. 4b), but it was biased at low y for all neutrino energies.

For the structure-function analysis, an unbiased data sample is required. In this analysis the charged-current trigger sample was used. To enhance the event statistics at high Q^2, the hard charged-current triggers with $E_{had} > 25$ GeV were added. The resulting sample of events with $E_{had} > 25$ GeV was normalized to the number of charged-current triggers in this region.

6. EVENT RECONSTRUCTION

Events were reconstructed by an off-line analysis program. A charged-current event was required to have at least two planes fired in four out of five consecutive drift chambers (this corresponds to a muon momentum cut-off of ~ 4 GeV). The reconstruction program performed a pattern recognition to find muon tracks. The vertex position of the interaction along the beam direction was defined by the most upstream scintillation counter fired along the muon track. A fit was made to the points found along this track in order to determine the muon momentum and angle. The energy loss due to ionization and the correlations due to multiple scattering were included in the fit. The measured energy deposition exceeding 1 GeV per module in the scintillators along the muon trajectory was used to correct for radiative energy losses. The hadronic energy was calculated as a sum of all pulse heights recorded in a box of 1.5 m iron-equivalent length and 1.2 m width, starting at the vertex of the interaction. It was corrected for the pulse height deposited by the muon, using the average observed pulse height in the 1.5 m long region following the hadronic shower box, truncated at 6 GeV. The effect of fluctuations in the muon energy loss was taken into account in the Monte Carlo simulation program.

A typical charged-current interaction event is shown in Fig. 5. Several thousand computer-reconstructed events were inspected visually for potential failures. The automatic reconstruction had an overall efficiency of better than 98.5%. Failing events were reconstructed interactively to check for potential biases. The remaining small bias at muon momenta below 7 GeV/c was corrected for by

an appropriate weighting of events in this region. The large sample of events available in this analysis permitted several checks of the measurement for uniformity and stability with time.

7. CALIBRATION AND RESOLUTION

7.1 Muon momentum and angle

The momentum of the outgoing muon was derived from the curvature of the track. The magnetic fields inside modules were measured with pick-up loops as a function of position. Their absolute value was known to better than 2%. The absolute momentum scale was checked at low momenta by comparing the fitted momentum with the momentum derived from the range for muons which stopped in the apparatus. High-energy tracks were divided into two parts and fitted separately. The resulting difference of the fitted momenta was compared with the calculated energy loss [22] (these calculated values were in good agreement with measurements of muon energy loss [23]). These tests confirmed that the absolute momentum scale was correct to better than 2% (Fig. 6).

The muon momentum resolution is dominated by multiple scattering in iron. It depends, as well, on the track length available for the fit. On the average, the momentum error was $\Delta p/p = 9\%$. The error on the muon angle was dominated by the multiple scattering between the interaction point and the first measurement used in the fit. A typical error on the muon angle was 10 mrad at $p_\mu = 10$ GeV and 2 mrad at $p_\mu = 100$ GeV. Several methods were used to calculate the expected resolution. Their comparison shows that the resolution of the muon angle and the momentum was known to $\pm 10\%$ of its value, or better. Tails in the resolution functions, due to erroneous assignment of hits in the hadronic shower region, were estimated with the help of the Monte Carlo simulation program (see Section 9).

7.2 Hadron energy

The complete pulse-height measurement chain, including photomultipliers, mixers, and ADCs, was calibrated using a system based on a laser and light-fibres feeding each scintillator. The long-term change in the response was monitored by means of cosmic muons recorded between beam bursts. The recorded pulse heights for neutrino events were corrected for attenuation along the scintillator, using the reconstructed vertex position. The attenuation length of each counter was measured in several dedicated runs with cosmic muons.

The conversion factor of the observed pulse height to hadron energy was calibrated in an auxiliary exposure of four calorimeter modules to a momentum-selected negative hadron beam with energies ranging from 15 GeV to 140 GeV. A weighting procedure was used to improve the resolution and to reduce the effect of fluctuations of the electromagnetic component of hadronic showers, especially at high energies. The response of each individual counter E_i was reduced by a factor depending on the total shower energy [24]. The weighted response of the calorimeter was found to be nearly linear with the shower energy (Fig. 7). The resolution was found to be Gaussian with a standard deviation $\Delta E/E = (0.52^2/E + 0.02^2)^{1/2}$. For neutrino interactions originating at the end of the fiducial region, the leakage of the hadronic shower into the downstream part of the detector was measured with a resolution $\Delta E/E = 0.7/E^{1/2}$ (E in GeV).

In the course of the analysis it was found that the pulse-height circuitry had a rate-dependent response. It was therefore necessary to correct the observed pulse height for the actual rate of data-taking. The change in the detector response as a function of the triggering frequency was determined in an auxiliary measurement. Owing to different event rates, this correction is different for neutrino and antineutrino exposures. This effect reduces the observed hadron energy on the average by 9% in the neutrino case and by 6% for antineutrino running, and worsens the hadron energy resolution by about 5% (Fig. 8). The effect was folded with the simulated rate distribution in the Monte Carlo calculation.

In a narrow-band beam exposure, events in a radial slice around the beam axis have a well-defined average total energy, known from the decay kinematics [4]. For small-y events the total energy is given predominantly by the muon momentum; at large y, the hadron energy dominates. This fact has been used to adjust the hadron energy scale relative to the muon momentum scale with a precision of 1%, scaling the test beam calibration by 2.5%. After this adjustment, the total energy of events for different y-slices is constant within 1% (Fig. 9). As a result of the rate-dependent response, we estimate that the overall hadron energy scale had an uncertainty of 2.5% with an offset of ± 0.5 GeV.

7.3 Resolution in x and Q^2

The finite resolution in the hadron energy and in the muon momentum and angle induces a smearing of events in x and Q^2. At large x the smearing is always dominated by the hadron energy resolution. At small x and large y the angular resolution dominates the smearing, whereas at small y the hadron energy resolution contributes significantly. Figure 10 shows the resolution of the detector in x and Q^2 for the wide-band beam neutrino spectrum. The solid lines represent the resolution for $y < 0.5$, whereas the dashed lines are for $y > 0.5$; the difference in resolution is very small. Systematic errors due to uncertainties in the understanding of the detector resolution were included in the overall systematic errors of differential cross-sections and structure functions.

8. EVENT SELECTION

Events used in the analysis were required to fulfil the following criteria:

- The interaction vertex had to be within modules 2 to 9. This requirement ensured uniform hadron energy resolution for the entire sample. Events originating in the first module were discarded to avoid a possible contamination with beam-related muons because of an inefficiency of the anticounter.
- The distance of the interaction point from the axis of the detector had to be smaller than 160 cm and larger than 35 cm to assure complete lateral containment of the hadronic shower. The total mass of the fiducial volume was about 250 t.
- Only events with a single reconstructed muon were accepted.
- The muon had to traverse at least five consecutive drift chambers, i.e. 2 m of iron. In the analysis, an additional cut was applied at 5 GeV/c on the reconstructed muon momentum.
- The muon track had to be well reconstructed. At least four points and at least half of all available points along the trajectory had to be used in the fit. At most, half of the muon trajectory was allowed to be in a non-magnetic region in the centre of the apparatus, and the estimated momentum uncertainty was required to be better than 30%. The fit probability had to exceed 0.001.
- The sign of the muon momentum had to correspond to the nominal beam polarity.
- The total energy of the incoming neutrino was required to be higher than 20 GeV and lower than 212 GeV. The low-energy cut was introduced to avoid regions of poor acceptance and lower trigger efficiency, whereas at very high energies smearing becomes more important.

The final event sample consists of 640000 neutrino events and 550000 antineutrino events. Some details of the event selection are given in Table 1. The total energy distributions of neutrino and antineutrino events in different radial slices are shown in Fig. 11.

9. MONTE CARLO SIMULATION

A Monte Carlo simulation of the experimental set-up was used to correct observed event rates for acceptance and detector response.

The neutrino beam energy and radial distributions cannot be reliably calculated. They were derived in an iterative procedure from the data, assuming a total cross-section rising linearly with neutrino energy. In the first step, neutrino events were generated using parametrizations of the observed energy spectrum and of published structure functions [25]. The calculated acceptance was applied to the data to obtain new energy and radial distributions, and the whole procedure was repeated until the input and output energies and radial distributions were the same.

Muons were propagated through the detector. Multiple Coulomb scattering and energy loss due to ionization, pair creation, and bremsstrahlung were taken into account. Radiative energy losses above 6 GeV were adjusted to agree with the observed distribution of pulse height recorded along the muon trajectory as a function of muon momentum. Triggering rates were simulated, and the hadronic energy was reduced to simulate the electronic response. Monte Carlo generated events were smeared according to the measured resolution function (in the case of hadronic energy) or to the calculated function (in the case of muon momentum and angle). The smeared Monte Carlo events were subject to cuts identical to those applied to the data.

The ratio of simulated events accepted, after cuts, in a given x–y–E_ν bin to the number of events generated in this bin gave the correction factor to be applied to the observed event rates. It was verified that the combined acceptance and smearing correction depends only weakly on the input structure functions. The final correction factor was obtained iteratively, replacing the initial parametrization of structure functions by a third-order polynomial fit in y to the differential cross-sections, as determined in this experiment, in every x–E_ν bin. After this procedure had converged, the Monte Carlo simulation reproduced well the observed distributions of all kinematical variables (see Fig. 12). Figure 13 shows the values of the correction factor as a function of x and y at several typical neutrino energies. In the determination of differential cross-sections, only bins with combined acceptance and smearing correction in the range 0.7 to 1.3 were retained.

A large sample of Monte Carlo events was reconstructed using the off-line reconstruction program as a check of possible biases in the pattern recognition and fitting procedure. The simulation included spurious hits in the shower region as well as δ-rays and noise hits along the muon trajectory. The distributions of reconstructed track parameters around their true values was in good agreement with the computed resolution functions for 99% of the events. About 1% of the events were found in tails of these distributions. These tails were incorporated into the smearing procedure; their effect on the final results is negligible.

10. DETERMINATION OF DIFFERENTIAL CROSS-SECTIONS

The differential cross-sections were determined in bins of x, y, and E_ν for both neutrino and antineutrino interactions. The total energy was computed as the sum of reconstructed muon momentum and hadron shower energy. A logarithmic binning in E_ν was used to reduce variations in bin population. To facilitate a subsequent extraction of structure functions, a logarithmic binning in y was also used in such a way that, in a given x bin, different E_ν and y bins corresponded to the same value of ν. The bin limits are given in Table 2. In every total energy bin the differential cross-sections were normalized to the energy-independent values of $\sigma_{tot}/E_\nu = 0.703 \times 10^{-38}$ cm^2/GeV per nucleon for the neutrino case and 0.331×10^{-38} cm^2/GeV per nucleon for the antineutrino one [18]. The differential cross-sections were determined according to the following formula, which is independent of the precise shape of the beam spectrum:

$$\frac{1}{E_\nu}\frac{d^2\sigma}{dxdy} = \frac{MC^s(E_\nu)}{D(E_\nu)MC^g(E_\nu)}\frac{D(x,y,E_\nu)}{MC^s(x,y,E_\nu)}\frac{MC^g(x,y,E_\nu)}{\Delta x\Delta y}\frac{\sigma_{tot}}{E_\nu}, \qquad (10.1)$$

where

$D(x,y,E_\nu)$, $MC^s(x,y,E_\nu)$, and $MC^g(x,y,E_\nu)$ denote the data, the Monte Carlo after smearing and cuts, and the generated Monte Carlo events in this bin;

$D(E_\nu)$, $MC^s(E_\nu)$, and $MC^g(E_\nu)$ are the data, the smeared Monte Carlo, and the generated Monte Carlo events in this neutrino energy interval.

The values of the differential cross-sections determined in this way are averaged over the bin size. The systematic error of the resulting cross-sections was evaluated by adding, in quadrature, the changes of differential cross-sections due to

- a change of the hadron energy scale by $\pm 2.5\%$, independently of muon momentum scale;
- a shift of the hadron energy by ± 0.5 GeV;
- a non-linearity of the hadron energy calibration, corresponding to a change of response by $\pm 4\%$ over 100 GeV;
- a simultaneous change of the muon momentum scale and the hadron energy scale by $\pm 2\%$;
- an independent change of the resolution on muon momentum, muon angle, and hadronic energy by $\pm 20\%$ of the resolution;
- a change of the shape of the neutrino and antineutrino energy spectra used in the simulation by $\pm 20\%$ over 200 GeV.

The first three effects cover the uncertainties in the corrections for the muon energy loss in the shower region and in the rate-dependence of the pulse-height response.

The combined systematic error is typically of the order of 5%, except for the region of low ν where the assumed ± 0.5 GeV shift of the hadron energy causes up to 15% change of the differential cross-sections. Differential cross-sections were evaluated for bins with $\nu > 5$ GeV to ensure sufficient resolution in hadron energy ($\Delta E/E < 25\%$). The resulting differential cross-sections and their errors are given in Table 3. The scale errors due to uncertainties in the values of the total cross-sections are not included in the systematic errors.

Figure 14 shows an example of the differential cross-sections for neutrinos and antineutrinos at $E_\nu = 65$ GeV. Scaling violations distort the y distributions considerably at fixed E_ν. The y distribution for neutrino–nucleon interactions at large x is not at all flat, as might be expected from the naïve quark–parton model, and neutrino and antineutrino cross-sections at very small x do not exhibit the expected quadratic y dependence.

11. DETERMINATION OF STRUCTURE FUNCTIONS

The structure functions were calculated from the appropriate combinations of the differential cross-sections determined according to the previous section, but also corrected for shifts in the effective bin centre using parametrizations of the structure functions [25]. These corrections are generally very small, except for the first and the last x bins ($x = 0.015$ and $x = 0.65$), where they can be as large as 7–8%.

The measured cross-sections include contributions from higher-order electroweak diagrams, whereas the structure functions are defined for the Born approximation only. Therefore radiative corrections were applied using the calculations of Ref. [26]. These calculations include the complete set of second-order electroweak diagrams for four-fermion interactions. They agree very well with other calculations available in the literature [27, 28]. In the quark–parton model they are convoluted with the quark densities to yield correction factors to be applied to the measured cross-sections. The dependence of these corrections on the assumed quark densities and their masses is very weak: in

general, the uncertainty of the correction factor in our kinematical domain is smaller than 1%. These corrections differ from the previously used calculations of Ref. [29] by up to 3% (see Fig. 15), although at very small x the differences are larger.

For the determination of structure functions from the differential cross-sections, the W propagator was taken into account using $m_W = 82\ \mathrm{GeV}/c^2$ [30, 31]. Fermi-motion corrections were not applied. A correction for the neutron excess in iron was included in the evaluation of the structure function using $d_v/u_v = 0.55(1-x)$ for the ratio of the valence-quark distributions in the proton [32].

In order to reduce the number of independent structure functions, approximate charge symmetry for $\Delta S = 0$ and $\Delta C = 0$ transitions is assumed, implying for i = 1, 2, and 3,

$$F_i^{\bar{\nu}p} = F_i^{\nu n},$$

$$F_i^{\nu p} = F_i^{\bar{\nu} n}.$$

A correction for $\Delta S = \Delta C = 1$ transitions was applied according to the quark–parton model. The charm content of the nucleon has been neglected. All structure functions in the following correspond to an isoscalar target.

The uncertainties in the structure functions due to the errors of the total neutrino and antineutrino cross-sections were estimated, allowing for a deviation from linearity of σ^{ν}/E_{ν} of 7% over 160 GeV centred at 50 GeV and for a 1% variation of the absolute values of these cross-sections. These errors are treated as being independent for neutrinos and antineutrinos. The resulting uncertainties for all structure functions are listed separately from other systematic errors. An additional common scale error of the cross-sections of 3% has to be applied to all structure functions.

11.1 The structure function $xF_3(x,Q^2)$

The average structure function $xF_3(x,Q^2) = 1/2[xF_3^{\nu}(x,Q^2) + xF_3^{\bar{\nu}}(x,Q^2)]$ was obtained from the difference between neutrino and antineutrino cross-sections according to the formula

$$xF_3(x,Q^2) = \frac{1}{\sigma_0} \frac{(d^2\sigma^{\nu Fe}/dxdy) - (d^2\sigma^{\bar{\nu}Fe}/dxdy)}{1 - (1-y)^2 + 2\delta\,(\,{}^1\!/_2\, y^2 + 1 - y - {}^1\!/_4\, y^2Q^2/\nu^2)}, \qquad (11.1)$$

where

$$\delta = \frac{N - Z}{N + Z} \times \frac{1 - d_v/u_v}{1 + d_v/u_v}$$

(N is the number of neutrons; Z is the number of protons). The term proportional to δ is the correction for the non-isoscalarity of the iron nucleus.

In the extraction of the structure function, only bins with $y > 0.1$ were used. Values of $xF_3(x,Q^2)$ corresponding to the same x and Q^2, but different E_{ν} and y, were averaged. The systematic errors were estimated by adding, in quadrature, changes of the function due to the systematic effects listed in Section 10. At small x the systematic error of xF_3 is dominated by the uncertainty in the antineutrino to neutrino cross-section ratio and its possible dependence on the neutrino energy. The systematic errors due to these cross-section uncertainties are given separately. The values, the statistical and the systematic errors are given in Table 4 and shown in Fig. 16. The structure function xF_3 evaluated at the same x and Q^2 but different y should be independent of y. Figure 17 shows that this is the case within statistical errors. This confirms the systematic quality of the measurement.

11.2 The structure functions $F_2(x,Q^2)$ and $2xF_1(x,Q^2)$

Assuming that $xF_3^{\nu} = xF_3^{\bar{\nu}}$, the sum of neutrino- and antineutrino-nucleon differential cross-sections is a linear combination of $F_2(x,Q^2)$ and $2xF_1(x,Q^2)$ with coefficients depending on y:

$$\frac{d^2\sigma^{\nu N}}{dxdy} + \frac{d^2\sigma^{\bar{\nu}N}}{dxdy} = 2\sigma_0 [\,{}^1\!/_2\, y^2\, 2xF_1 + (1 - y - {}^1\!/_2\, Mxy/E_\nu)F_2] \,. \tag{11.2}$$

In order to separate the two functions, an assumption on their difference, or on the ratio $R(x,Q^2)$, is needed. The large experimental uncertainty in R, especially at small values of x, causes sizeable uncertainties in the resulting structure functions. The correction due to R depends on the average value of y of the events used. Therefore the data are presented in the form of a y-dependent function which allows a determination of $2xF_1$ and F_2 for any possible value of R. An auxiliary function $F_w(x,Q^2)$ is defined as a weighted average of $F_2(x,Q^2)$ and $2xF_1(x,Q^2)$ with weights depending on the y range used for its determination:

$$F_w(x,Q^2) = \langle a \rangle_y\, 2xF_1(x,Q^2) + (1 - \langle a \rangle_y)\, F_2(x,Q^2) \tag{11.3}$$

with

$$\langle a \rangle_y = \langle (y^2)/2/[y^2/2 + (1-y) - Mxy/2E_\nu] \rangle_y \,. \tag{11.4}$$

From the tabulated values of F_w and $\langle a \rangle_y$, the structure functions $2xF_1$ and F_2 for any given value of R can be obtained as

$$2xF_1(x,Q^2) = \frac{F_w(x,Q^2)}{1 + (1 + \langle a \rangle_y)\,(R - Q^2/\nu^2)/(1 + Q^2/\nu^2)} \,, \tag{11.5}$$

$$F_2(x,Q^2) = \frac{F_w(x,Q^2)}{1 + \langle a \rangle_y\,(Q^2/\nu^2 - R)/(1 + R)} \,. \tag{11.6}$$

The difference between F_2, $2xF_1$, and F_w, assuming a parametrization of R as $R_0(x,Q^2) \equiv 1.5 \times (1 - x)^4/\ln(Q^2/0.2^2)$, is shown in Fig. 18. This parametrization is consistent with the results presented in subsection 11.4.

The strange and charmed seas are not necessarily equal, therefore the structure functions xF_3^{ν} and $xF_3^{\bar{\nu}}$ are expected to differ slightly. As a result, they do not cancel completely in the sum of cross-sections. The quark-parton model was used to calculate a correction for this effect. We have assumed that the strange sea has the same x distribution as the non-strange sea, and we have neglected the charm content of the nucleon. The normalization of the strange sea was taken to be $C_s = xs(x)/\bar{q}(x) = 0.1$. This number was derived from opposite-sign dimuon rates at hadron energies < 50 GeV, but not corrected for slow rescaling effects [33].

With the corrections for the strange sea and the non-isoscalarity of the iron nucleus taken into account, the final formulae for F_w and $\langle a \rangle_y$ become

$$F_w(x,Q^2) = \frac{1}{\sigma_0} \left\langle \frac{(1 - A)d^2\sigma^{\nu Fe}/dxdy + (1 + A)d^2\sigma^{\bar{\nu}Fe}/dxdy}{2[{}^1\!/_2 y^2 + C_s(y - {}^1\!/_2 y^2) + 1 - y - {}^1\!/_4 y^2Q^2/\nu^2]} \right\rangle_y \,. \tag{11.7a}$$

and

$$\langle a\rangle_y = \left\langle \frac{{}^1\!/_2y^2 + C_s(y - {}^1\!/_2y^2)}{1 - y - {}^1\!/_4y^2Q^2/\nu^2 + {}^1\!/_2y^2 + C_s(y - {}^1\!/_2y^2)} \right\rangle_y , \qquad (11.7b)$$

where

$$A = \frac{(\delta - C_s)\,[1 - (1-y)^2]}{1 - (1-y)^2 + \delta\,[1 + (1-y)^2 + {}^1\!/_2y^2Q^2/\nu^2]} .$$

The values of the auxiliary function F_w and the corresponding values of the weights $\langle a\rangle_y$ for all available x and Q^2 data points are given in Table 4 together with the systematic errors. As in the case of xF_3, the third error reflects the uncertainty due to possible errors in the neutrino and antineutrino total cross-sections.

The uncertainty in the structure function F_2, which is due to insufficient knowledge of R, may be reduced by limiting the determination of the structure function to the region of small y. To achieve this, only those data points in x, y, and E_ν were used, for which the difference between the values of F_2, as determined assuming $R = 0$ and $R = R_0$, is smaller than the combined statistical and systematic errors. The results of this determination are given in Table 4. They are compared in Fig. 19 with the structure function F_2 obtained from the measured values of F_w using $R = R_0(x,Q^2)$.

Charm production, which is of the order of 10% in neutrino interactions, will lead to a partial suppression of the measured cross-sections owing to the mass of the c-quark. This, in turn, affects a comparison of the structure functions with those measured in other processes such as charged lepton scattering, μ-pair production, or high-p_T jet production. The slow rescaling model [34] is usually used to correct the differential cross-sections for this effect. The magnitude of the slow rescaling effect on F_2 and the strange-sea correction mentioned above are shown in Fig. 20.

11.3 The structure function $\bar{q}^{\bar{\nu}}(x,Q^2)$

The contribution of left-handed constituents to the antineutrino-nucleon scattering is suppressed by $(1-y)^2$. This fact is used to determine the right-handed antiquark content of the nucleon, $\bar{q}^{\bar{\nu}}(x,Q^2) = x(\bar{u} + \bar{d} + 2\bar{s})$. The combination of differential cross-sections

$$\frac{d^2\sigma^{\bar{\nu}N}}{dxdy} - (1-y)^2\frac{d^2\sigma^{\nu N}}{dxdy} = \sigma_0\{[1 - (1-y)^4]\bar{q}^{\bar{\nu}} + [(1-y) - (1-y)^3]F_L\} \qquad (11.8)$$

is a linear combination of $\bar{q}^{\bar{\nu}}(x,Q^2)$ and the longitudinal structure function $F_L(x,Q^2)$. The structure function $\bar{q}^{\bar{\nu}}(x,Q^2)$ can be evaluated once $F_L(x,Q^2)$ is known. In analogy with the F_2 and $2xF_1$ cases, we define an auxiliary function

$$\bar{q}_w(x,Q^2) = \langle b\rangle_y\,\bar{q}^{\bar{\nu}}(x,Q^2) + (1 - \langle b\rangle_y)F_L(x,Q^2) . \qquad (11.9)$$

With all corrections taken into account, $\bar{q}_w$ is defined as

$$\bar{q}_w(x,Q^2) = \left\langle \frac{1}{\sigma_0 B}\,\frac{(1+\delta)d^2\sigma^{\bar{\nu}Fe}/dxdy - (1-\delta)(1-y)^2d^2\sigma^{\nu Fe}/dxdy}{1 + (1-y)^2 - 2C_s(1-y)^2/(1+C_s) + (1-y)} \right\rangle_y , \qquad (11.10)$$

where

$$B = 1 - (1-y)^2 + \delta[1 + (1-y)^2] ,$$

$$\langle b \rangle_y = \left\langle \frac{1 + (1-y)^2 - 2C_s(1-y)^2/(1+C_s)}{1 + (1-y)^2 - 2C_s(1-y)^2/(1+C_s) + (1-y)} \right\rangle_y .$$

The values of the resulting function $\bar{q}_w(x,Q^2)$ with their statistical and systematic errors and the corresponding values of $\langle b \rangle_y$ are given in Table 4. With an assumption on the value of F_L, the structure function $\bar{q}^{\bar{\nu}}(x,Q^2)$ can be extracted from $\bar{q}_w$ using the relation

$$\bar{q}^{\bar{\nu}}(x,Q^2) = \frac{1}{\langle b \rangle_y} [\bar{q}_w(x,Q^2) - (1 - \langle b \rangle_y) F_L(x,Q^2)] . \qquad (11.11)$$

Figure 21 shows the antiquark distribution evaluated assuming $F_L = R_0(x,Q^2) \cdot 2xF_1$.

11.4 Separation of the structure functions $F_L(x,Q^2)$ and $\bar{q}^{\bar{\nu}}(x,Q^2)$

The difference between antineutrino and neutrino cross-sections defined in Eq. (11.8) is a combination of the structure functions $\bar{q}^{\bar{\nu}}(x,Q^2)$ and $F_L(x,Q^2)$. The two components can be separated as their y dependence is different. To reduce the systematic error due to the uncertainties in the neutrino and antineutrino cross-section ratio, only points with $y > 0.5$ were used in the analysis. The differential cross-sections were determined according to the procedure described in Section 10. However, the binning in y was modified to optimize the range available for fitting (see Table 2); in particular, the upper edge of the highest-y bin was chosen to be $y_{max} = 1 - p_\mu^{cut}/E_\nu$ to reduce the acceptance correction. The differential cross-sections were corrected for shifts to the bin centres, for non-isoscalarity, and for the strange sea as described above. Radiative corrections and the W-boson propagator effect were taken into account. A two-parameter fit was performed for each x and Q^2 point, yielding F_L and $\bar{q}^{\bar{\nu}}$. An example of the y distribution at fixed x and Q^2, and a fit to it, is shown in Fig. 22. The results of these fits were averaged over Q^2 to obtain the values of $F_L(x)$ and $\bar{q}^{\bar{\nu}}(x)$ given in Table 5 and shown in Figs. 23 and 24 (notice that the average value of Q^2 is proportional to x). Their systematic error was estimated by adding, in quadrature, variations of the results due to the systematic effects already described, including the uncertainties of the energy dependence of the total cross-sections. The values of $F_L(x)$ fall with x in a way that is consistent with QCD expectations. In the case of neutrino-induced reactions, a sizeable contribution to the longitudinal structure function is expected owing to the effects of the finite c-quark mass [35]. For the same reason, the observed antiquark distribution may be reduced. To estimate the size of this effect, we have determined the values of F_L and $\bar{q}^{\bar{\nu}}$ using differential cross-sections corrected according to the slow rescaling model [34]. The resulting structure functions are shown as open points in Figs. 23 and 24. The values of the longitudinal structure function can be converted to R using values of $2xF_1$ derived from Table 4, assuming $R = R_0(x,Q^2)$. In Fig. 25 they are compared with the measurement obtained previously from narrow-band beam data [36]. They agree within stated errors. The present results are, however, more precise, chiefly owing to the increase in the statistics.

We have repeated the analysis in coarser x-bins and averaging over only parts of the available Q^2 range to look for a possible Q^2 dependence of F_L. The results, given in Table 6 and shown in Figs. 26 and 27, indicate a fall of F_L with Q^2, and demonstrate the rise of the sea with increasing Q^2. The larger errors in the antiquark distribution are primarily due to the intrinsic correlation with $F_L(x,Q^2)$, which cannot be determined more precisely without further assumptions.

11.5 Limits on the structure function $F_2(x)$ at large x

The observation of a difference between the nucleon structure functions determined from muon scattering on iron and on deuterium [37] has created considerable interest in nuclear effects in

deep-inelastic scattering. The presence of collective phenomena inside the nucleon, such as multinucleon bags or clusters, may lead to a non-vanishing cross-section for scattering at values of x exceeding 1. In principle, for neutrino scattering off a nucleus, the kinematically allowed x-values range from zero to A, where A is the atomic number.

The measurement of the structure functions at very large values of x is difficult. The resolution in x is poor, primarily because of the resolution in hadron energy at low values of ν. The smallness of the cross-section makes the observed event rates very sensitive to tails of the resolution functions. An upper limit on the structure function can be set by all observed events, without any allowance for smearing effects. Sufficient resolution is maintained if $\nu > 20$ GeV. A possible contamination of wrong-sign muons is reduced by imposing $p_\mu < 80$ GeV/c. The p_μ and ν cuts may be translated to a total energy-dependent $y_{cut} = \max [20/E_\nu, (1 - 80/E_\nu)]$. Figures 28 and 29 show that the total-energy distributions and the y distributions of events with $x > 0.8$ and $x > 1.0$ are very similar to the distribution of all events for neutrinos and of events with $x > 0.45$ for antineutrinos. The observed number of events with $x > 0.8$ were corrected for the acceptance, assuming a flat y-distribution. Ignoring the sea contribution at very large x, we have implied that the differential cross-section is proportional to $F_2(x)$. The corrected number of events in each x bin can then be expressed as

$$N(x_1 < x < x_2) = \int dE_\nu \, \phi(E_\nu) \frac{G_F^2 M E_\nu}{\pi} \int_{x_1}^{x_2} dx \, F_2(x) , \tag{11.12}$$

where $N(x_1 < x < x_2)$ is the number of events corrected for p_μ and ν cuts, and $\phi(E_\nu)$ is the neutrino or antineutrino flux.

The integrated flux is given by the observed event rates with $x > 0$, assuming the value of the total cross-section as discussed above. The upper limits on the structure function F_2 obtained from neutrino and antineutrino data were averaged; the results after bin centre correction are shown in Fig. 30 and in Table 7. The systematic errors are dominated by uncertainties in the hadron energy.

The number of events with $x > 1$ is fully consistent with the expectation from smearing effects due to resolution, thus leaving little room for a genuine structure function. We observe that the long tails in the Fermi momentum distribution of Ref. [38] are inconsistent with the data. This conclusion is independent of the resolution and of the actual shape of the structure functions for $x > 0.65$ (Fig. 30).

12. COMPARISON WITH QCD PREDICTIONS

Perturbative QCD does not make any prediction about the shape of structure functions F_2, $2xF_1$ and xF_3, but describes their evolution with Q^2. The magnitude of a change of the structure function with Q^2 depends on the value of the strong coupling constant $\alpha_s(Q^2)$ or equivalently on the QCD scale parameter Λ. In leading order they are related through

$$\alpha_s(Q^2) = \frac{4\pi}{[11 - {}^2/_3 n_f] \ln Q^2/\Lambda^2}, \tag{12.1}$$

where n_f is the number of active quark flavours. The Q^2 evolution of the non-singlet structure function xF_3 is particularly simple since it depends only on Λ. The structure function xF_3 is therefore very suitable for an unambiguous determination of this parameter.

The scaling violations of the singlet structure functions F_2 and $2xF_1$ depend also on the gluon structure function. This fact permits a determination of the shape of the gluon distribution, in addition to Λ.

The structure functions determined in this experiment exhibit the familiar pattern of scaling violations: with increasing Q^2 there is a rise at small values of x, a fall at large x, and an increase of the quark–antiquark sea (Figs. 1b, 19, and 21). Equivalently, the comparison of the structure functions determined at three different values of Q^2 exhibits a clear shrinkage (Fig. 31).

12.1 Moments of structure functions

QCD predictions for scaling violations are most conveniently expressed in terms of moments of the structure functions, defined as

$$M_n(Q^2) = \int_0^1 dx\, x^{n-2} f(x,Q^2)\,, \qquad \text{where } f = 2xF_1,\ F_2, \text{ or } xF_3\,. \tag{12.2}$$

Owing to kinematical limitations, however, the shape of the structure functions cannot, in general, be measured over the entire x range for a given Q^2. From the experimental point of view it is therefore desirable to study the scaling violations as a function of ν rather than of Q^2, since the whole range of x is kinematically accessible at any fixed value of ν. The QCD predictions for the moments at fixed ν are, however, much weaker. We have calculated the integrals and average values of x for xF_3, F_2, and $\bar{q}^{\nu}$ as a function of ν (Fig. 32). Contributions to the integral from the region $x > 0.7$ were estimated using the fitted shape of the structure functions, assuming a $(1-x)^{\beta}$ behaviour near $x = 1$. These contributions were below 10% for all moments presented here. The moments show quantitatively the increase in the amount of sea with ν and the shrinkage of all structure functions, especially for $\nu < 50$ GeV, as expected from QCD.

The Gross–Llewellyn Smith [39] sum rule can be expressed in terms of the first moment of xF_3 calculated at fixed ν [40]:

$$\int_0^1 dx\, \frac{1}{x} xF_3(x,\nu) = 3\left[1 - 2.36\,\frac{\alpha_s(2M\nu)}{\pi}\right]\,. \tag{12.3}$$

In Fig. 33 we have compared the measured moment with this prediction. The data clearly indicate the presence of the α_s term. The difference between the data and the prediction at low ν may be attributed to sizeable contributions from low Q^2, where perturbative QCD may not be valid.

12.2 A comparison of xF_3 with QCD and a determination of Λ

Given the shape of the valence-quark structure function q_v at some Q_0^2, its evolution to any value of Q^2 is predicted in QCD by the Altarelli–Parisi equation [41]:

$$\frac{dq_v(x,Q^2)}{d\ln Q^2} = \frac{\alpha_s(Q^2)}{2\pi}\int_x^1 \frac{dz}{z}\,\frac{x}{z}\,P_{qq}\left(\frac{x}{z}\right)\, q_v(z,Q^2)\,; \tag{12.4}$$

q_v can be identified with xF_3 after target mass corrections. In contrast to the moments, no analytic solution exists. Several computer programs are available to calculate the Q^2 evolution, including next-to-leading-order corrections in the $\overline{\text{MS}}$ scheme and target mass effects. We have made a detailed comparison of three different programs [42–44] and found good agreement in leading order and in the treatment of the target mass effects. Differences in the next-to-leading order did not seriously affect the results of our fits. In the following we have compared the results on xF_3 with the QCD predictions, using the program of Ref. [42]. The shape of the valence-quark structure function was parametrized at $Q_0^2 = 5$ GeV^2 as

$$q_v(x,Q^2) = A\,x^{\alpha}(1-x)^{\beta}(1+\gamma x)/B\,.$$

The factor B is a normalization factor chosen so that A can be interpreted as the number of valence quarks; A, α, β, and γ are free parameters. The χ^2 was computed using statistical and systematic errors added in quadrature. This prescription decreases the weight of points, which suffer large systematic uncertainties in the fitting procedure. On the other hand, the absolute value of the χ^2 loses its statistical meaning. Fits were performed in next-to-leading order, including target mass effects [45] for different cuts in Q^2 and W^2. A fit to all data with $Q^2 > 2$ GeV^2 is shown in Fig. 16. Systematic deviations of the measured values from the best-fit lines are observed in the large-x region, occurring at relatively low values of W^2, and in the small-x region where the data tend to rise with Q^2 more quickly than is predicted by QCD, especially at low values of Q^2. However, in view of the large systematic errors in this regime, due to the uncertainty in the neutrino total cross-section, this cannot be considered significant. The best-fit values for Λ in the second-order QCD program developed by Abbott and Barnett [42] are shown in Fig. 34 as a function of minimum Q^2 and minimum W^2. Other second-order programs [43, 44] give values of Λ larger by (10–30)%. The most important result here, in our opinion, is the fact that the QCD predictions for the Q^2 evolution of the non-singlet structure function, to our knowledge the most quantitative, direct and unambiguous prediction of QCD, are confirmed by experiment for reasonably large Q^2. For $W^2 > 11$ GeV^2 and $Q^2 > 10$ GeV^2, the value of $\Lambda_{\overline{MS}}$ is 100^{+90}_{-60} MeV. The resulting fit parameters are given in Table 8.

A simple illustration of QCD predictions is provided by the x-dependence of the logarithmic derivative d ln F/d ln Q^2 of a structure function F, later referred to as 'slope'. Figure 35 shows the slopes of xF_3 calculated for two different choices of the kinematic domain. The error bars take into account the correlations induced by systematic effects. The ν cut was chosen to keep an equal number of high-Q^2 points in every x bin, although the average Q^2 varies from bin to bin.

As in Fig. 16, deviations from the QCD expectations are observed, but since the systematic errors dominate and are strongly correlated between neighbouring points, we do not consider these differences to be significant. The difference between the calculated slopes and the QCD prediction becomes less significant for slopes computed for high Q^2 and ν cuts, indicating the presence of non-perturbative effects at the low-Q^2 end of the range covered by the data.

12.3 A comparison of differential cross-sections with the QCD predictions and a determination of the gluon distribution

The evolution of the singlet-quark distributions q_s such as F_2 or $2xF_1$ is coupled to the gluon distribution, as given by the Altarelli–Parisi equations [41]:

$$\frac{dq_s(x,Q^2)}{d\ln Q^2} = \frac{\alpha_s(Q^2)}{2\pi}\int_x^1 \frac{x\,dz}{z^2}\left[P_{qq}\left(\frac{x}{z}\right) q_s(z,Q^2) + 2n_f P_{gq}\left(\frac{x}{z}\right) G(z,Q^2)\right], \qquad (12.5a)$$

$$\frac{dG(x,Q^2)}{d\ln Q^2} = \frac{\alpha_s(Q^2)}{2\pi}\int_x^1 \frac{x\,dz}{z^2}\left[P_{qg}\left(\frac{x}{z}\right) q_s(z,Q^2) + P_{gg}\left(\frac{x}{z}\right) G(z,Q^2)\right]. \qquad (12.5b)$$

It has been observed that in the QCD fits to the singlet structure function there exists a strong correlation between the value of Λ and the shape of the gluon distribution [13]. To reduce this correlation, some other experimental information is needed. The measured antiquark distribution

was frequently used for this purpose, although it is not a completely independent measurement; its correlation with F_2 was always ignored.

The extraction of the singlet structure function depends on the assumed value of R, which in turn depends strongly on the unknown gluon distribution. However, the gluon distribution fitted to the Q^2 variation of F_2 or $2xF_1$ is not necessarily consistent with the assumption on R. To avoid these problems we have performed fits to the differential cross-sections rather than to the structure functions. At $Q_0^2 = 20\ \mathrm{GeV}^2$ we have parametrized

$$q_v(x,Q_0^2) = A_v\, x^{\alpha_v}\,(1-x)^{\beta_v}\,(1+\gamma_v x)/B_v\,,$$

$$q_s(x,Q_0^2) = q_v\,(x,Q_0^2) + A_s\, e^{-\beta_s x}\,(1-x)\,,$$

$$G(x,Q_0^2) = A_g\,(1-x)^{\beta_g}\,.$$

The constant A_v was calculated from the Gross-Llewellyn Smith sum rule and $1/B_v = \int dx\, x^{\alpha_v - 1}\,(1-x)^{B_v}\,(1+\gamma_v x)$; all the other parameters were free. This particular ansatz for the difference $q_s - q_v$, which in the parton model is twice the sea-quark distribution, gives among several parametrizations the best χ^2. At every iteration the value of R, as well as target mass corrections, were evaluated. The resulting structure functions were used to compute neutrino and antineutrino cross-sections according to Eq. (2.1). Differential cross-sections were corrected for slow rescaling and shift of the bin centre; radiative corrections and the W-boson propagator were taken into account also. Statistical and systematic errors were combined in quadrature. Potential changes in the normalization and the energy dependence of the total cross-sections were studied separately.

Fits were performed in leading order only, using a modified version of the program of Ref. [42]. The momentum sum rule $\int dx\,(q + \bar{q} + G) = 1$ was not enforced. All data points with $Q^2 > 5\ \mathrm{GeV}^2$ and $W^2 > 11\ \mathrm{GeV}^2$ were used in the fit. The fits describe the measured cross-sections satisfactorily, yielding a χ^2 of the order of 505 for 855 degrees of freedom. Examples of the agreement of the fitted curves with the measured values of the differential cross-sections and the extracted structure function F_2 are shown in Figs. 14 and 19. The value of Λ was found to be independent of the integral and of the shape of the quark and gluon parametrizations. A χ^2 minimum is observed around $\Lambda = 130\ \mathrm{MeV}$.

In order to estimate the uncertainty in the gluon distribution we have tried, in addition to the functional forms mentioned above other parametrizations for G and q_s. The fits are not sensitive to more than two parameters in the parametrization of $G(x,Q^2)$. The variation of the functional forms of G and q_s introduces uncertainties in the determination of the gluon distribution of about equal size, in total $\pm 20\%$ at $x = 0.08$ and $\pm 30\%$ at $x = 0.35$. The largest uncertainty in the gluon distribution arises from the energy dependence of the total cross-sections. These systematic errors induce an additional uncertainty in the gluon distribution of $\approx 30\%$ at $x = 0.08$ and up to $\approx 40\%$ at $x = 0.35$. Figure 36 displays the gluon distribution; the errors due to parametrizations and total cross-sections are given separately.

The gluon distribution appears to be soft, concentrated in the region $x < 0.4$. The difference to our previously published gluon structure function can be ascribed to the treatment of $R(x,Q^2)$ and to the difference in the energy dependence of total cross-sections. The complete set of parameters for the typical fit are given in Table 9. Figure 37 shows the corresponding shapes of the quark and gluon distributions at $Q^2 = 20\ \mathrm{GeV}^2$.

13. COMPARISON OF STRUCTURE FUNCTIONS WITH OTHER MEASUREMENTS

Our previously published structure functions were determined from the narrow-band beam data taken in 1978/79 [15]. Owing to the flat neutrino spectrum, the systematic errors were smaller than for the data reported here. A comparison of the shape of differential cross-sections in Table 3 with those derived from the old data using the procedure described in Section 10 shows agreement at the level of 5–10%. A comparison of structure functions with other published ones should take into account the following differences in their extraction:

- The total cross-section σ_{tot}/E_ν was assumed to be independent of energy and equal to 0.703×10^{-38} cm^2/GeV per nucleon for the neutrino and 0.331×10^{-38} cm^2/GeV per nucleon for the antineutrino case. In the past, the energy dependence of the total cross-sections was contained in the data themselves. The average value of σ_{tot}/E_ν for $40 < E_\nu < 90$ GeV for the data of Ref. [15] was 0.62×10^{-38} cm^2/GeV per nucleon for neutrinos and 0.30×10^{-38} cm^2/GeV per nucleon for antineutrinos, approximately 10% lower than the more recent cross-section measurements.
- Different radiative corrections were applied.
- The strange-sea correction (in the case of the F_2 structure function) is evaluated in this analysis using $C_s = 0.1$ rather than 0.2.
- A constant value of $R = 0.1$ was used in the past. The sensitivity of F_2 to the R correction depends on the total energy spectrum.

We have extracted values of the structure function $F_2(x,Q^2)$ from the old data, using the procedure described in Section 11. Figure 38 shows their comparison with the structure functions determined in this analysis. The agreement between the two data sets is reasonably good, at the level of 5–10%.

Figure 39 shows the comparison of the values of R(x) with those obtained in other deep-inelastic scattering experiments at high Q^2 using neutrino [46] and muon beams [47, 48]. These measurements correspond, in general, to different values of Q^2. There is agreement that at large x and high Q^2 the value of R is very small, less than 0.05, whereas at small x it goes up to ~ 0.3. Large statistical errors do not permit any conclusions about the Q^2 dependence of R. On the other hand, the comparison of our results with those of the recent SLAC experiment at low energy [49] (Fig. 40) indicates a significant variation of R with Q^2.

Figure 41 shows the comparison of the values of the structure function $xF_3(x,Q^2)$ with the neutrino data of Refs. [16] and [17]. The agreement, within error bars, is very good.

Within the quark-parton model there is a very close connection between the structure function F_2 measured in neutrino- and charged-lepton-induced reactions given by the average square of electric charges of the quarks. This comparison may be affected by the change of the flavour composition of the nucleon as a function of x, and by different threshold effects due to the c-quark mass. Figure 42 shows the comparison of the structure function $F_2(x,Q^2)$ with the measurements of the EMC [47] and BCDMS [48] Collaborations multiplied by 18/5. For the purpose of this comparison the data have been corrected for slow rescaling and extracted using $R = 0$. At large values of x, all three experiments agree very well. In the small-x region the two muon experiments disagree; our structure function is higher than the EMC measurement by 5–10% but exhibits similar Q^2 variation. Scaling violations seen in the neutrino and muon data are compared in Fig. 43, where the logarithmic derivatives of the structure function $F_2(x,Q^2)$ are shown. All high-Q^2 data agree reasonably well at large x, whereas there is a systematic difference between slopes at small x.

Acknowledgements

We thank our technical collaborators from the participating institutes for the construction and maintenance of the beam and the detector. We also acknowledge useful discussions with Profs. D.Y. Bardin, M. Roos, E. Paschos and F.J. Yndurain on radiative corrections, and on the QCD analysis of the data.

REFERENCES

[1] E.D. Bloom et al., Phys. Rev. Lett. **23** (1969) 930.
[2] M. Breidenbach et al., Phys. Rev. Lett. **23** (1969) 935.
[3] G. Miller et al., Phys. Rev. **D5** (1972) 528.
[4] H. de Groot et al., Z. Phys. **C1** (1979) 143.
[5] P.C. Bosetti et al., Nucl. Phys. **B142** (1978) 1.
[6] D. Fox et al., Phys. Rev. Lett. **33** (1974) 1504.
[7] Y. Watanabe et al., Phys. Rev. Lett. **35** (1975) 898.
[8] C. Chang et al., Phys. Rev. Lett. **35** (1975) 901.
[9] H.L. Anderson et al., Phys. Rev. Lett. **37** (1976) 4.
[10] H.L. Anderson et al., Phys. Rev. Lett. **38** (1977) 1450.
[11] H. de Groot et al., Phys. Lett. **82B** (1979) 292.
[12] H. de Groot et al., Phys. Lett. **82B** (1979) 456.
[13] H. Abramowicz et al., Z. Phys. **C12** (1982) 289.
[14] H. Abramowicz et al., Z. Phys. **C13** (1982) 199.
[15] H. Abramowicz et al., Z. Phys. **C17** (1983) 283.
[16] F. Bergsma et al., Phys. Lett. **123B** (1983) 269.
[17] D.B. MacFarlane et al., Z. Phys. **C26** (1984) 1.
[18] P. Berge et al., Z. Phys. **C35** (1987) 443.
[19] S. van der Meer, CERN Report 61-7 (1961).
[20] M. Holder et al., Nucl. Instrum. Methods **151** (1978) 69.
[21] W. von Rüden, IEEE Trans. Nucl. Sci. **NS-29** (1982) 360.
CDHS Collab., Request for approval of WA1 improvement programme, Memorandum CERN/SPSC/79-34/M 160 Rev. (1979).
[22] C. Richard-Serre, CERN Report 71-18 (1971).
[23] R. Kopp et al., Z. Phys. **C28** (1985) 171.
[24] H. Abramowicz et al., Nucl. Instrum. Methods **180** (1981) 429.
[25] H.D. Brummel, Diploma Thesis, Dortmund Univ. (1983).
[26] D.Yu. Bardin et al., Yad. Phys. **30** (1979) 418.
D.Yu. Bardin et al., Yad. Phys. **36** (1982) 282.
D.Yu. Bardin and V.A. Dokuchaeva, JINR-E2-86-260 (1986) and references quoted therein.
[27] J.F. Wheater and C.H. Llewellyn Smith, Nucl. Phys. **B208** (1982) 27.
[28] L. Liede et al., Helsinki University report HU-TFP-8345 (1983).
[29] A. De Rújula et al., Nucl. Phys. **B154** (1979) 394.
[30] G. Arnison et al., Phys. Lett. **122B** (1983) 103.
[31] M. Banner et al., Phys. Lett. **122B** (1983) 476.
[32] H. Abramowicz et al., Z. Phys. **C25** (1984) 29.
[33] J. Knobloch and K. Kleinknecht, Determination of the structure function of strange and charm quarks in the nucleon, CDHSW internal note (1983).
[34] R.M. Barnett, Phys. Rev. **D14** (1976) 70.
[35] A. De Rújula, H. Georgi and H.D. Politzer, Ann. Phys. (USA) **103** (1977) 315.
[36] H. Abramowicz et al., Phys. Lett. **107B** (1981) 141.
[37] J.J. Aubert et al., Phys. Lett. **123B** (1983) 275.
[38] A. Bodek and J. Ritchie, Phys. Rev. **D24** (1981) 1400.
[39] D.J. Gross and C.H. Llewellyn Smith, Nucl. Phys. **B14** (1969) 337.
[40] C. Lopez and F.J. Yndurain, Nucl. Phys. **B194** (1982) 397.
[41] G. Altarelli and G. Parisi, Nucl. Phys. **B126** (1977) 298.

[42] L.F. Abbott and R.M. Barnett, Ann. Phys. (USA) **125** (1980) 276.
[43] A. Devoto et al., Phys. Rev. **D27** (1983) 508.
[44] A. Gonzalez-Arroyo, C. Lopez and F.J. Yndurain, Nucl. Phys. **B153** (1979) 493.
[45] R. Barbieri et al., Nucl. Phys. **B117** (1976) 50.
[46] F. Bergsma et al., Phys. Lett. **141B** (1984) 129.
[47] J.J. Aubert et al., Nucl. Phys. **B272** (1986) 158.
[48] A.C. Benvenuti et al., Phys. Lett. **195B** (1987) 91.
[49] S. Dasu et al., Phys. Rev. Lett. **61** (1988) 1061.

Table 1

Summary of the data reduction statistics

	Neutrinos	Antineutrinos
Initial number of single-muon events	1822938	1812654
Rejected by cuts:		
Wrong-sign muon	43107	309410
Vertex in module 1	78943	56000
Vertex after module 9	379882	332923
Radius < 0.35 m	100982	77626
Radius > 1.60 m	154438	161445
Trajectory in the hole	421	216
$E_\nu < 20$ GeV or $E_\nu > 212$ GeV	149727	266613
$p_\mu < 5$ GeV/c	14736	4770
HCC triggers with $\nu < 25$ GeV	262097	52261
Final event sample	638605	551390
HCC triggers with $\nu > 25$ GeV in the final sample	187688	13625

Table 2

Limits of bins used in the determination of the differential cross-sections. The row 'bin number 0' defines a lower limit of the first bin. The column '$y(F_L)$' specifies the y binning used for the simultaneous determination of F_L and $\bar{q}^{\bar{\nu}}$

Bin number	Upper limit of the bin			E_ν (GeV)
	x	y	$y(F_L)$	
0	0.00	0.032	0.298	20.0
1	0.03	0.042	0.339	26.0
2	0.06	0.054	0.387	33.8
3	0.10	0.070	0.441	43.9
4	0.15	0.091	0.503	57.1
5	0.20	0.119	0.573	74.3
6	0.25	0.154	0.654	96.5
7	0.30	0.201	0.745	125.5
8	0.40	0.261	0.850	163.1
9	0.50	0.339	0.969	212.1
10	0.60	0.441		
11	0.70	0.573		
12		0.745		
13		0.969		

Table 3

Differential cross-sections for neutrino–iron and antineutrino–iron scattering in units of 10^{-38} cm^2/GeV per nucleon. The first error is statistical, the second is systematic. Errors due to the uncertainties in the total cross-section are not included.

$d\sigma/E_\nu dxdy$ in bin 1; $\langle E_\nu \rangle$ = 23.0 GeV; neutrino beam

x = 0 \ y =	0.032	0.042	0.054	0.070	0.091	0.119	0.154	0.201	0.261	0.339	0.441	0.573	0.745	0.969
0.03									0.733 ±0.052 ±0.092	0.771 ±0.047 ±0.084	0.873 ±0.046 ±0.078	0.856 ±0.039 ±0.075		
0.06									1.290 ±0.078 ±0.156	1.156 ±0.059 ±0.141	1.283 ±0.059 ±0.130	1.268 ±0.050 ±0.123		
0.10									1.553 ±0.076 ±0.154	1.541 ±0.065 ±0.129	1.462 ±0.056 ±0.110	1.564 ±0.049 ±0.100		
0.15									1.599 ±0.069 ±0.161	1.611 ±0.060 ±0.139	1.635 ±0.054 ±0.122	1.531 ±0.045 ±0.113		
0.20									1.426 ±0.061 ±0.119	1.698 ±0.063 ±0.101	1.537 ±0.051 ±0.088	1.525 ±0.046 ±0.080		
0.25									1.464 ±0.070 ±0.125	1.434 ±0.056 ±0.108	1.459 ±0.050 ±0.095	1.409 ±0.043 ±0.087		
0.30									1.317 ±0.061 ±0.087	1.297 ±0.052 ±0.070	1.409 ±0.051 ±0.057	1.219 ±0.042 ±0.049		
0.40									1.063 ±0.041 ±0.065	1.091 ±0.037 ±0.057	0.991 ±0.030 ±0.051	1.002 ±0.028 ±0.047		
0.50									0.773 ±0.034 ±0.057	0.673 ±0.027 ±0.052	0.713 ±0.025 ±0.048	0.627 ±0.021 ±0.046		
0.60									0.468 ±0.025 ±0.038	0.472 ±0.023 ±0.034	0.406 ±0.018 ±0.031	0.372 ±0.016 ±0.029		
0.70									0.279 ±0.018 ±0.027	0.266 ±0.015 ±0.021	0.221 ±0.013 ±0.016	0.175 ±0.010 ±0.014		

Table 3 (cont'd)

$d\sigma/E_\nu dxdy$ in bin 2; $\langle E_\nu \rangle$ = 29.9 GeV; neutrino beam

x = 0 \ y =	0.032	0.042	0.054	0.070	0.091	0.119	0.154	0.201	0.261	0.339	0.441	0.573	0.745	0.969
0								0.792 ±0.062 ±0.102	0.813 ±0.061 ±0.093	0.868 ±0.051 ±0.085	0.985 ±0.052 ±0.078	1.055 ±0.048 ±0.075		
0.03								1.125 ±0.069 ±0.170	1.351 ±0.075 ±0.154	1.277 ±0.067 ±0.139	1.437 ±0.062 ±0.128	1.399 ±0.054 ±0.121		
0.06								1.521 ±0.077 ±0.180	1.505 ±0.071 ±0.154	1.506 ±0.062 ±0.130	1.589 ±0.057 ±0.111	1.559 ±0.050 ±0.100		
0.10								1.597 ±0.074 ±0.184	1.644 ±0.067 ±0.161	1.615 ±0.063 ±0.139	1.668 ±0.056 ±0.122	1.602 ±0.045 ±0.112		
0.15								1.575 ±0.077 ±0.137	1.562 ±0.067 ±0.119	1.643 ±0.063 ±0.102	1.590 ±0.055 ±0.089	1.557 ±0.047 ±0.082		
0.20								1.502 ±0.073 ±0.143	1.388 ±0.064 ±0.125	1.514 ±0.058 ±0.108	1.454 ±0.051 ±0.095	1.536 ±0.046 ±0.087		
0.25								1.339 ±0.063 ±0.109	1.253 ±0.056 ±0.089	1.388 ±0.054 ±0.070	1.266 ±0.048 ±0.056	1.295 ±0.044 ±0.047		
0.30								1.084 ±0.043 ±0.072	1.053 ±0.039 ±0.064	1.052 ±0.036 ±0.057	1.073 ±0.033 ±0.051	0.961 ±0.026 ±0.048		
0.40								0.775 ±0.036 ±0.063	0.714 ±0.031 ±0.057	0.673 ±0.027 ±0.052	0.641 ±0.024 ±0.049	0.615 ±0.021 ±0.046		
0.50								0.466 ±0.027 ±0.042	0.435 ±0.022 ±0.038	0.398 ±0.019 ±0.034	0.411 ±0.019 ±0.030	0.378 ±0.016 ±0.029		
0.60								0.257 ±0.018 ±0.034	0.253 ±0.015 ±0.027	0.215 ±0.013 ±0.021	0.193 ±0.011 ±0.017	0.167 ±0.009 ±0.014		
0.70														

Table 3 (cont'd)

$d\sigma/E_\nu dxdy$ in bin 3; $\langle E_\nu \rangle$ = 38.9 GeV; neutrino beam

x = 0	y = 0.032	0.042	0.054	0.070	0.091	0.119	0.154	0.201	0.261	0.339	0.441	0.573	0.745	0.969
0.03							0.858 ±0.070 ±0.121	0.973 ±0.067 ±0.110	1.013 ±0.062 ±0.098	1.086 ±0.067 ±0.088	1.144 ±0.063 ±0.079	1.190 ±0.052 ±0.074		
0.06							1.336 ±0.103 ±0.151	1.177 ±0.075 ±0.139	1.315 ±0.074 ±0.126	1.494 ±0.073 ±0.114	1.525 ±0.072 ±0.105	1.517 ±0.055 ±0.099		
0.10							1.585 ±0.094 ±0.178	1.568 ±0.081 ±0.157	1.623 ±0.079 ±0.134	1.654 ±0.070 ±0.113	1.621 ±0.066 ±0.097	1.779 ±0.054 ±0.088		
0.15							1.604 ±0.087 ±0.171	1.756 ±0.079 ±0.153	1.664 ±0.070 ±0.134	1.642 ±0.062 ±0.117	1.684 ±0.059 ±0.104	1.760 ±0.047 ±0.096		
0.20							1.587 ±0.085 ±0.132	1.586 ±0.074 ±0.121	1.716 ±0.072 ±0.110	1.574 ±0.060 ±0.100	1.648 ±0.056 ±0.092	1.782 ±0.047 ±0.087		
0.25							1.450 ±0.081 ±0.110	1.499 ±0.079 ±0.098	1.418 ±0.065 ±0.087	1.528 ±0.060 ±0.076	1.466 ±0.059 ±0.068	1.562 ±0.044 ±0.063		
0.30							1.418 ±0.080 ±0.095	1.342 ±0.072 ±0.084	1.437 ±0.065 ±0.073	1.347 ±0.056 ±0.063	1.282 ±0.052 ±0.055	1.423 ±0.043 ±0.051		
0.40							1.144 ±0.053 ±0.073	1.011 ±0.042 ±0.063	0.985 ±0.038 ±0.052	1.027 ±0.036 ±0.042	0.946 ±0.031 ±0.034	0.998 ±0.025 ±0.029		
0.50							0.696 ±0.040 ±0.053	0.671 ±0.033 ±0.047	0.664 ±0.030 ±0.042	0.657 ±0.027 ±0.037	0.661 ±0.027 ±0.033	0.634 ±0.020 ±0.031		
0.60							0.480 ±0.032 ±0.051	0.479 ±0.032 ±0.045	0.385 ±0.021 ±0.039	0.377 ±0.019 ±0.034	0.320 ±0.016 ±0.029	0.324 ±0.013 ±0.027		
0.70							0.253 ±0.022 ±0.033	0.244 ±0.018 ±0.034	0.209 ±0.014 ±0.027	0.191 ±0.013 ±0.021	0.140 ±0.010 ±0.017	0.148 ±0.008 ±0.014		

Table 3 (cont'd)

$d\sigma/E_\nu dxdy$ in bin 4; $\langle E_\nu \rangle$ = 50.5 GeV; neutrino beam

x = 0 \ y =	0.032	0.042	0.054	0.070	0.091	0.119	0.154	0.201	0.261	0.339	0.441	0.573	0.745	0.969
0.03						0.858 ±0.091 ±0.128	1.059 ±0.089 ±0.119	1.021 ±0.076 ±0.110	1.028 ±0.067 ±0.100	1.110 ±0.066 ±0.091	1.081 ±0.054 ±0.085	1.244 ±0.045 ±0.081		
0.06						1.352 ±0.118 ±0.158	1.487 ±0.114 ±0.149	1.423 ±0.097 ±0.140	1.435 ±0.085 ±0.130	1.530 ±0.077 ±0.121	1.540 ±0.063 ±0.114	1.583 ±0.048 ±0.110		
0.10						1.785 ±0.132 ±0.199	1.562 ±0.098 ±0.179	1.449 ±0.083 ±0.157	1.676 ±0.081 ±0.135	1.784 ±0.078 ±0.114	1.853 ±0.059 ±0.098	1.772 ±0.048 ±0.089		
0.15						1.696 ±0.114 ±0.191	1.507 ±0.089 ±0.175	1.667 ±0.085 ±0.156	1.734 ±0.075 ±0.137	1.738 ±0.068 ±0.119	1.695 ±0.050 ±0.106	1.798 ±0.042 ±0.098		
0.20						1.746 ±0.107 ±0.143	1.749 ±0.106 ±0.133	1.614 ±0.079 ±0.122	1.688 ±0.074 ±0.111	1.611 ±0.067 ±0.101	1.736 ±0.054 ±0.093	1.610 ±0.040 ±0.088		
0.25						1.629 ±0.103 ±0.119	1.449 ±0.085 ±0.109	1.611 ±0.081 ±0.098	1.570 ±0.076 ±0.087	1.505 ±0.064 ±0.077	1.516 ±0.051 ±0.069	1.519 ±0.038 ±0.065		
0.30						1.256 ±0.091 ±0.101	1.501 ±0.087 ±0.092	1.464 ±0.078 ±0.082	1.266 ±0.062 ±0.072	1.254 ±0.055 ±0.063	1.303 ±0.045 ±0.056	1.308 ±0.036 ±0.052		
0.40						1.088 ±0.060 ±0.083	1.052 ±0.057 ±0.074	1.036 ±0.048 ±0.063	1.009 ±0.042 ±0.053	0.991 ±0.036 ±0.043	0.977 ±0.028 ±0.035	0.920 ±0.021 ±0.031		
0.50						0.845 ±0.053 ±0.058	0.748 ±0.045 ±0.053	0.683 ±0.037 ±0.047	0.637 ±0.031 ±0.042	0.642 ±0.029 ±0.036	0.624 ±0.022 ±0.032	0.575 ±0.016 ±0.030		
0.60						0.451 ±0.038 ±0.056	0.411 ±0.030 ±0.051	0.371 ±0.025 ±0.045	0.364 ±0.024 ±0.039	0.345 ±0.020 ±0.034	0.341 ±0.016 ±0.030	0.328 ±0.012 ±0.027		
0.70						0.282 ±0.026 ±0.036	0.218 ±0.020 ±0.033	0.187 ±0.016 ±0.034	0.177 ±0.015 ±0.027	0.148 ±0.012 ±0.021	0.157 ±0.009 ±0.017	0.131 ±0.006 ±0.014		

Table 3 (cont'd)

$d\sigma/E_\nu dxdy$ in bin 5; $\langle E_\nu \rangle$ = 65.7 GeV; neutrino beam

x = 0 \ y =	0.032	0.042	0.054	0.070	0.091	0.119	0.154	0.201	0.261	0.339	0.441	0.573	0.745	0.969
0.03					0.967 ±0.111 ±0.086	1.128 ±0.117 ±0.086	1.029 ±0.097 ±0.086	1.019 ±0.079 ±0.086	1.272 ±0.081 ±0.086	1.257 ±0.059 ±0.086	1.240 ±0.044 ±0.086	1.212 ±0.041 ±0.086	1.245 ±0.041 ±0.086
0.06					1.503 ±0.142 ±0.209	1.598 ±0.139 ±0.192	1.727 ±0.119 ±0.173	1.725 ±0.110 ±0.152	1.837 ±0.100 ±0.131	1.849 ±0.074 ±0.111	1.702 ±0.053 ±0.096	1.510 ±0.046 ±0.087	1.709 ±0.050 ±0.085
0.10					1.629 ±0.131 ±0.132	1.582 ±0.121 ±0.129	1.934 ±0.111 ±0.125	1.752 ±0.096 ±0.121	1.915 ±0.090 ±0.116	1.749 ±0.063 ±0.112	1.801 ±0.049 ±0.109	1.717 ±0.045 ±0.107	1.768 ±0.044 ±0.107
0.15					1.734 ±0.122 ±0.133	1.709 ±0.111 ±0.126	1.754 ±0.098 ±0.119	1.880 ±0.091 ±0.110	1.781 ±0.078 ±0.102	1.860 ±0.059 ±0.094	1.890 ±0.045 ±0.088	1.704 ±0.040 ±0.084	1.731 ±0.041 ±0.083
0.20					1.598 ±0.118 ±0.149	1.656 ±0.105 ±0.138	1.712 ±0.098 ±0.124	1.730 ±0.086 ±0.110	1.756 ±0.078 ±0.095	1.669 ±0.056 ±0.082	1.744 ±0.043 ±0.071	1.566 ±0.038 ±0.065	1.691 ±0.042 ±0.063
0.25					1.757 ±0.124 ±0.110	1.615 ±0.104 ±0.102	1.593 ±0.091 ±0.091	1.729 ±0.086 ±0.080	1.485 ±0.069 ±0.069	1.380 ±0.049 ±0.058	1.528 ±0.040 ±0.050	1.447 ±0.037 ±0.046	1.470 ±0.038 ±0.044
0.30					1.525 ±0.116 ±0.093	1.211 ±0.090 ±0.085	1.303 ±0.086 ±0.076	1.470 ±0.080 ±0.066	1.408 ±0.070 ±0.056	1.288 ±0.049 ±0.046	1.251 ±0.037 ±0.039	1.214 ±0.033 ±0.035	1.160 ±0.032 ±0.034
0.40					1.108 ±0.073 ±0.072	1.122 ±0.062 ±0.066	1.063 ±0.053 ±0.059	1.036 ±0.048 ±0.051	1.046 ±0.043 ±0.044	0.964 ±0.031 ±0.036	0.961 ±0.023 ±0.031	0.951 ±0.022 ±0.028	
0.50					0.757 ±0.056 ±0.064	0.797 ±0.053 ±0.060	0.684 ±0.043 ±0.055	0.703 ±0.038 ±0.050	0.598 ±0.031 ±0.044	0.575 ±0.023 ±0.039	0.565 ±0.017 ±0.035	0.601 ±0.017 ±0.032	
0.60					0.405 ±0.038 ±0.059	0.451 ±0.036 ±0.054	0.430 ±0.030 ±0.048	0.416 ±0.026 ±0.042	0.372 ±0.022 ±0.035	0.332 ±0.016 ±0.030	0.312 ±0.012 ±0.025	0.306 ±0.011 ±0.022	
0.70								0.176 ±0.016 ±0.028	0.158 ±0.013 ±0.025	0.144 ±0.009 ±0.022	0.134 ±0.007 ±0.019	0.134 ±0.007 ±0.018	0.097 ±0.006 ±0.017

Table 3 (cont'd)

$d\sigma/E_\nu dxdy$ in bin 6; $\langle E_\nu \rangle$ = 85.4 GeV; neutrino beam

x \ y	0.032	0.042	0.054	0.070	0.091	0.119	0.154	0.201	0.261	0.339	0.441	0.573	0.745	0.969
0				1.244 ±0.147 ±0.084	1.168 ±0.124 ±0.084	1.175 ±0.109 ±0.084	1.066 ±0.090 ±0.084	1.231 ±0.090 ±0.084	1.255 ±0.064 ±0.084	1.264 ±0.050 ±0.083	1.309 ±0.046 ±0.083	1.503 ±0.047 ±0.083	1.354 ±0.043 ±0.083
0.03				1.386 ±0.158 ±0.220	1.602 ±0.148 ±0.206	1.711 ±0.134 ±0.189	1.719 ±0.118 ±0.170	1.713 ±0.103 ±0.149	1.810 ±0.084 ±0.128	1.727 ±0.057 ±0.108	1.732 ±0.052 ±0.093	1.904 ±0.052 ±0.084	1.609 ±0.046 ±0.082
0.06				1.941 ±0.162 ±0.140	1.655 ±0.141 ±0.136	1.761 ±0.126 ±0.133	1.712 ±0.104 ±0.128	2.026 ±0.100 ±0.123	1.987 ±0.076 ±0.119	2.009 ±0.057 ±0.114	1.916 ±0.050 ±0.110	2.007 ±0.048 ±0.108	1.883 ±0.046 ±0.108
0.10				1.660 ±0.133 ±0.133	1.739 ±0.127 ±0.127	1.885 ±0.110 ±0.121	1.771 ±0.094 ±0.113	1.845 ±0.087 ±0.105	1.899 ±0.067 ±0.097	1.916 ±0.050 ±0.089	1.866 ±0.044 ±0.083	1.863 ±0.041 ±0.080	1.775 ±0.040 ±0.079
0.15				1.842 ±0.141 ±0.145	1.752 ±0.120 ±0.136	1.705 ±0.109 ±0.126	1.710 ±0.093 ±0.114	1.651 ±0.082 ±0.102	1.647 ±0.061 ±0.089	1.718 ±0.047 ±0.077	1.777 ±0.043 ±0.067	1.703 ±0.040 ±0.062	1.660 ±0.039 ±0.060
0.20				1.465 ±0.125 ±0.111	1.608 ±0.115 ±0.104	1.409 ±0.095 ±0.096	1.441 ±0.085 ±0.087	1.394 ±0.076 ±0.076	1.574 ±0.061 ±0.066	1.531 ±0.044 ±0.057	1.497 ±0.039 ±0.049	1.494 ±0.037 ±0.045	1.422 ±0.037 ±0.044
0.25				1.447 ±0.124 ±0.101	1.424 ±0.109 ±0.094	1.270 ±0.095 ±0.086	1.364 ±0.086 ±0.077	1.308 ±0.071 ±0.066	1.341 ±0.055 ±0.056	1.350 ±0.042 ±0.046	1.331 ±0.036 ±0.039	1.242 ±0.033 ±0.035	1.147 ±0.031 ±0.033
0.30				1.042 ±0.079 ±0.077	1.055 ±0.066 ±0.072	0.947 ±0.055 ±0.066	0.981 ±0.050 ±0.059	1.058 ±0.047 ±0.051	0.992 ±0.034 ±0.043	0.997 ±0.025 ±0.036	0.954 ±0.023 ±0.030	0.949 ±0.021 ±0.027	0.943 ±0.022 ±0.026
0.40				0.664 ±0.058 ±0.066	0.726 ±0.056 ±0.063	0.628 ±0.044 ±0.059	0.741 ±0.044 ±0.054	0.610 ±0.033 ±0.049	0.566 ±0.025 ±0.043	0.586 ±0.018 ±0.039	0.560 ±0.016 ±0.035	0.533 ±0.015 ±0.032	0.506 ±0.015 ±0.032
0.50				0.389 ±0.042 ±0.062	0.424 ±0.039 ±0.058	0.398 ±0.033 ±0.053	0.338 ±0.027 ±0.048	0.342 ±0.024 ±0.042	0.335 ±0.018 ±0.035	0.304 ±0.012 ±0.030	0.289 ±0.011 ±0.025	0.279 ±0.010 ±0.022	0.270 ±0.011 ±0.022
0.60				0.305 ±0.035 ±0.063	0.207 ±0.025 ±0.059	0.238 ±0.024 ±0.053	0.201 ±0.019 ±0.046	0.170 ±0.015 ±0.039	0.161 ±0.013 ±0.031	0.142 ±0.008 ±0.025	0.125 ±0.007 ±0.019	0.136 ±0.007 ±0.016	0.096 ±0.006 ±0.015
0.70														

$d\sigma/E_\nu dxdy$ in bin 7; $\langle E_\nu \rangle$ = 111.0 GeV; neutrino beam

Table 3 (cont'd)

x = 0 \ y =	0.032	0.042	0.054	0.070	0.091	0.119	0.154	0.201	0.261	0.339	0.441	0.573	0.745	0.969
0.03			1.137 ±0.168 ±0.107	1.166 ±0.150 ±0.106	1.110 ±0.129 ±0.104	1.126 ±0.114 ±0.102	1.324 ±0.110 ±0.100	1.496 ±0.091 ±0.097	1.318 ±0.060 ±0.094	1.421 ±0.057 ±0.092	1.459 ±0.051 ±0.090	1.540 ±0.049 ±0.089	1.394 ±0.045 ±0.088
0.06			2.042 ±0.231 ±0.145	1.639 ±0.182 ±0.142	1.471 ±0.152 ±0.139	1.707 ±0.144 ±0.136	1.713 ±0.128 ±0.132	1.800 ±0.100 ±0.128	1.839 ±0.073 ±0.123	1.782 ±0.064 ±0.119	1.967 ±0.063 ±0.116	1.917 ±0.057 ±0.114	1.730 ±0.052 ±0.114
0.10			1.367 ±0.176 ±0.135	1.987 ±0.186 ±0.132	2.055 ±0.165 ±0.129	1.958 ±0.141 ±0.125	2.005 ±0.131 ±0.120	1.855 ±0.090 ±0.115	1.924 ±0.069 ±0.110	1.997 ±0.060 ±0.105	1.917 ±0.055 ±0.102	1.946 ±0.051 ±0.099	1.867 ±0.049 ±0.099
0.15			1.817 ±0.180 ±0.082	2.355 ±0.192 ±0.081	1.838 ±0.139 ±0.081	1.807 ±0.121 ±0.080	1.827 ±0.111 ±0.080	1.806 ±0.086 ±0.079	1.965 ±0.061 ±0.078	1.919 ±0.054 ±0.077	1.917 ±0.049 ±0.077	1.916 ±0.047 ±0.077	1.828 ±0.044 ±0.077
0.20			1.789 ±0.177 ±0.126	1.736 ±0.167 ±0.122	1.926 ±0.141 ±0.117	1.787 ±0.119 ±0.112	1.819 ±0.110 ±0.106	1.545 ±0.072 ±0.099	1.673 ±0.057 ±0.092	1.684 ±0.051 ±0.086	1.650 ±0.045 ±0.081	1.679 ±0.043 ±0.078	1.647 ±0.040 ±0.077
0.25			1.436 ±0.157 ±0.133	1.575 ±0.145 ±0.127	1.540 ±0.125 ±0.119	1.637 ±0.114 ±0.109	1.538 ±0.109 ±0.098	1.484 ±0.071 ±0.086	1.497 ±0.052 ±0.074	1.490 ±0.046 ±0.063	1.496 ±0.043 ±0.054	1.541 ±0.040 ±0.049	1.479 ±0.039 ±0.048
0.30			1.311 ±0.149 ±0.102	1.149 ±0.122 ±0.098	1.345 ±0.126 ±0.093	1.298 ±0.100 ±0.087	1.317 ±0.098 ±0.080	1.249 ±0.065 ±0.072	1.347 ±0.050 ±0.064	1.324 ±0.044 ±0.057	1.252 ±0.038 ±0.052	1.249 ±0.036 ±0.048	1.226 ±0.036 ±0.048
0.40			0.957 ±0.089 ±0.066	1.113 ±0.084 ±0.064	1.162 ±0.076 ±0.062	1.073 ±0.069 ±0.060	1.025 ±0.057 ±0.057	0.960 ±0.040 ±0.054	1.020 ±0.031 ±0.051	0.961 ±0.027 ±0.049	0.954 ±0.025 ±0.046	0.924 ±0.023 ±0.045	0.854 ±0.022 ±0.045
0.50			0.718 ±0.074 ±0.097	0.702 ±0.064 ±0.091	0.662 ±0.055 ±0.083	0.702 ±0.053 ±0.075	0.645 ±0.043 ±0.065	0.590 ±0.030 ±0.054	0.592 ±0.022 ±0.044	0.566 ±0.020 ±0.033	0.578 ±0.019 ±0.026	0.544 ±0.017 ±0.021	0.540 ±0.017 ±0.020
0.60			0.442 ±0.055 ±0.050	0.388 ±0.045 ±0.048	0.384 ±0.040 ±0.045	0.360 ±0.034 ±0.042	0.352 ±0.029 ±0.038	0.314 ±0.023 ±0.034	0.312 ±0.015 ±0.030	0.298 ±0.013 ±0.026	0.277 ±0.012 ±0.023	0.292 ±0.011 ±0.021	0.264 ±0.012 ±0.021
0.70			0.250 ±0.039 ±0.060	0.229 ±0.032 ±0.063	0.244 ±0.029 ±0.059	0.203 ±0.024 ±0.043	0.204 ±0.021 ±0.046	0.171 ±0.015 ±0.039	0.151 ±0.010 ±0.031	0.149 ±0.009 ±0.025	0.120 ±0.007 ±0.019	0.128 ±0.007 ±0.016	0.106 ±0.006 ±0.015

Table 3 (cont'd)

$d\sigma/E_\nu dxdy$ in bin 8; $\langle E_\nu \rangle$ = 144.3 GeV; neutrino beam

x = 0	y = 0.032	0.042	0.054	0.070	0.091	0.119	0.154	0.201	0.261	0.339	0.441	0.573	0.745	0.969
0.03		1.156 ±0.247 ±0.117	1.552 ±0.252 ±0.116	0.860 ±0.166 ±0.115	1.271 ±0.178 ±0.114	1.332 ±0.162 ±0.112	1.320 ±0.121 ±0.111	1.543 ±0.098 ±0.109	1.599 ±0.087 ±0.107	1.629 ±0.079 ±0.105	1.739 ±0.076 ±0.103	1.725 ±0.069 ±0.103	1.613 ±0.062 ±0.103
0.06		1.651 ±0.297 ±0.164	1.527 ±0.252 ±0.162	1.667 ±0.232 ±0.160	1.772 ±0.211 ±0.157	1.697 ±0.183 ±0.153	1.851 ±0.142 ±0.149	2.017 ±0.113 ±0.144	2.039 ±0.102 ±0.140	2.070 ±0.091 ±0.136	2.038 ±0.081 ±0.132	2.087 ±0.074 ±0.130	1.781 ±0.064 ±0.130
0.10		1.828 ±0.364 ±0.162	2.047 ±0.267 ±0.160	2.610 ±0.265 ±0.156	1.820 ±0.194 ±0.152	1.875 ±0.172 ±0.147	1.928 ±0.132 ±0.142	2.017 ±0.099 ±0.136	2.101 ±0.093 ±0.129	1.963 ±0.076 ±0.123	2.087 ±0.071 ±0.119	1.925 ±0.061 ±0.116	1.938 ±0.060 ±0.115
0.15		1.142 ±0.202 ±0.093	1.728 ±0.218 ±0.093	1.770 ±0.194 ±0.092	1.943 ±0.178 ±0.092	1.792 ±0.150 ±0.092	1.807 ±0.114 ±0.092	1.907 ±0.085 ±0.092	1.928 ±0.075 ±0.092	1.884 ±0.066 ±0.092	1.812 ±0.057 ±0.092	1.748 ±0.053 ±0.092	1.761 ±0.050 ±0.092
0.20		1.762 ±0.250 ±0.153	1.788 ±0.221 ±0.149	1.958 ±0.203 ±0.144	1.986 ±0.212 ±0.139	2.016 ±0.170 ±0.132	1.760 ±0.113 ±0.124	1.861 ±0.082 ±0.116	1.772 ±0.073 ±0.108	1.733 ±0.064 ±0.100	1.628 ±0.056 ±0.094	1.651 ±0.052 ±0.090	1.575 ±0.048 ±0.089
0.25		1.442 ±0.282 ±0.154	1.552 ±0.204 ±0.149	2.018 ±0.205 ±0.141	1.507 ±0.155 ±0.133	1.638 ±0.143 ±0.122	1.575 ±0.108 ±0.110	1.557 ±0.076 ±0.097	1.476 ±0.064 ±0.084	1.609 ±0.062 ±0.072	1.457 ±0.053 ±0.062	1.435 ±0.048 ±0.057	1.415 ±0.046 ±0.055
0.30		1.337 ±0.215 ±0.116	1.584 ±0.205 ±0.112	1.200 ±0.157 ±0.108	1.176 ±0.136 ±0.102	1.320 ±0.127 ±0.096	1.262 ±0.093 ±0.089	1.293 ±0.067 ±0.081	1.265 ±0.060 ±0.073	1.236 ±0.054 ±0.065	1.301 ±0.050 ±0.060	1.230 ±0.044 ±0.056	1.261 ±0.044 ±0.055
0.40		1.103 ±0.136 ±0.075	1.070 ±0.118 ±0.074	1.025 ±0.102 ±0.072	1.007 ±0.089 ±0.070	0.928 ±0.086 ±0.067	1.016 ±0.060 ±0.064	0.980 ±0.042 ±0.061	0.980 ±0.037 ±0.058	0.956 ±0.034 ±0.055	0.909 ±0.029 ±0.053	0.903 ±0.027 ±0.052	0.889 ±0.027 ±0.051
0.50		0.753 ±0.110 ±0.118	0.594 ±0.086 ±0.112	0.823 ±0.089 ±0.105	0.645 ±0.069 ±0.097	0.685 ±0.063 ±0.087	0.677 ±0.048 ±0.076	0.660 ±0.033 ±0.063	0.596 ±0.029 ±0.050	0.552 ±0.025 ±0.039	0.562 ±0.023 ±0.029	0.553 ±0.022 ±0.024	0.503 ±0.019 ±0.023
0.60		0.508 ±0.113 ±0.060	0.488 ±0.075 ±0.058	0.393 ±0.059 ±0.055	0.329 ±0.047 ±0.052	0.352 ±0.043 ±0.048	0.308 ±0.031 ±0.044	0.311 ±0.021 ±0.039	0.312 ±0.019 ±0.034	0.290 ±0.017 ±0.030	0.260 ±0.014 ±0.026	0.254 ±0.013 ±0.024	0.253 ±0.014 ±0.024
0.70		0.288 ±0.062 ±0.065	0.211 ±0.046 ±0.060	0.239 ±0.043 ±0.063	0.160 ±0.031 ±0.059	0.204 ±0.030 ±0.053	0.169 ±0.021 ±0.046	0.155 ±0.014 ±0.039	0.141 ±0.012 ±0.031	0.136 ±0.010 ±0.025	0.118 ±0.009 ±0.019	0.106 ±0.008 ±0.016	0.129 ±0.009 ±0.015

Table 3 (cont'd)

$d\sigma/E_\nu dxdy$ in bin 9; $\langle E_\nu \rangle$ = 187.6 GeV; neutrino beam

x = 0 \ y =	0.032	0.042	0.054	0.070	0.091	0.119	0.154	0.201	0.261	0.339	0.441	0.573	0.745	0.969
0.03	1.095 ±0.387 ±0.172	0.848 ±0.300 ±0.170	1.150 ±0.307 ±0.167	1.659 ±0.326 ±0.164	1.591 ±0.282 ±0.161	1.553 ±0.213 ±0.157	1.779 ±0.160 ±0.152	1.497 ±0.130 ±0.146	1.444 ±0.114 ±0.141	1.522 ±0.106 ±0.136	1.652 ±0.100 ±0.132	1.599 ±0.089 ±0.130	1.722 ±0.096 ±0.129
0.06	1.693 ±0.511 ±0.208	2.383 ±0.533 ±0.206	1.941 ±0.424 ±0.204	2.083 ±0.387 ±0.202	2.016 ±0.337 ±0.199	1.946 ±0.244 ±0.195	2.258 ±0.191 ±0.191	2.247 ±0.170 ±0.186	2.262 ±0.152 ±0.182	2.368 ±0.149 ±0.177	2.098 ±0.121 ±0.174	1.947 ±0.103 ±0.172	1.733 ±0.088 ±0.172
0.10	1.741 ±0.466 ±0.217	2.111 ±0.450 ±0.214	1.851 ±0.371 ±0.210	2.060 ±0.344 ±0.206	1.639 ±0.270 ±0.200	2.180 ±0.237 ±0.193	2.071 ±0.161 ±0.185	2.202 ±0.147 ±0.177	2.201 ±0.131 ±0.168	2.067 ±0.117 ±0.160	2.132 ±0.105 ±0.153	2.029 ±0.091 ±0.149	2.131 ±0.093 ±0.148
0.15	2.011 ±0.450 ±0.124	2.016 ±0.396 ±0.123	1.974 ±0.344 ±0.123	1.847 ±0.293 ±0.122	1.749 ±0.251 ±0.121	2.199 ±0.256 ±0.121	2.020 ±0.143 ±0.120	2.215 ±0.138 ±0.118	1.901 ±0.112 ±0.117	1.970 ±0.101 ±0.116	1.882 ±0.090 ±0.116	1.852 ±0.077 ±0.115	1.811 ±0.072 ±0.115
0.20	2.048 ±0.458 ±0.196	1.814 ±0.379 ±0.193	1.580 ±0.310 ±0.188	1.828 ±0.293 ±0.182	1.556 ±0.238 ±0.175	2.035 ±0.209 ±0.167	1.857 ±0.144 ±0.158	1.838 ±0.121 ±0.148	1.860 ±0.108 ±0.138	1.843 ±0.095 ±0.128	1.707 ±0.083 ±0.121	1.673 ±0.074 ±0.116	1.479 ±0.066 ±0.115
0.25	2.090 ±0.468 ±0.184	1.126 ±0.301 ±0.179	1.981 ±0.351 ±0.173	2.097 ±0.317 ±0.166	1.799 ±0.258 ±0.157	1.690 ±0.190 ±0.146	1.786 ±0.135 ±0.133	1.828 ±0.131 ±0.120	1.476 ±0.099 ±0.106	1.611 ±0.089 ±0.093	1.458 ±0.075 ±0.083	1.383 ±0.068 ±0.077	1.369 ±0.065 ±0.076
0.30	1.170 ±0.353 ±0.163	0.899 ±0.271 ±0.158	1.320 ±0.288 ±0.153	1.400 ±0.260 ±0.147	1.299 ±0.220 ±0.139	1.624 ±0.189 ±0.130	1.368 ±0.119 ±0.119	1.319 ±0.102 ±0.107	1.439 ±0.099 ±0.096	1.364 ±0.084 ±0.085	1.249 ±0.069 ±0.076	1.226 ±0.062 ±0.071	1.156 ±0.060 ±0.070
0.40	1.293 ±0.264 ±0.100	1.156 ±0.219 ±0.099	1.012 ±0.179 ±0.097	1.040 ±0.159 ±0.095	1.202 ±0.150 ±0.092	1.352 ±0.123 ±0.088	1.136 ±0.076 ±0.085	1.129 ±0.067 ±0.080	1.008 ±0.058 ±0.076	0.888 ±0.046 ±0.072	0.902 ±0.041 ±0.069	0.813 ±0.036 ±0.067	0.877 ±0.038 ±0.067
0.50	0.624 ±0.180 ±0.158	0.793 ±0.178 ±0.153	0.995 ±0.174 ±0.145	0.664 ±0.123 ±0.136	0.902 ±0.125 ±0.126	0.768 ±0.109 ±0.113	0.626 ±0.054 ±0.098	0.552 ±0.044 ±0.082	0.551 ±0.038 ±0.066	0.503 ±0.034 ±0.050	0.465 ±0.028 ±0.039	0.498 ±0.028 ±0.032	0.474 ±0.027 ±0.030
0.60	0.199 ±0.089 ±0.070	0.490 ±0.123 ±0.068	0.566 ±0.116 ±0.066	0.345 ±0.079 ±0.063	0.433 ±0.078 ±0.060	0.394 ±0.060 ±0.056	0.374 ±0.038 ±0.052	0.290 ±0.030 ±0.048	0.265 ±0.025 ±0.043	0.265 ±0.022 ±0.039	0.233 ±0.019 ±0.035	0.230 ±0.020 ±0.033	0.225 ±0.019 ±0.033
0.70						0.197 ±0.038 ±0.056	0.217 ±0.027 ±0.060	0.164 ±0.021 ±0.051	0.137 ±0.017 ±0.041	0.137 ±0.015 ±0.032	0.117 ±0.012 ±0.025	0.093 ±0.012 ±0.021	0.100 ±0.012 ±0.020

Table 3 (cont'd)

$d\sigma/E_\nu dxdy$ in bin 1; $\langle E_\nu \rangle$ = 23.0 GeV; antineutrino beam

x = 0 \ y =	0.032	0.042	0.054	0.070	0.091	0.119	0.154	0.201	0.261	0.339	0.441	0.573	0.745	0.969
0.03									0.702 ±0.030 ±0.081	0.711 ±0.026 ±0.069	0.636 ±0.021 ±0.060	0.505 ±0.016 ±0.054		
0.06									0.867 ±0.033 ±0.105	0.842 ±0.029 ±0.084	0.760 ±0.024 ±0.068	0.632 ±0.019 ±0.059		
0.10									1.040 ±0.033 ±0.127	0.978 ±0.028 ±0.098	0.804 ±0.023 ±0.076	0.629 ±0.017 ±0.063		
0.15									1.026 ±0.029 ±0.116	0.892 ±0.024 ±0.086	0.740 ±0.019 ±0.063	0.508 ±0.014 ±0.049		
0.20									0.900 ±0.028 ±0.087	0.826 ±0.024 ±0.061	0.630 ±0.018 ±0.040	0.412 ±0.012 ±0.028		
0.25									0.803 ±0.026 ±0.084	0.701 ±0.021 ±0.060	0.511 ±0.016 ±0.042	0.315 ±0.010 ±0.032		
0.30									0.753 ±0.026 ±0.055	0.606 ±0.020 ±0.040	0.393 ±0.014 ±0.028	0.235 ±0.009 ±0.021		
0.40									0.560 ±0.016 ±0.043	0.433 ±0.012 ±0.031	0.296 ±0.009 ±0.022	0.159 ±0.005 ±0.017		
0.50									0.388 ±0.013 ±0.028	0.265 ±0.009 ±0.020	0.192 ±0.007 ±0.013	0.094 ±0.004 ±0.009		
0.60									0.229 ±0.010 ±0.021	0.180 ±0.008 ±0.014	0.101 ±0.005 ±0.008	0.039 ±0.003 ±0.005		
0.70									0.131 ±0.007 ±0.014	0.080 ±0.005 ±0.009	0.043 ±0.003 ±0.005	0.014 ±0.001 ±0.003		

$d\sigma/E_\nu dxdy$ in bin 2; $\langle E_\nu \rangle$ = 29.9 GeV; antineutrino beam

Table 3 (cont'd)

x = 0 \ y =	0.032	0.042	0.054	0.070	0.091	0.119	0.154	0.201	0.261	0.339	0.441	0.573	0.745	0.969
0.03								0.686 ±0.032 ±0.092	0.704 ±0.028 ±0.079	0.675 ±0.026 ±0.068	0.684 ±0.024 ±0.059	0.670 ±0.022 ±0.053		
0.06								0.947 ±0.039 ±0.151	0.975 ±0.035 ±0.118	0.905 ±0.031 ±0.087	0.863 ±0.028 ±0.064	0.777 ±0.023 ±0.050		
0.10								1.097 ±0.039 ±0.158	1.151 ±0.036 ±0.127	0.974 ±0.030 ±0.099	0.838 ±0.024 ±0.077	0.649 ±0.018 ±0.064		
0.15								1.151 ±0.035 ±0.147	1.058 ±0.031 ±0.115	0.944 ±0.026 ±0.086	0.743 ±0.021 ±0.062	0.576 ±0.016 ±0.049		
0.20								1.009 ±0.033 ±0.117	0.974 ±0.030 ±0.088	0.783 ±0.024 ±0.061	0.625 ±0.019 ±0.040	0.429 ±0.014 ±0.028		
0.25								1.017 ±0.033 ±0.109	0.803 ±0.026 ±0.084	0.659 ±0.022 ±0.061	0.533 ±0.018 ±0.042	0.360 ±0.012 ±0.032		
0.30								0.860 ±0.031 ±0.074	0.741 ±0.026 ±0.056	0.559 ±0.020 ±0.040	0.429 ±0.015 ±0.028	0.259 ±0.010 ±0.021		
0.40								0.606 ±0.018 ±0.056	0.507 ±0.015 ±0.043	0.418 ±0.012 ±0.031	0.287 ±0.009 ±0.022	0.169 ±0.006 ±0.017		
0.50								0.420 ±0.015 ±0.035	0.332 ±0.012 ±0.027	0.245 ±0.009 ±0.019	0.179 ±0.007 ±0.013	0.080 ±0.004 ±0.009		
0.60								0.270 ±0.011 ±0.028	0.197 ±0.009 ±0.020	0.141 ±0.007 ±0.014	0.089 ±0.005 ±0.008	0.047 ±0.003 ±0.005		
0.70								0.137 ±0.008 ±0.020	0.112 ±0.006 ±0.014	0.068 ±0.004 ±0.009	0.042 ±0.003 ±0.005	0.023 ±0.002 ±0.003		

Table 3 (cont'd)

$d\sigma/E_\nu dxdy$ in bin 3; $\langle E_\nu \rangle$ = 38.9 GeV; antineutrino beam

x = 0	y = 0.032	0.042	0.054	0.070	0.091	0.119	0.154	0.201	0.261	0.339	0.441	0.573	0.745	0.969
0.03							0.717 ±0.040 ±0.107	0.785 ±0.038 ±0.094	0.856 ±0.035 ±0.081	0.800 ±0.032 ±0.068	0.818 ±0.031 ±0.058	0.777 ±0.026 ±0.053		
0.06							0.982 ±0.049 ±0.135	1.020 ±0.043 ±0.117	1.047 ±0.041 ±0.099	1.020 ±0.038 ±0.082	0.970 ±0.034 ±0.069	0.882 ±0.029 ±0.061		
0.10							1.214 ±0.049 ±0.146	1.220 ±0.045 ±0.123	1.150 ±0.038 ±0.100	1.024 ±0.033 ±0.079	0.915 ±0.028 ±0.062	0.743 ±0.022 ±0.052		
0.15							1.207 ±0.045 ±0.148	1.191 ±0.039 ±0.121	1.134 ±0.034 ±0.094	0.969 ±0.029 ±0.068	0.730 ±0.023 ±0.049	0.630 ±0.019 ±0.037		
0.20							1.176 ±0.045 ±0.108	1.087 ±0.038 ±0.088	1.010 ±0.032 ±0.068	0.843 ±0.027 ±0.048	0.636 ±0.021 ±0.034	0.475 ±0.016 ±0.025		
0.25							1.109 ±0.044 ±0.095	0.970 ±0.036 ±0.079	0.845 ±0.030 ±0.062	0.694 ±0.024 ±0.046	0.535 ±0.020 ±0.034	0.371 ±0.014 ±0.027		
0.30							0.998 ±0.041 ±0.062	0.863 ±0.034 ±0.051	0.750 ±0.028 ±0.039	0.585 ±0.022 ±0.029	0.392 ±0.017 ±0.021	0.259 ±0.012 ±0.016		
0.40							0.730 ±0.025 ±0.052	0.660 ±0.022 ±0.041	0.562 ±0.018 ±0.032	0.436 ±0.014 ±0.021	0.296 ±0.010 ±0.013	0.183 ±0.007 ±0.009		
0.50							0.471 ±0.020 ±0.035	0.429 ±0.017 ±0.028	0.325 ±0.013 ±0.020	0.249 ±0.010 ±0.014	0.154 ±0.007 ±0.009	0.096 ±0.005 ±0.006		
0.60							0.342 ±0.017 ±0.038	0.248 ±0.013 ±0.030	0.200 ±0.010 ±0.021	0.129 ±0.007 ±0.014	0.088 ±0.005 ±0.007	0.049 ±0.004 ±0.004		
0.70							0.192 ±0.013 ±0.022	0.147 ±0.009 ±0.017	0.103 ±0.007 ±0.012	0.065 ±0.005 ±0.007	0.044 ±0.004 ±0.004	0.022 ±0.002 ±0.002		

Table 3 (cont'd)

$d\sigma/E_\nu dxdy$ in bin 4; $\langle E_\nu \rangle$ = 50.5 GeV; antineutrino beam

x \ y	0.032	0.042	0.054	0.070	0.091	0.119	0.154	0.201	0.261	0.339	0.441	0.573	0.745	0.969
0														
0.03						0.815 ±0.059 ±0.114	0.929 ±0.055 ±0.103	0.906 ±0.048 ±0.092	0.924 ±0.043 ±0.080	0.871 ±0.037 ±0.069	0.823 ±0.032 ±0.061	0.733 ±0.028 ±0.056		
0.06						1.161 ±0.072 ±0.147	1.166 ±0.063 ±0.133	1.169 ±0.054 ±0.116	1.080 ±0.047 ±0.099	1.123 ±0.044 ±0.084	1.059 ±0.037 ±0.072	0.869 ±0.031 ±0.065		
0.10						1.306 ±0.066 ±0.163	1.321 ±0.059 ±0.143	1.338 ±0.053 ±0.121	1.191 ±0.045 ±0.099	1.140 ±0.039 ±0.078	0.919 ±0.031 ±0.062	0.820 ±0.027 ±0.053		
0.15						1.280 ±0.059 ±0.168	1.321 ±0.054 ±0.145	1.159 ±0.044 ±0.119	1.092 ±0.038 ±0.092	1.045 ±0.034 ±0.068	0.822 ±0.026 ±0.049	0.607 ±0.020 ±0.038		
0.20						1.275 ±0.060 ±0.124	1.270 ±0.052 ±0.106	1.063 ±0.042 ±0.087	0.980 ±0.036 ±0.067	0.828 ±0.029 ±0.048	0.681 ±0.024 ±0.034	0.486 ±0.018 ±0.025		
0.25						1.218 ±0.060 ±0.109	1.056 ±0.047 ±0.095	0.968 ±0.040 ±0.078	0.775 ±0.033 ±0.062	0.679 ±0.027 ±0.047	0.531 ±0.021 ±0.035	0.332 ±0.015 ±0.028		
0.30						0.990 ±0.054 ±0.071	0.945 ±0.045 ±0.061	0.849 ±0.039 ±0.050	0.650 ±0.029 ±0.039	0.567 ±0.025 ±0.029	0.422 ±0.018 ±0.021	0.252 ±0.013 ±0.016		
0.40						0.880 ±0.037 ±0.061	0.686 ±0.029 ±0.052	0.624 ±0.024 ±0.041	0.538 ±0.019 ±0.031	0.393 ±0.015 ±0.021	0.269 ±0.011 ±0.013	0.155 ±0.007 ±0.009		
0.50						0.543 ±0.029 ±0.040	0.483 ±0.025 ±0.034	0.421 ±0.019 ±0.027	0.314 ±0.014 ±0.020	0.231 ±0.011 ±0.014	0.150 ±0.008 ±0.009	0.079 ±0.005 ±0.006		
0.60						0.357 ±0.023 ±0.046	0.286 ±0.017 ±0.039	0.237 ±0.014 ±0.030	0.163 ±0.010 ±0.022	0.114 ±0.007 ±0.014	0.083 ±0.006 ±0.007	0.042 ±0.003 ±0.004		
0.70						0.170 ±0.014 ±0.026	0.141 ±0.011 ±0.022	0.092 ±0.008 ±0.017	0.067 ±0.006 ±0.012	0.048 ±0.004 ±0.007	0.035 ±0.003 ±0.004	0.018 ±0.002 ±0.002		

Table 3 (cont'd)

$d\sigma/E_\nu dxdy$ in bin 5; $\langle E_\nu \rangle$ = 65.7 GeV; antineutrino beam

x = 0 \ y =	0.032	0.042	0.054	0.070	0.091	0.119	0.154	0.201	0.261	0.339	0.441	0.573	0.745	0.969
0.03					0.801 ±0.067 ±0.130	0.833 ±0.062 ±0.121	0.979 ±0.060 ±0.112	1.019 ±0.054 ±0.101	0.981 ±0.048 ±0.090	0.945 ±0.041 ±0.080	0.919 ±0.036 ±0.072	0.876 ±0.031 ±0.068	0.728 ±0.029 ±0.066
0.06					1.098 ±0.082 ±0.124	1.243 ±0.077 ±0.114	1.246 ±0.069 ±0.103	1.391 ±0.067 ±0.091	1.349 ±0.059 ±0.079	1.251 ±0.049 ±0.068	1.144 ±0.040 ±0.059	0.901 ±0.032 ±0.054	0.770 ±0.031 ±0.052
0.10					1.459 ±0.086 ±0.152	1.456 ±0.077 ±0.138	1.444 ±0.066 ±0.123	1.442 ±0.060 ±0.107	1.283 ±0.050 ±0.090	1.205 ±0.041 ±0.075	1.052 ±0.034 ±0.063	0.794 ±0.027 ±0.056	0.596 ±0.024 ±0.054
0.15					1.458 ±0.080 ±0.126	1.362 ±0.066 ±0.112	1.339 ±0.059 ±0.097	1.295 ±0.051 ±0.080	1.220 ±0.044 ±0.062	1.041 ±0.035 ±0.046	0.828 ±0.027 ±0.034	0.626 ±0.021 ±0.027	0.467 ±0.019 ±0.024
0.20					1.435 ±0.079 ±0.094	1.331 ±0.067 ±0.085	1.243 ±0.056 ±0.074	1.144 ±0.048 ±0.061	1.001 ±0.039 ±0.049	0.828 ±0.030 ±0.037	0.648 ±0.024 ±0.029	0.472 ±0.019 ±0.023	0.302 ±0.014 ±0.022
0.25					1.145 ±0.069 ±0.083	1.092 ±0.060 ±0.074	1.089 ±0.052 ±0.063	0.976 ±0.044 ±0.051	0.795 ±0.036 ±0.039	0.673 ±0.027 ±0.028	0.502 ±0.021 ±0.019	0.358 ±0.016 ±0.015	0.224 ±0.013 ±0.013
0.30					1.092 ±0.069 ±0.079	0.929 ±0.055 ±0.070	0.922 ±0.049 ±0.059	0.877 ±0.042 ±0.048	0.728 ±0.034 ±0.036	0.531 ±0.024 ±0.025	0.351 ±0.017 ±0.016	0.259 ±0.013 ±0.011	0.133 ±0.010 ±0.010
0.40					0.869 ±0.044 ±0.066	0.825 ±0.038 ±0.058	0.719 ±0.031 ±0.048	0.632 ±0.025 ±0.038	0.512 ±0.020 ±0.028	0.409 ±0.016 ±0.019	0.265 ±0.011 ±0.011	0.149 ±0.007 ±0.007	0.072 ±0.005 ±0.006
0.50					0.554 ±0.035 ±0.040	0.497 ±0.028 ±0.035	0.445 ±0.023 ±0.030	0.358 ±0.018 ±0.024	0.308 ±0.015 ±0.018	0.233 ±0.012 ±0.012	0.150 ±0.008 ±0.008	0.078 ±0.005 ±0.005	0.027 ±0.003 ±0.004
0.60					0.293 ±0.023 ±0.048	0.318 ±0.022 ±0.042	0.237 ±0.016 ±0.035	0.195 ±0.013 ±0.028	0.163 ±0.011 ±0.020	0.111 ±0.008 ±0.012	0.074 ±0.006 ±0.007	0.040 ±0.003 ±0.003	0.016 ±0.002 ±0.002
0.70					0.165 ±0.016 ±0.021	0.153 ±0.014 ±0.019	0.117 ±0.011 ±0.016	0.100 ±0.009 ±0.013	0.065 ±0.006 ±0.009	0.051 ±0.005 ±0.006	0.039 ±0.004 ±0.004	0.014 ±0.002 ±0.003	0.006 ±0.001 ±0.002

$d\sigma/E_\nu dxdy$ in bin 6; $\langle E_\nu \rangle$ = 85.4 GeV; antineutrino beam

Table 3 (cont'd)

x = 0 \ y =	0.032	0.042	0.054	0.070	0.091	0.119	0.154	0.201	0.261	0.339	0.441	0.573	0.745	0.969
0.03				0.976 ±0.099 ±0.141	0.931 ±0.089 ±0.133	1.041 ±0.078 ±0.124	0.949 ±0.068 ±0.114	1.130 ±0.064 ±0.103	1.033 ±0.051 ±0.091	0.976 ±0.043 ±0.080	0.936 ±0.039 ±0.072	0.922 ±0.036 ±0.067	0.889 ±0.035 ±0.066
0.06				1.249 ±0.117 ±0.131	1.449 ±0.110 ±0.123	1.403 ±0.095 ±0.114	1.526 ±0.087 ±0.103	1.347 ±0.072 ±0.091	1.302 ±0.060 ±0.079	1.231 ±0.051 ±0.067	1.092 ±0.043 ±0.058	1.026 ±0.040 ±0.053	0.790 ±0.034 ±0.052
0.10				1.506 ±0.111 ±0.165	1.461 ±0.099 ±0.154	1.575 ±0.091 ±0.141	1.546 ±0.078 ±0.125	1.483 ±0.067 ±0.108	1.440 ±0.056 ±0.091	1.202 ±0.045 ±0.075	1.095 ±0.038 ±0.063	0.867 ±0.030 ±0.055	0.652 ±0.026 ±0.053
0.15				1.383 ±0.096 ±0.135	1.529 ±0.088 ±0.124	1.486 ±0.078 ±0.111	1.456 ±0.068 ±0.095	1.368 ±0.059 ±0.079	1.277 ±0.049 ±0.062	1.053 ±0.038 ±0.046	0.823 ±0.029 ±0.034	0.653 ±0.023 ±0.027	0.432 ±0.019 ±0.025
0.20				1.347 ±0.097 ±0.106	1.455 ±0.089 ±0.097	1.339 ±0.074 ±0.087	1.220 ±0.061 ±0.076	1.151 ±0.053 ±0.063	1.076 ±0.044 ±0.050	0.800 ±0.032 ±0.038	0.665 ±0.027 ±0.029	0.483 ±0.020 ±0.023	0.319 ±0.016 ±0.022
0.25				1.205 ±0.088 ±0.093	1.194 ±0.078 ±0.085	1.039 ±0.064 ±0.075	1.090 ±0.057 ±0.064	0.949 ±0.047 ±0.052	0.854 ±0.039 ±0.040	0.690 ±0.030 ±0.029	0.510 ±0.023 ±0.020	0.322 ±0.016 ±0.015	0.223 ±0.014 ±0.013
0.30				1.038 ±0.084 ±0.087	0.977 ±0.071 ±0.079	0.936 ±0.062 ±0.070	0.925 ±0.054 ±0.059	0.862 ±0.045 ±0.048	0.641 ±0.034 ±0.036	0.501 ±0.025 ±0.025	0.400 ±0.020 ±0.016	0.273 ±0.015 ±0.011	0.117 ±0.009 ±0.010
0.40				0.860 ±0.054 ±0.072	0.807 ±0.046 ±0.066	0.744 ±0.039 ±0.058	0.753 ±0.035 ±0.049	0.584 ±0.027 ±0.039	0.531 ±0.022 ±0.028	0.389 ±0.016 ±0.019	0.274 ±0.012 ±0.011	0.155 ±0.008 ±0.007	0.064 ±0.005 ±0.006
0.50				0.661 ±0.048 ±0.045	0.554 ±0.038 ±0.040	0.428 ±0.030 ±0.036	0.387 ±0.025 ±0.030	0.385 ±0.021 ±0.024	0.274 ±0.015 ±0.018	0.213 ±0.012 ±0.012	0.152 ±0.009 ±0.008	0.070 ±0.006 ±0.005	0.024 ±0.003 ±0.004
0.60				0.399 ±0.035 ±0.053	0.324 ±0.028 ±0.048	0.251 ±0.021 ±0.042	0.230 ±0.018 ±0.035	0.176 ±0.014 ±0.027	0.153 ±0.011 ±0.019	0.107 ±0.008 ±0.012	0.070 ±0.006 ±0.007	0.031 ±0.004 ±0.003	0.015 ±0.002 ±0.002
0.70				0.204 ±0.023 ±0.023	0.168 ±0.018 ±0.021	0.145 ±0.015 ±0.018	0.118 ±0.012 ±0.015	0.088 ±0.009 ±0.012	0.072 ±0.008 ±0.009	0.058 ±0.006 ±0.006	0.028 ±0.003 ±0.004	0.012 ±0.002 ±0.003	0.005 ±0.001 ±0.002

Table 3 (cont'd)

$d\sigma/E_\nu dxdy$ in bin 7; $\langle E_\nu \rangle$ = 111.0 GeV; antineutrino beam

x = 0 \ y =	0.032	0.042	0.054	0.070	0.091	0.119	0.154	0.201	0.261	0.339	0.441	0.573	0.745	0.969
0.03			0.962 ±0.144 ±0.106	1.038 ±0.131 ±0.105	0.941 ±0.110 ±0.105	1.101 ±0.110 ±0.105	1.240 ±0.102 ±0.105	1.156 ±0.081 ±0.105	1.107 ±0.067 ±0.105	1.085 ±0.060 ±0.105	1.150 ±0.055 ±0.105	1.090 ±0.051 ±0.105	0.916 ±0.046 ±0.105
0.06			1.441 ±0.177 ±0.136	1.195 ±0.147 ±0.133	1.537 ±0.145 ±0.130	1.296 ±0.114 ±0.126	1.663 ±0.114 ±0.122	1.457 ±0.094 ±0.118	1.470 ±0.078 ±0.113	1.331 ±0.066 ±0.109	1.222 ±0.057 ±0.105	0.954 ±0.046 ±0.103	0.833 ±0.042 ±0.103
0.10			1.592 ±0.170 ±0.199	1.621 ±0.158 ±0.189	1.559 ±0.129 ±0.177	1.552 ±0.113 ±0.162	1.557 ±0.100 ±0.145	1.431 ±0.081 ±0.127	1.189 ±0.063 ±0.108	1.127 ±0.054 ±0.091	1.127 ±0.050 ±0.078	0.830 ±0.038 ±0.070	0.699 ±0.034 ±0.068
0.15			1.362 ±0.139 ±0.131	1.423 ±0.125 ±0.124	1.540 ±0.114 ±0.117	1.552 ±0.100 ±0.107	1.403 ±0.086 ±0.097	1.450 ±0.075 ±0.085	1.321 ±0.060 ±0.073	0.953 ±0.045 ±0.062	0.872 ±0.038 ±0.054	0.643 ±0.030 ±0.049	0.446 ±0.025 ±0.048
0.20			1.528 ±0.146 ±0.138	1.270 ±0.117 ±0.129	1.428 ±0.109 ±0.119	1.325 ±0.092 ±0.107	1.224 ±0.078 ±0.093	1.129 ±0.065 ±0.078	1.045 ±0.052 ±0.063	0.831 ±0.041 ±0.048	0.643 ±0.033 ±0.037	0.444 ±0.025 ±0.031	0.275 ±0.018 ±0.029
0.25			1.426 ±0.149 ±0.135	1.448 ±0.130 ±0.127	1.499 ±0.125 ±0.117	1.160 ±0.086 ±0.105	1.040 ±0.072 ±0.092	0.889 ±0.058 ±0.077	0.841 ±0.047 ±0.062	0.674 ±0.038 ±0.049	0.530 ±0.030 ±0.038	0.328 ±0.021 ±0.032	0.183 ±0.015 ±0.030
0.30			0.941 ±0.115 ±0.108	1.150 ±0.111 ±0.101	1.026 ±0.092 ±0.092	1.094 ±0.084 ±0.082	0.869 ±0.066 ±0.070	0.796 ±0.054 ±0.057	0.665 ±0.042 ±0.043	0.540 ±0.034 ±0.031	0.382 ±0.025 ±0.021	0.235 ±0.018 ±0.016	0.128 ±0.013 ±0.014
0.40			0.912 ±0.083 ±0.087	0.836 ±0.069 ±0.081	0.773 ±0.057 ±0.074	0.686 ±0.047 ±0.065	0.676 ±0.042 ±0.055	0.622 ±0.034 ±0.044	0.492 ±0.026 ±0.033	0.373 ±0.020 ±0.023	0.258 ±0.015 ±0.015	0.144 ±0.010 ±0.010	0.058 ±0.006 ±0.009
0.50			0.573 ±0.062 ±0.080	0.568 ±0.055 ±0.074	0.516 ±0.046 ±0.067	0.538 ±0.041 ±0.058	0.406 ±0.032 ±0.048	0.305 ±0.023 ±0.037	0.318 ±0.021 ±0.026	0.229 ±0.016 ±0.016	0.143 ±0.011 ±0.008	0.085 ±0.007 ±0.003	0.028 ±0.004 ±0.002
0.60			0.424 ±0.050 ±0.053	0.352 ±0.040 ±0.049	0.309 ±0.033 ±0.044	0.228 ±0.025 ±0.038	0.237 ±0.023 ±0.032	0.196 ±0.018 ±0.025	0.151 ±0.014 ±0.018	0.102 ±0.010 ±0.011	0.065 ±0.007 ±0.006	0.044 ±0.006 ±0.003	0.013 ±0.003 ±0.002
0.70			0.203 ±0.032 ±0.034	0.147 ±0.024 ±0.032	0.109 ±0.018 ±0.029	0.090 ±0.015 ±0.025	0.101 ±0.014 ±0.021	0.082 ±0.011 ±0.017	0.068 ±0.008 ±0.012	0.052 ±0.007 ±0.008	0.026 ±0.005 ±0.004	0.012 ±0.003 ±0.003	0.003 ±0.001 ±0.002

Table 3 (cont'd)

$d\sigma/E_\nu dxdy$ in bin 8; $\langle E_\nu \rangle$ = 144.3 GeV; antineutrino beam

x = 0 \ y =	0.032	0.042	0.054	0.070	0.091	0.119	0.154	0.201	0.261	0.339	0.441	0.573	0.745	0.969
0.03		0.954 ±0.255 ±0.120	0.897 ±0.218 ±0.120	1.187 ±0.221 ±0.120	1.082 ±0.186 ±0.120	0.869 ±0.147 ±0.120	1.067 ±0.138 ±0.120	1.499 ±0.149 ±0.120	1.306 ±0.118 ±0.120	1.277 ±0.105 ±0.120	1.138 ±0.091 ±0.120	1.165 ±0.086 ±0.120	1.038 ±0.077 ±0.120
0.06		0.994 ±0.266 ±0.162	1.428 ±0.280 ±0.159	1.362 ±0.241 ±0.156	1.586 ±0.229 ±0.152	1.262 ±0.181 ±0.147	1.118 ±0.145 ±0.142	1.587 ±0.148 ±0.136	1.246 ±0.117 ±0.130	1.540 ±0.116 ±0.125	1.226 ±0.100 ±0.121	1.089 ±0.080 ±0.118	0.922 ±0.074 ±0.118
0.10		2.169 ±0.362 ±0.237	1.620 ±0.274 ±0.228	1.920 ±0.262 ±0.216	1.858 ±0.226 ±0.202	1.511 ±0.179 ±0.185	1.693 ±0.161 ±0.166	1.366 ±0.122 ±0.146	1.324 ±0.106 ±0.124	1.318 ±0.093 ±0.105	1.043 ±0.076 ±0.089	0.786 ±0.059 ±0.081	0.711 ±0.052 ±0.078
0.15		1.527 ±0.270 ±0.153	1.578 ±0.241 ±0.148	1.524 ±0.208 ±0.141	1.846 ±0.201 ±0.132	1.655 ±0.167 ±0.122	1.278 ±0.124 ±0.110	1.351 ±0.109 ±0.097	1.121 ±0.089 ±0.084	1.040 ±0.075 ±0.072	0.809 ±0.059 ±0.062	0.612 ±0.046 ±0.057	0.430 ±0.037 ±0.056
0.20		1.179 ±0.236 ±0.169	1.599 ±0.242 ±0.161	1.428 ±0.200 ±0.151	1.080 ±0.153 ±0.139	1.301 ±0.148 ±0.125	1.317 ±0.127 ±0.109	1.054 ±0.096 ±0.091	0.988 ±0.082 ±0.073	0.820 ±0.067 ±0.056	0.726 ±0.057 ±0.043	0.415 ±0.037 ±0.036	0.312 ±0.030 ±0.034
0.25		1.209 ±0.237 ±0.157	1.256 ±0.213 ±0.150	1.358 ±0.194 ±0.141	1.374 ±0.181 ±0.130	1.313 ±0.148 ±0.118	1.188 ±0.120 ±0.103	0.930 ±0.090 ±0.087	0.754 ±0.072 ±0.070	0.704 ±0.062 ±0.055	0.494 ±0.047 ±0.043	0.290 ±0.031 ±0.037	0.189 ±0.023 ±0.035
0.30		1.094 ±0.224 ±0.134	1.093 ±0.197 ±0.127	1.147 ±0.177 ±0.118	0.996 ±0.146 ±0.108	1.071 ±0.133 ±0.096	0.957 ±0.108 ±0.082	0.793 ±0.083 ±0.066	0.767 ±0.073 ±0.051	0.547 ±0.055 ±0.036	0.477 ±0.048 ±0.025	0.243 ±0.029 ±0.018	0.123 ±0.019 ±0.016
0.40		1.067 ±0.153 ±0.104	0.963 ±0.128 ±0.099	0.775 ±0.101 ±0.092	0.676 ±0.083 ±0.084	0.705 ±0.075 ±0.074	0.644 ±0.064 ±0.063	0.509 ±0.048 ±0.050	0.496 ±0.042 ±0.038	0.399 ±0.033 ±0.026	0.231 ±0.024 ±0.017	0.166 ±0.017 ±0.012	0.065 ±0.010 ±0.010
0.50		0.533 ±0.103 ±0.091	0.738 ±0.107 ±0.086	0.612 ±0.086 ±0.080	0.386 ±0.060 ±0.072	0.400 ±0.055 ±0.063	0.368 ±0.045 ±0.052	0.321 ±0.038 ±0.041	0.257 ±0.031 ±0.029	0.249 ±0.026 ±0.018	0.130 ±0.017 ±0.009	0.049 ±0.009 ±0.004	0.019 ±0.005 ±0.003
0.60		0.400 ±0.085 ±0.063	0.353 ±0.071 ±0.059	0.275 ±0.055 ±0.055	0.309 ±0.052 ±0.050	0.283 ±0.044 ±0.043	0.177 ±0.030 ±0.036	0.182 ±0.026 ±0.028	0.143 ±0.020 ±0.020	0.106 ±0.016 ±0.013	0.050 ±0.010 ±0.007	0.034 ±0.007 ±0.003	0.010 ±0.004 ±0.002
0.70							0.115 ±0.022 ±0.019	0.056 ±0.013 ±0.015	0.043 ±0.010 ±0.011	0.051 ±0.010 ±0.008	0.024 ±0.006 ±0.005	0.007 ±0.003 ±0.003	0.006 ±0.003 ±0.003

Table 3 (cont'd)

$d\sigma/E_\nu dxdy$ in bin 9; $\langle E_\nu \rangle$ = 187.6 GeV; antineutrino beam

x = 0	y = 0.032	0.042	0.054	0.070	0.091	0.119	0.154	0.201	0.261	0.339	0.441	0.573	0.745	0.969
0.03	1.726 ±0.772 ±0.162	1.331 ±0.595 ±0.161	1.233 ±0.503 ±0.161	1.429 ±0.477 ±0.160	0.861 ±0.325 ±0.159	1.219 ±0.327 ±0.158	1.285 ±0.288 ±0.157	1.511 ±0.276 ±0.155	1.074 ±0.207 ±0.154	0.989 ±0.178 ±0.152	1.126 ±0.172 ±0.151	1.346 ±0.191 ±0.151	1.434 ±0.197 ±0.151
0.06	0.782 ±0.553 ±0.179	0.904 ±0.522 ±0.178	2.091 ±0.697 ±0.177	1.614 ±0.538 ±0.175	1.247 ±0.416 ±0.173	0.971 ±0.308 ±0.171	0.935 ±0.260 ±0.169	1.792 ±0.317 ±0.166	1.313 ±0.240 ±0.163	1.206 ±0.204 ±0.160	1.233 ±0.184 ±0.158	1.042 ±0.152 ±0.157	0.793 ±0.133 ±0.157
0.10	1.425 ±0.638 ±0.306	1.985 ±0.662 ±0.297	2.051 ±0.592 ±0.285	1.593 ±0.460 ±0.271	1.860 ±0.439 ±0.254	2.523 ±0.441 ±0.234	1.644 ±0.301 ±0.211	1.557 ±0.260 ±0.186	1.201 ±0.203 ±0.160	1.371 ±0.194 ±0.136	1.280 ±0.168 ±0.117	0.801 ±0.120 ±0.107	0.476 ±0.083 ±0.104
0.15	2.038 ±0.680 ±0.210	2.101 ±0.607 ±0.203	0.814 ±0.332 ±0.196	1.684 ±0.421 ±0.186	1.311 ±0.328 ±0.174	1.282 ±0.281 ±0.160	1.257 ±0.234 ±0.144	1.536 ±0.229 ±0.127	1.380 ±0.216 ±0.109	1.013 ±0.148 ±0.092	0.916 ±0.126 ±0.080	0.500 ±0.083 ±0.072	0.472 ±0.083 ±0.070
0.20	1.357 ±0.554 ±0.208	1.573 ±0.525 0.200	1.895 ±0.507 ±0.191	1.259 ±0.364 ±0.180	1.224 ±0.316 ±0.166	1.458 ±0.299 ±0.149	1.334 ±0.240 ±0.130	1.116 ±0.195 ±0.110	0.856 ±0.152 ±0.089	1.106 ±0.154 ±0.069	0.613 ±0.102 ±0.054	0.396 ±0.074 ±0.045	0.263 ±0.054 ±0.043
0.25	0.910 ±0.455 ±0.218	1.405 ±0.497 ±0.210	0.815 ±0.333 ±0.200	0.842 ±0.298 ±0.188	1.144 ±0.306 ±0.174	1.084 ±0.256 ±0.156	0.858 ±0.192 ±0.137	0.909 ±0.175 ±0.115	0.743 ±0.141 ±0.093	0.739 ±0.136 ±0.072	0.303 ±0.071 ±0.057	0.312 ±0.065 ±0.047	0.216 ±0.058 ±0.045
0.30	0.460 ±0.325 ±0.160	0.888 ±0.397 ±0.154	1.097 ±0.388 ±0.146	1.484 ±0.397 ±0.137	1.068 ±0.296 ±0.125	1.096 ±0.259 ±0.111	0.644 ±0.166 ±0.096	0.805 ±0.165 ±0.079	0.711 ±0.137 ±0.061	0.438 ±0.096 ±0.045	0.333 ±0.075 ±0.032	0.122 ±0.041 ±0.025	0.231 ±0.065 ±0.023
0.40	0.355 ±0.205 ±0.143	1.274 ±0.341 ±0.137	1.121 ±0.281 ±0.130	0.756 ±0.202 ±0.121	0.957 ±0.200 ±0.110	0.659 ±0.141 ±0.097	0.687 ±0.122 ±0.082	0.682 ±0.107 ±0.066	0.493 ±0.080 ±0.049	0.357 ±0.060 ±0.034	0.268 ±0.047 ±0.022	0.133 ±0.030 ±0.015	0.070 ±0.020 ±0.013
0.50	1.124 ±0.375 ±0.142	0.478 ±0.214 ±0.136	0.511 ±0.193 ±0.128	0.836 ±0.216 ±0.118	0.595 ±0.159 ±0.106	0.760 ±0.153 ±0.093	0.447 ±0.098 ±0.077	0.259 ±0.065 ±0.059	0.323 ±0.063 ±0.041	0.163 ±0.040 ±0.025	0.068 ±0.023 ±0.012	0.094 ±0.024 ±0.005	0.029 ±0.013 ±0.003
0.60	0.547 ±0.223 ±0.063	0.423 ±0.173 ±0.061	0.273 ±0.122 ±0.057	0.296 ±0.112 ±0.053	0.197 ±0.081 ±0.048	0.173 ±0.066 ±0.042	0.192 ±0.058 ±0.036	0.110 ±0.039 ±0.028	0.165 ±0.043 ±0.021	0.071 ±0.025 ±0.014	0.044 ±0.018 ±0.008	0.019 ±0.011 ±0.005	0.035 ±0.014 ±0.004
0.70									0.046 ±0.021 ±0.014	0.015 ±0.011 ±0.010	0.020 ±0.011 ±0.006	0.018 ±0.010 ±0.004	0.012 ±0.008 ±0.004

Table 4

Values of the auxiliary functions
F_w, a, $\bar{q}_w$, b, and the structure functions xF_3 and F_2 as a function of x and Q^2.
The structure function $F_2(x,Q^2)$ is evaluated using only the small-y region to minimize the uncertainty due to R. The first error is statistical, the second is systematic, and the third gives the uncertainty associated with errors in the total cross-section.
The systematic uncertainties on F_2 are equivalent to those listed for F_w.

x = 0.015

Q^2	a	F_w	F_2	xF_3	$\bar{q}_w$	b
0.19	0.051	0.559 ±0.013 ±0.053 ±0.006	0.559 ±0.013	0.106 ±0.048 ±0.030 ±0.020		
0.25	0.082	0.633 ±0.013 ±0.049 ±0.005	0.633 ±0.013	0.123 ±0.036 ±0.026 ±0.015		
0.33	0.127	0.690 ±0.012 ±0.048 ±0.004	0.690 ±0.014	0.181 ±0.027 ±0.023 ±0.012	0.197 ±0.011 ±0.029 ±0.012	0.709
0.43	0.212	0.740 ±0.012 ±0.048 ±0.005	0.758 ±0.016	0.222 ±0.021 ±0.020 ±0.011	0.196 ±0.007 ±0.024 ±0.011	0.747
0.56	0.211	0.868 ±0.014 ±0.049 ±0.006	0.857 ±0.019	0.252 ±0.025 ±0.019 ±0.010	0.257 ±0.009 ±0.021 ±0.011	0.746
0.72	0.208	0.926 ±0.014 ±0.052 ±0.008	0.922 ±0.019	0.258 ±0.026 ±0.019 ±0.012	0.288 ±0.010 ±0.021 ±0.011	0.742
0.94	0.236	0.985 ±0.014 ±0.057 ±0.012	0.971 ±0.020	0.290 ±0.024 ±0.019 ±0.014	0.284 ±0.011 ±0.023 ±0.011	0.743
1.22	0.281	1.057 ±0.016 ±0.064 ±0.016	1.086 ±0.028	0.251 ±0.025 ±0.021 ±0.018	0.328 ±0.012 ±0.027 ±0.013	0.742
1.59	0.467	1.159 ±0.016 ±0.072 ±0.021	1.167 ±0.046	0.312 ±0.022 ±0.024 ±0.023	0.370 ±0.011 ±0.034 ±0.014	0.807
2.06	0.533	1.260 ±0.020 ±0.081 ±0.026	1.067 ±0.084	0.285 ±0.026 ±0.027 ±0.030	0.441 ±0.014 ±0.044 ±0.017	0.820
2.68	0.617	1.314 ±0.028 ±0.093 ±0.033		0.288 ±0.033 ±0.032 ±0.038	0.467 ±0.020 ±0.056 ±0.019	0.838
3.48	0.680	1.455 ±0.047 ±0.106 ±0.040		0.294 ±0.055 ±0.038 ±0.048	0.546 ±0.038 ±0.070 ±0.023	0.858
4.53	0.745	1.711 ±0.114 ±0.120 ±0.049		0.144 ±0.133 ±0.044 ±0.059	0.756 ±0.106 ±0.087 ±0.027	0.877

x = 0.045

Q^2	a	F_w	F_2	xF_3	$\bar{q}_w$	b
0.58	0.049	0.835 ±0.017 ±0.084 ±0.006	0.834 ±0.017	0.415 ±0.064 ±0.059 ±0.024		
0.76	0.081	0.890 ±0.015 ±0.075 ±0.005	0.889 ±0.015	0.328 ±0.045 ±0.050 ±0.020		
0.99	0.125	0.963 ±0.015 ±0.069 ±0.006	0.968 ±0.017	0.377 ±0.035 ±0.043 ±0.017	0.214 ±0.013 ±0.029 ±0.012	0.709
1.28	0.212	1.043 ±0.014 ±0.065 ±0.008	1.074 ±0.020	0.425 ±0.026 ±0.038 ±0.016	0.235 ±0.008 ±0.025 ±0.012	0.747
1.67	0.218	1.142 ±0.016 ±0.064 ±0.012	1.159 ±0.022	0.414 ±0.029 ±0.034 ±0.016	0.290 ±0.009 ±0.023 ±0.011	0.747
2.17	0.221	1.219 ±0.016 ±0.065 ±0.016	1.233 ±0.023	0.436 ±0.029 ±0.031 ±0.017	0.332 ±0.011 ±0.023 ±0.011	0.743
2.82	0.243	1.284 ±0.016 ±0.068 ±0.021	1.286 ±0.024	0.457 ±0.027 ±0.031 ±0.020	0.336 ±0.012 ±0.024 ±0.012	0.743
3.66	0.283	1.281 ±0.017 ±0.073 ±0.027	1.329 ±0.032	0.441 ±0.028 ±0.032 ±0.024	0.335 ±0.012 ±0.028 ±0.013	0.743
4.76	0.459	1.446 ±0.019 ±0.081 ±0.034	1.511 ±0.053	0.562 ±0.025 ±0.034 ±0.030	0.382 ±0.011 ±0.033 ±0.014	0.808
6.19	0.546	1.401 ±0.021 ±0.092 ±0.042	1.540 ±0.104	0.542 ±0.026 ±0.039 ±0.037	0.378 ±0.013 ±0.041 ±0.016	0.822
8.04	0.614	1.477 ±0.029 ±0.104 ±0.052		0.558 ±0.034 ±0.045 ±0.045	0.416 ±0.019 ±0.050 ±0.019	0.841
10.45	0.666	1.491 ±0.045 ±0.119 ±0.062		0.518 ±0.053 ±0.053 ±0.055	0.453 ±0.035 ±0.061 ±0.021	0.851
13.59	0.745	1.388 ±0.083 ±0.137 ±0.073		0.550 ±0.096 ±0.062 ±0.067	0.404 ±0.071 ±0.074 ±0.025	0.877

x = 0.080

Q^2	a	F_w	F_2	xF_3	$\bar{q}_w$	b
1.04	0.049	1.031 ±0.017 ±0.100 ±0.009	1.030 ±0.017	0.599 ±0.065 ±0.065 ±0.031		
1.35	0.077	1.067 ±0.015 ±0.089 ±0.008	1.065 ±0.015	0.469 ±0.046 ±0.056 ±0.025		
1.75	0.126	1.104 ±0.015 ±0.080 ±0.007	1.102 ±0.015	0.494 ±0.033 ±0.048 ±0.021	0.219 ±0.012 ±0.040 ±0.012	0.709
2.28	0.207	1.159 ±0.014 ±0.073 ±0.008	1.165 ±0.016	0.591 ±0.025 ±0.043 ±0.018	0.219 ±0.007 ±0.034 ±0.011	0.747
2.96	0.225	1.220 ±0.015 ±0.069 ±0.010	1.252 ±0.018	0.601 ±0.026 ±0.039 ±0.017	0.234 ±0.008 ±0.029 ±0.010	0.749
3.85	0.217	1.299 ±0.015 ±0.067 ±0.012	1.298 ±0.017	0.661 ±0.027 ±0.036 ±0.017	0.248 ±0.009 ±0.026 ±0.009	0.746
5.01	0.237	1.332 ±0.015 ±0.067 ±0.016	1.330 ±0.017	0.649 ±0.025 ±0.036 ±0.019	0.296 ±0.010 ±0.025 ±0.009	0.743
6.51	0.277	1.354 ±0.016 ±0.070 ±0.020	1.387 ±0.020	0.652 ±0.026 ±0.037 ±0.023	0.292 ±0.011 ±0.025 ±0.010	0.745
8.46	0.457	1.408 ±0.016 ±0.075 ±0.026	1.420 ±0.027	0.706 ±0.021 ±0.039 ±0.029	0.305 ±0.009 ±0.026 ±0.011	0.812
11.00	0.526	1.440 ±0.020 ±0.082 ±0.032	1.481 ±0.043	0.744 ±0.024 ±0.044 ±0.036	0.311 ±0.011 ±0.029 ±0.012	0.824
14.30	0.599	1.440 ±0.025 ±0.092 ±0.040	1.606 ±0.089	0.715 ±0.030 ±0.050 ±0.045	0.332 ±0.015 ±0.033 ±0.015	0.838
18.59	0.665	1.483 ±0.038 ±0.104 ±0.048		0.752 ±0.044 ±0.058 ±0.055	0.345 ±0.025 ±0.039 ±0.017	0.855
24.16	0.745	1.481 ±0.069 ±0.118 ±0.057		0.997 ±0.076 ±0.068 ±0.067	0.234 ±0.045 ±0.047 ±0.020	0.877

$x = 0.125$

Q^2	a	F_w	F_2	xF_3	$\bar{q}_w$	b
1.62	0.048	1.050 ±0.016 ±0.094 ±0.008	1.048 ±0.016	0.654 ±0.060 ±0.056 ±0.027		
2.11	0.076	1.102 ±0.015 ±0.080 ±0.007	1.100 ±0.015	0.660 ±0.043 ±0.050 ±0.023		
2.74	0.121	1.125 ±0.014 ±0.068 ±0.008	1.122 ±0.014	0.669 ±0.032 ±0.046 ±0.020	0.173 ±0.011 ±0.021 ±0.008	0.710
3.56	0.205	1.136 ±0.013 ±0.059 ±0.009	1.157 ±0.015	0.690 ±0.023 ±0.043 ±0.018	0.163 ±0.006 ±0.017 ±0.008	0.750
4.63	0.220	1.178 ±0.014 ±0.054 ±0.011	1.191 ±0.016	0.694 ±0.024 ±0.042 ±0.018	0.183 ±0.007 ±0.015 ±0.008	0.748
6.02	0.222	1.241 ±0.013 ±0.050 ±0.014	1.236 ±0.016	0.732 ±0.023 ±0.041 ±0.019	0.207 ±0.008 ±0.014 ±0.008	0.746
7.82	0.239	1.290 ±0.013 ±0.050 ±0.017	1.299 ±0.015	0.809 ±0.022 ±0.042 ±0.022	0.191 ±0.008 ±0.013 ±0.008	0.745
10.17	0.275	1.259 ±0.014 ±0.052 ±0.022	1.278 ±0.018	0.781 ±0.023 ±0.044 ±0.026	0.201 ±0.009 ±0.014 ±0.009	0.745
13.22	0.449	1.300 ±0.014 ±0.057 ±0.028	1.320 ±0.024	0.793 ±0.019 ±0.047 ±0.031	0.221 ±0.007 ±0.016 ±0.009	0.812
17.18	0.521	1.293 ±0.017 ±0.065 ±0.035	1.269 ±0.034	0.829 ±0.021 ±0.052 ±0.037	0.209 ±0.008 ±0.019 ±0.010	0.830
22.34	0.593	1.286 ±0.021 ±0.075 ±0.043	1.342 ±0.071	0.819 ±0.025 ±0.057 ±0.045	0.216 ±0.011 ±0.024 ±0.011	0.843
29.04	0.662	1.255 ±0.030 ±0.088 ±0.051		0.833 ±0.034 ±0.064 ±0.054	0.200 ±0.018 ±0.029 ±0.012	0.855
37.75	0.745	1.310 ±0.060 ±0.104 ±0.061		0.820 ±0.067 ±0.073 ±0.065	0.236 ±0.045 ±0.036 ±0.014	0.877

x = 0.175

Q^2	a	F_w	F_2	xF_3	$\bar{q}_w$	b
2.27	0.051	1.017 ±0.015 ±0.063 ±0.009	1.015 ±0.015	0.671 ±0.057 ±0.035 ±0.027		
2.95	0.075	1.069 ±0.015 ±0.055 ±0.008	1.066 ±0.015	0.751 ±0.044 ±0.035 ±0.023		
3.83	0.123	1.075 ±0.013 ±0.048 ±0.007	1.071 ±0.013	0.753 ±0.031 ±0.035 ±0.020	0.133 ±0.010 ±0.018 ±0.007	0.710
4.98	0.200	1.071 ±0.013 ±0.044 ±0.008	1.081 ±0.014	0.753 ±0.023 ±0.035 ±0.018	0.121 ±0.005 ±0.015 ±0.006	0.751
6.48	0.214	1.092 ±0.013 ±0.041 ±0.009	1.103 ±0.016	0.776 ±0.024 ±0.035 ±0.017	0.124 ±0.006 ±0.013 ±0.006	0.750
8.42	0.210	1.139 ±0.013 ±0.039 ±0.012	1.117 ±0.015	0.830 ±0.023 ±0.036 ±0.017	0.135 ±0.007 ±0.011 ±0.006	0.748
10.95	0.239	1.132 ±0.012 ±0.040 ±0.015	1.136 ±0.014	0.810 ±0.021 ±0.037 ±0.019	0.138 ±0.007 ±0.011 ±0.006	0.745
14.24	0.275	1.131 ±0.014 ±0.042 ±0.018	1.154 ±0.017	0.796 ±0.021 ±0.038 ±0.022	0.137 ±0.008 ±0.011 ±0.006	0.746
18.51	0.432	1.146 ±0.014 ±0.046 ±0.023	1.122 ±0.021	0.838 ±0.018 ±0.040 ±0.027	0.142 ±0.006 ±0.011 ±0.006	0.818
24.06	0.520	1.149 ±0.016 ±0.051 ±0.029	1.173 ±0.034	0.819 ±0.019 ±0.042 ±0.032	0.146 ±0.007 ±0.013 ±0.007	0.831
31.28	0.594	1.118 ±0.019 ±0.059 ±0.035	1.135 ±0.062	0.846 ±0.022 ±0.044 ±0.039	0.127 ±0.008 ±0.015 ±0.008	0.849
40.66	0.663	1.102 ±0.028 ±0.068 ±0.042		0.799 ±0.031 ±0.047 ±0.047	0.144 ±0.015 ±0.018 ±0.009	0.858
52.86	0.745	1.019 ±0.048 ±0.079 ±0.051		0.755 ±0.052 ±0.050 ±0.056	0.127 ±0.029 ±0.022 ±0.010	0.877

x = 0.225

Q^2	a	F_w	F_2	xF_3	$\bar{q}_w$	b
2.92	0.047	0.967 ±0.015 ±0.072 ±0.008	0.964 ±0.015	0.732 ±0.059 ±0.087 ±0.025		
3.79	0.077	0.949 ±0.014 ±0.056 ±0.007	0.945 ±0.014	0.701 ±0.040 ±0.067 ±0.021		
4.93	0.122	0.971 ±0.013 ±0.043 ±0.007	0.966 ±0.013	0.756 ±0.029 ±0.050 ±0.018	0.088 ±0.009 ±0.022 ±0.002	0.711
6.41	0.204	0.974 ±0.012 ±0.034 ±0.007	0.969 ±0.012	0.758 ±0.022 ±0.037 ±0.016	0.084 ±0.005 ±0.018 ±0.004	0.753
8.33	0.205	0.979 ±0.013 ±0.027 ±0.008	0.974 ±0.013	0.776 ±0.023 ±0.027 ±0.015	0.095 ±0.006 ±0.014 ±0.006	0.751
10.83	0.212	0.988 ±0.012 ±0.023 ±0.010	0.984 ±0.012	0.780 ±0.022 ±0.021 ±0.016	0.095 ±0.006 ±0.012 ±0.007	0.749
14.08	0.236	0.994 ±0.011 ±0.023 ±0.013	0.991 ±0.011	0.808 ±0.019 ±0.018 ±0.017	0.078 ±0.006 ±0.010 ±0.008	0.747
18.30	0.270	0.977 ±0.013 ±0.025 ±0.016	0.974 ±0.013	0.765 ±0.020 ±0.018 ±0.020	0.092 ±0.007 ±0.009 ±0.008	0.747
23.79	0.436	0.994 ±0.013 ±0.030 ±0.021	0.993 ±0.015	0.786 ±0.016 ±0.022 ±0.024	0.093 ±0.005 ±0.009 ±0.008	0.818
30.93	0.515	0.987 ±0.015 ±0.039 ±0.026	1.001 ±0.019	0.778 ±0.018 ±0.029 ±0.029	0.095 ±0.006 ±0.010 ±0.008	0.831
40.21	0.578	0.954 ±0.018 ±0.050 ±0.032	0.924 ±0.026	0.809 ±0.021 ±0.039 ±0.035	0.076 ±0.007 ±0.011 ±0.008	0.848
52.27	0.661	0.942 ±0.026 ±0.065 ±0.038	0.925 ±0.049	0.761 ±0.029 ±0.053 ±0.042	0.086 ±0.012 ±0.014 ±0.007	0.863
67.96	0.745	0.938 ±0.050 ±0.082 ±0.045		0.724 ±0.054 ±0.071 ±0.051	0.103 ±0.032 ±0.017 ±0.005	0.877

x = 0.275

Q^2	a	F_w	F_2	xF_3	$\bar{q}_w$	b
3.56	0.049	0.862 ±0.014 ±0.043 ±0.006	0.859 ±0.014	0.662 ±0.053 ±0.074 ±0.022		
4.63	0.077	0.847 ±0.013 ±0.035 ±0.006	0.844 ±0.013	0.651 ±0.037 ±0.059 ±0.018		
6.03	0.119	0.877 ±0.012 ±0.028 ±0.006	0.873 ±0.012	0.790 ±0.029 ±0.046 ±0.016	0.038 ±0.009 ±0.016 ±0.004	0.711
7.83	0.198	0.838 ±0.011 ±0.022 ±0.007	0.832 ±0.011	0.680 ±0.020 ±0.036 ±0.015	0.056 ±0.004 ±0.013 ±0.003	0.753
10.18	0.206	0.845 ±0.012 ±0.019 ±0.008	0.840 ±0.012	0.700 ±0.022 ±0.028 ±0.014	0.057 ±0.005 ±0.011 ±0.003	0.752
13.24	0.208	0.853 ±0.012 ±0.017 ±0.010	0.849 ±0.011	0.750 ±0.020 ±0.023 ±0.015	0.054 ±0.005 ±0.009 ±0.003	0.750
17.21	0.236	0.830 ±0.011 ±0.017 ±0.013	0.827 ±0.011	0.738 ±0.018 ±0.020 ±0.016	0.046 ±0.005 ±0.007 ±0.003	0.746
22.37	0.276	0.836 ±0.012 ±0.019 ±0.016	0.833 ±0.012	0.691 ±0.018 ±0.020 ±0.018	0.057 ±0.006 ±0.007 ±0.003	0.748
29.08	0.449	0.804 ±0.011 ±0.022 ±0.020	0.800 ±0.011	0.659 ±0.014 ±0.022 ±0.022	0.060 ±0.004 ±0.006 ±0.003	0.829
37.81	0.532	0.796 ±0.013 ±0.027 ±0.025	0.793 ±0.013	0.666 ±0.015 ±0.027 ±0.026	0.051 ±0.004 ±0.007 ±0.004	0.848
49.15	0.582	0.805 ±0.017 ±0.034 ±0.030	0.803 ±0.017	0.690 ±0.019 ±0.035 ±0.031	0.055 ±0.006 ±0.008 ±0.004	0.851
63.89	0.641	0.802 ±0.023 ±0.043 ±0.036	0.800 ±0.023	0.730 ±0.026 ±0.045 ±0.037	0.041 ±0.009 ±0.009 ±0.004	0.855
83.06	0.745	0.824 ±0.049 ±0.053 ±0.043	0.822 ±0.049	0.588 ±0.055 ±0.057 ±0.044	0.114 ±0.035 ±0.011 ±0.004	0.877

x = 0.350

Q^2	a	F_w	F_2	xF_3	$\bar{q}_w$	b
4.54	0.048	0.690 ±0.009 ±0.029 ±0.006	0.687 ±0.009	0.609 ±0.035 ±0.046 ±0.019		
5.90	0.073	0.675 ±0.008 ±0.025 ±0.005	0.672 ±0.008	0.601 ±0.025 ±0.035 ±0.015		
7.67	0.119	0.654 ±0.008 ±0.021 ±0.005	0.649 ±0.008	0.555 ±0.018 ±0.027 ±0.013	0.038 ±0.005 ±0.009 ±0.002	0.712
9.97	0.191	0.655 ±0.007 ±0.019 ±0.005	0.650 ±0.007	0.582 ±0.013 ±0.021 ±0.011	0.025 ±0.003 ±0.007 ±0.002	0.755
12.96	0.212	0.633 ±0.008 ±0.017 ±0.005	0.628 ±0.007	0.548 ±0.013 ±0.016 ±0.010	0.034 ±0.003 ±0.006 ±0.002	0.754
16.85	0.215	0.634 ±0.007 ±0.016 ±0.007	0.631 ±0.007	0.554 ±0.012 ±0.014 ±0.010	0.033 ±0.003 ±0.005 ±0.002	0.750
21.90	0.242	0.615 ±0.007 ±0.017 ±0.008	0.612 ±0.007	0.550 ±0.011 ±0.013 ±0.011	0.025 ±0.003 ±0.004 ±0.002	0.750
28.47	0.268	0.614 ±0.007 ±0.018 ±0.011	0.612 ±0.007	0.553 ±0.012 ±0.014 ±0.013	0.023 ±0.003 ±0.003 ±0.002	0.750
37.01	0.314	0.612 ±0.009 ±0.020 ±0.014	0.609 ±0.008	0.553 ±0.012 ±0.017 ±0.015	0.023 ±0.004 ±0.003 ±0.002	0.752
48.12	0.499	0.591 ±0.008 ±0.023 ±0.017	0.588 ±0.008	0.548 ±0.010 ±0.022 ±0.019	0.022 ±0.002 ±0.003 ±0.002	0.849
62.55	0.587	0.567 ±0.010 ±0.027 ±0.021	0.564 ±0.010	0.507 ±0.012 ±0.028 ±0.023	0.023 ±0.003 ±0.003 ±0.002	0.862
81.32	0.645	0.560 ±0.014 ±0.032 ±0.025	0.558 ±0.014	0.512 ±0.016 ±0.037 ±0.028	0.024 ±0.005 ±0.003 ±0.003	0.865
105.70	0.746	0.574 ±0.025 ±0.038 ±0.030	0.573 ±0.025	0.517 ±0.027 ±0.048 ±0.034	0.027 ±0.011 ±0.004 ±0.003	0.878

x = 0.450

Q^2	a	F_w	F_2	xF_3	$\bar{q}_w$	b
5.83	0.047	0.480 ±0.008 ±0.023 ±0.005	0.478 ±0.008	0.463 ±0.029 ±0.044 ±0.012		
7.58	0.077	0.448 ±0.007 ±0.023 ±0.003	0.445 ±0.007	0.399 ±0.019 ±0.038 ±0.009		
9.86	0.116	0.431 ±0.006 ±0.023 ±0.003	0.428 ±0.006	0.402 ±0.014 ±0.034 ±0.008	0.019 ±0.004 ±0.008 ±0.001	0.712
12.82	0.197	0.413 ±0.006 ±0.023 ±0.002	0.409 ±0.006	0.375 ±0.010 ±0.030 ±0.007	0.016 ±0.002 ±0.006 ±0.001	0.755
16.66	0.205	0.397 ±0.006 ±0.023 ±0.003	0.394 ±0.006	0.375 ±0.010 ±0.026 ±0.006	0.007 ±0.002 ±0.005 ±0.001	0.756
21.66	0.207	0.381 ±0.005 ±0.022 ±0.004	0.379 ±0.005	0.364 ±0.010 ±0.024 ±0.007	0.012 ±0.002 ±0.004 ±0.001	0.751
28.16	0.241	0.370 ±0.005 ±0.022 ±0.006	0.367 ±0.005	0.342 ±0.008 ±0.022 ±0.008	0.009 ±0.002 ±0.003 ±0.002	0.752
36.61	0.264	0.366 ±0.006 ±0.021 ±0.008	0.364 ±0.005	0.347 ±0.009 ±0.021 ±0.010	0.008 ±0.002 ±0.002 ±0.002	0.751
47.59	0.320	0.352 ±0.006 ±0.020 ±0.011	0.350 ±0.006	0.327 ±0.009 ±0.020 ±0.012	0.006 ±0.003 ±0.002 ±0.003	0.753
61.86	0.513	0.335 ±0.006 ±0.020 ±0.014	0.334 ±0.006	0.315 ±0.007 ±0.020 ±0.015	0.008 ±0.001 ±0.002 ±0.003	0.859
80.42	0.555	0.330 ±0.008 ±0.019 ±0.018	0.329 ±0.008	0.333 ±0.009 ±0.021 ±0.019	0.006 ±0.002 ±0.002 ±0.004	0.858
104.50	0.666	0.322 ±0.010 ±0.017 ±0.023	0.321 ±0.010	0.305 ±0.011 ±0.023 ±0.024	0.005 ±0.002 ±0.002 ±0.005	0.874
135.90	0.746	0.308 ±0.018 ±0.016 ±0.028	0.307 ±0.018	0.288 ±0.019 ±0.026 ±0.029	0.010 ±0.007 ±0.003 ±0.006	0.878

$x = 0.550$

Q^2	a	F_w	F_2	xF_3	$\bar{q}_w$	b
7.13	0.047	0.294 ±0.006 ±0.026 ±0.002	0.292 ±0.006	0.257 ±0.021 ±0.019 ±0.006		
9.27	0.072	0.283 ±0.005 ±0.024 ±0.001	0.281 ±0.005	0.273 ±0.015 ±0.019 ±0.005		
12.05	0.118	0.250 ±0.004 ±0.023 ±0.002	0.248 ±0.004	0.235 ±0.010 ±0.018 ±0.005	0.008 ±0.003 ±0.002 ±0.001	0.713
15.66	0.181	0.234 ±0.004 ±0.021 ±0.002	0.231 ±0.004	0.236 ±0.008 ±0.017 ±0.004	0.001 ±0.001 ±0.002 ±0.001	0.758
20.36	0.197	0.220 ±0.004 ±0.020 ±0.002	0.217 ±0.004	0.212 ±0.007 ±0.016 ±0.004	0.006 ±0.002 ±0.002 ±0.001	0.754
26.47	0.218	0.207 ±0.004 ±0.019 ±0.002	0.206 ±0.004	0.197 ±0.006 ±0.016 ±0.004	0.007 ±0.002 ±0.002 ±0.001	0.753
34.42	0.231	0.198 ±0.003 ±0.018 ±0.003	0.197 ±0.003	0.192 ±0.006 ±0.015 ±0.004	0.003 ±0.002 ±0.002 ±0.001	0.752
44.74	0.269	0.187 ±0.004 ±0.016 ±0.003	0.186 ±0.004	0.183 ±0.006 ±0.014 ±0.005	0.004 ±0.002 ±0.001 ±0.001	0.750
58.16	0.315	0.176 ±0.004 ±0.015 ±0.004	0.175 ±0.004	0.171 ±0.006 ±0.013 ±0.005	0.001 ±0.002 ±0.001 ±0.001	0.754
75.61	0.489	0.173 ±0.004 ±0.014 ±0.005	0.172 ±0.004	0.167 ±0.005 ±0.013 ±0.006	0.004 ±0.001 ±0.001 ±0.001	0.860
98.29	0.560	0.162 ±0.005 ±0.013 ±0.006	0.161 ±0.005	0.158 ±0.006 ±0.012 ±0.008	0.003 ±0.001 ±0.001 ±0.001	0.859
127.80	0.648	0.155 ±0.007 ±0.012 ±0.007	0.154 ±0.007	0.154 ±0.008 ±0.011 ±0.009	0.002 ±0.002 ±0.001 ±0.001	0.868
166.10	0.746	0.157 ±0.014 ±0.011 ±0.008	0.157 ±0.014	0.126 ±0.015 ±0.011 ±0.011	0.015 ±0.007 ±0.001 ±0.001	0.878

$x = 0.650$

Q^2	a	F_w	F_2	xF_3	$\bar{q}_w$	b
8.43	0.051	0.168 ±0.004 ±0.018 ±0.009	0.167 ±0.004	0.158 ±0.015 ±0.014 ±0.010		
10.95	0.078	0.151 ±0.004 ±0.017 ±0.007	0.149 ±0.004	0.155 ±0.010 ±0.013 ±0.008		
14.24	0.127	0.130 ±0.003 ±0.015 ±0.005	0.128 ±0.003	0.137 ±0.007 ±0.013 ±0.006	−0.001 ±0.002 ±0.003 ±0.001	0.714
18.51	0.195	0.112 ±0.003 ±0.014 ±0.004	0.111 ±0.003	0.115 ±0.005 ±0.012 ±0.005	−0.001 ±0.001 ±0.002 ±0.001	0.761
24.07	0.214	0.099 ±0.003 ±0.013 ±0.003	0.097 ±0.003	0.093 ±0.004 ±0.012 ±0.004	0.004 ±0.001 ±0.002 ±0.001	0.755
31.29	0.224	0.096 ±0.002 ±0.012 ±0.002	0.095 ±0.002	0.091 ±0.004 ±0.011 ±0.003	0.003 ±0.001 ±0.001 ±0.001	0.752
40.67	0.252	0.088 ±0.002 ±0.011 ±0.002	0.087 ±0.002	0.079 ±0.003 ±0.011 ±0.002	0.003 ±0.001 ±0.001 ±0.001	0.753
52.87	0.273	0.083 ±0.002 ±0.010 ±0.002	0.082 ±0.002	0.083 ±0.004 ±0.010 ±0.002	0.000 ±0.001 ±0.001 ±0.001	0.752
68.74	0.460	0.074 ±0.002 ±0.010 ±0.001	0.073 ±0.002	0.070 ±0.003 ±0.010 ±0.002	0.001 ±0.001 ±0.001 ±0.001	0.851
89.36	0.509	0.070 ±0.002 ±0.009 ±0.002	0.069 ±0.002	0.068 ±0.003 ±0.009 ±0.002	0.001 ±0.001 ±0.001 ±0.001	0.858
116.20	0.579	0.066 ±0.003 ±0.009 ±0.002	0.065 ±0.003	0.067 ±0.003 ±0.009 ±0.002	0.000 ±0.001 ±0.001 ±0.001	0.867
151.00	0.647	0.076 ±0.005 ±0.009 ±0.003	0.075 ±0.005	0.072 ±0.005 ±0.008 ±0.003	0.002 ±0.001 ±0.001 ±0.001	0.871
196.30	0.747	0.068 ±0.008 ±0.009 ±0.004	0.068 ±0.008	0.058 ±0.009 ±0.008 ±0.004	0.005 ±0.004 ±0.001 ±0.001	0.878

Table 5

Values of the structure functions $F_L(x)$ and $\bar{q}^{\bar{\nu}}(x)$ averaged over the available Q^2 range; $\langle Q^2 \rangle$ is the weighted average in each x bin. The systematic error includes uncertainties due to the error in the total cross-section.

x	$F_L(x)$				$\bar{q}^{\bar{\nu}}(x)$			
	$\langle Q^2 \rangle$ (GeV^2)	Value	Error		$\langle Q^2 \rangle$ (GeV^2)	Value	Error	
			Stat.	Syst.			Stat.	Syst.
0.015	1.4	0.299	0.081	0.104	1.5	0.368	0.021	0.026
0.045	4.2	0.264	0.087	0.088	4.8	0.377	0.022	0.021
0.080	7.9	0.337	0.071	0.076	9.1	0.278	0.017	0.017
0.125	12.7	0.139	0.054	0.058	14.8	0.211	0.012	0.013
0.175	18.1	0.052	0.045	0.047	21.2	0.150	0.010	0.010
0.225	23.3	0.038	0.037	0.035	26.7	0.096	0.008	0.008
0.275	30.5	0.031	0.027	0.041	33.9	0.053	0.007	0.006
0.350	35.5	0.027	0.017	0.019	41.1	0.019	0.003	0.003
0.450	49.1	−0.006	0.012	0.017	56.5	0.008	0.002	0.002
0.550	63.4	−0.006	0.007	0.010	72.7	0.003	0.001	0.002
0.650	69.4	−0.011	0.005	0.008	81.5	0.002	0.001	0.002

Table 6

Values of the structure functions $F_L(x,Q^2)$ and $\bar{q}^{\bar{\nu}}(x,Q^2)$.
The systematic error includes uncertainties due to the error in the total cross-section.

x	$\langle Q^2 \rangle$ (GeV^2)	$F_L(x)$			$\bar{q}^{\bar{\nu}}(x)$		
		Value	Error		Value	Error	
			Stat.	Syst.		Stat.	Syst.
0.05	3.1	0.495	0.113	0.165	0.180	0.033	0.040
	5.7	0.431	0.071	0.188	0.276	0.019	0.047
	9.8	0.274	0.074	0.183	0.375	0.017	0.023
	16.8	−0.263	0.173	0.217	0.488	0.031	0.063
0.15	6.8	0.246	0.101	0.105	0.132	0.029	0.043
	12.7	0.145	0.058	0.086	0.173	0.015	0.021
	22.0	0.083	0.055	0.074	0.185	0.012	0.021
	36.1	−0.238	0.114	0.168	0.208	0.019	0.030
0.25	10.8	0.166	0.076	0.083	0.045	0.021	0.020
	20.0	0.115	0.040	0.057	0.054	0.010	0.013
	34.5	0.009	0.038	0.043	0.081	0.008	0.008
	58.6	−0.294	0.068	0.216	0.103	0.012	0.029
0.40	18.1	0.068	0.036	0.029	0.007	0.010	0.008
	33.9	0.013	0.017	0.022	0.014	0.004	0.006
	57.0	−0.002	0.016	0.020	0.014	0.003	0.003
	90.9	−0.036	0.036	0.094	0.020	0.005	0.008
0.60	26.3	0.071	0.017	0.034	−0.019	0.004	0.011
	51.3	−0.001	0.007	0.014	0.001	0.001	0.003
	82.8	−0.027	0.006	0.014	0.004	0.001	0.002
	129.6	−0.037	0.010	0.011	0.005	0.001	0.002

Table 7

Upper limits on the structure function F_2 at large x

x	Upper limit on F_2	Statistical error	Systematic error
0.89	1.3×10^{-2}	9.7×10^{-4}	2.3×10^{-4}
1.09	2.8×10^{-3}	4.6×10^{-4}	4.7×10^{-4}
1.33	6.7×10^{-4}	1.6×10^{-4}	1.1×10^{-4}
1.85	2.9×10^{-5}	1.4×10^{-5}	4.8×10^{-6}

Table 8

Results of the QCD fit to the structure function $xF_3(x,Q^2)$ for $Q^2 > 10\ GeV^2$ and $W^2 > 11\ GeV^2$. At $Q_0^2 = 5\ GeV^2$ the function is parametrized as $xF_3(x) = A\, x^{\alpha}(1-x)^{\beta}(1+\gamma x)/B$. The fit was performed in next-to-leading order and including target mass corrections $\chi^2/NDF = 24.3/69$

Fit parameter	Value
$\Lambda_{\overline{MS}}$	$100\ ^{+90}_{-60}$ MeV
α	$0.63\ ^{+0.13}_{-0.24}$
β	$3.69\ ^{+0.24}_{-0.43}$
γ	$0.93\ ^{+3.03}_{-1.25}$
A	$2.92\ ^{+0.65}_{-0.27}$

Table 9

$$q_v(x) = A_v\, x^{\alpha_v}\,(1-x)^{\beta_v}(1+\gamma_v x)/B_v$$
$$q_s(x) = q_v(x) + A_s\, e^{-\beta_s x}\,(1-x)$$
$$G(x) = A_g(1-x)^{\beta_g}$$
$$Q_0^2 = 20\ \mathrm{GeV}^2$$
$$\Lambda = 128\ \mathrm{MeV}$$
$$\chi^2/\mathrm{NDF} = 505/855$$

A_v	2.92
α_v	0.476
β_v	3.97
γ_v	2.74
A_s	1.53
β_s	7.65
A_g	5.44
β_g	8.08

*) B_v is determined such that
$\int dx\, q_v(x)/x = A_v$

Figure captions

Fig. 1 Kinematics of inelastic charged-current neutrino interactions.

Fig. 2 Upgraded CDHS detector.

Fig. 3 Layout of the new calorimeter module.

Fig. 4 a) Efficiency of the charged-current trigger as a function of the total energy.
b) Efficiency of the hard charged-current trigger as a function of hadronic energy.

Fig. 5 Typical reconstructed charged-current event. The top view shows the profile of the pulse height recorded along the detector.

Fig. 6 a) Difference between the muon momentum derived from range and from curvature as a function of the momentum.
b) Test of the absolute muon momentum scale by comparing the difference between the momenta of the same track determined at different points along the muon trajectory with the calculated energy loss.

Fig. 7 Hadron calibration curve. Open circles and full triangles correspond to two different calibration runs.

Fig. 8 Effective change of the calorimeter response due to the frequency dependence of the ADCs for the neutrino and the antineutrino case as a function of hadron energy. The error bars indicate the contribution to the resolution due to the spectrum of the triggering rate.

Fig. 9 Average total energy of events in different y bins (wide-band beam, after correction for the rate effect), compared to a Monte Carlo calculation.

Fig. 10 Resolution in x and Q^2. The solid error bars represent the resolution for $y < 0.5$, the dashed ones for $y > 0.5$.

Fig. 11 Total energy distributions of neutrino- and antineutrino-induced events in different slices of the detector radius.

Fig. 12 Comparison of x and y distributions of data and simulated events, after smearing and cuts, for the neutrino and the antineutrino case. The solid lines represent the Monte Carlo; the data are shown as points.

Fig. 13 Values of the correction factor for acceptance and smearing effects in the x–y plane.

Fig. 14 Differential cross-sections for a) neutrino–iron and b) antineutrino–iron scattering at E_ν = 65 GeV. The solid lines are QCD fits for $Q^2 > 5$ GeV^2 and $W^2 > 11$ GeV^2; the dashed and lower solid lines show the contribution of quarks and gluons, respectively.

Fig. 15 Comparison of the radiative corrections according to Refs. [26] and [29]. The shaded area indicates uncertainties due to the quark masses in the range 1–300 MeV.

Fig. 16 The structure function $xF_3(x,Q^2)$. The solid line is the QCD fit for $Q^2 > 2$ GeV^2 and no W cut (see Section 12).

Fig. 17 Values of the structure function $xF_3(x,Q^2)$ extracted at different values of y.

Fig. 18 The difference between the auxiliary function $F_w(x,Q^2)$ and the structure functions $F_2(x,Q^2)$ and $2xF_1(x,Q^2)$, assuming $R = R_0(x,Q^2)$ in the case of the wide-band beam spectrum.

Fig. 19 The structure function $F_2(x,Q^2)$ determined at low y (open circles) and derived from the function $F_w(x,Q^2)$, assuming $R = R_0(x,Q^2)$ (full circles). The lines show the result of a QCD fit for $Q^2 > 5$ GeV^2 and $W^2 > 11$ GeV^2.

Fig. 20 The effect of the strange sea and slow rescaling corrections on the structure function $F_2(x,Q^2)$.

Fig. 21 The structure function $\bar{q}^{\bar{\nu}}(x,Q^2)$ derived from the auxiliary function $\bar{q}_w(x,Q^2)$ assuming $R = R_0(x,Q^2)$.

Fig. 22 Fit to the y distribution of $\Sigma^{\bar{\nu}} = [d\sigma^{\bar{\nu}}/dx\,dy - (1-y)^2\,d\sigma^{\nu}/dx\,dy]/\sigma_0[1-(1-y)^4]$ at $x = 0.08$ and $Q^2 = 5.3$ GeV^2.

Fig. 23 The longitudinal structure function $F_L(x)$ averaged over the available Q^2 range without (full circles) and with (open circles) slow rescaling correction.

Fig. 24 The antiquark distribution $\bar{q}^{\bar{\nu}}(x)$ averaged over the available Q^2 range without (full circles) and with (open circles) slow rescaling correction.

Fig. 25 Comparison of R(x) with our previous determination [36].

Fig. 26 The structure function $F_L(x,Q^2)$ determined from the simultaneous fit of F_L and $\bar{q}^{\bar{\nu}}$. Results of the fits are averaged over a fraction of the available Q^2 range.

Fig. 27 The antiquark distribution as a function of x and Q^2. Relatively large error bars, compared to those in Fig. 21, reflect experimental uncertainties of $F_L(x,Q^2)$.

Fig. 28 a) Total energy distribution of neutrino-induced events with $x > 0.8$ (full circles) and $x > 1$ (open circles), and all events (line).
b) Total energy distribution for antineutrino-induced events with $x > 0.8$ (full circles) and $x > 1$ (open circles), and $x > 0.45$ (line).

Fig. 29 a) The y distribution of neutrino-induced events with $x > 0.8$ (full circles) and $x > 1$ (open circles), and all events (line).
b) The y distribution for antineutrino-induced events with $x > 0.8$ (full circles), $x > 1$ (open circles), and $x > 0.45$ (line).

Fig. 30 Upper limits on the structure function F_2 at large x (full circles). The dashed line is the prediction of the Fermi momentum model [38], where the structure function for $x > 0.65$ was suppressed to zero. The dash-dotted line shows the prediction of the minimal Fermi motion model. The structure functions of Ref. [25] were used.

Fig. 31 The structure functions $F_2(x,Q^2)$, $xF_3(x,Q^2)$, and $\bar{q}^{\bar{\nu}}(x,Q^2)$ at three different values of Q^2.

Fig. 32 Integral (a) and average x (b) of the $F_2(x,Q^2)$, $xF_3(x,Q^2)$, and $\bar{q}^{\bar{\nu}}(x,Q^2)$ as a function of ν.

Fig. 33 Integral of F_3 as a function of ν.

Fig. 34 a) Values of $\Lambda_{\overline{MS}}$ as a function of the W^2 cut for $Q^2 > 5$ GeV^2.
b) Values of $\Lambda_{\overline{MS}}$ as a function of the Q^2 cut for $W^2 > 11$ GeV^2.

Fig. 35 Logarithmic derivatives $d \ln xF_3(x,Q^2)/d \ln Q^2$ as a function of x. Slopes are calculated for $Q^2 > 2$ GeV^2, $\nu > 5$ GeV (circles), and for $Q^2 > 5$ GeV^2, $\nu > 23$ GeV (squares).

Fig. 36 The gluon distribution at $Q^2 = 20$ GeV^2 with uncertainties due to shape variations (black band) and the systematic errors of the total cross-sections (dashed lines).

Fig. 37 Shape of the quark distributions $q - \bar{q}$ and $q + \bar{q}$ and the gluon distribution G(x) at $Q_0^2 = 20$ GeV^2.

Fig. 38 Comparison of the structure function $F_2(x,Q^2)$ determined from the narrow-band beam (open circles) and wide-band beam (full circles) data, using the same set of corrections.

Fig. 39 Comparison of the values of R(x) with other deep-inelastic scattering experiments at high Q^2.

Fig. 40 Comparison of the values of R(x) with the measurements performed at SLAC.

Fig. 41 Comparison of the structure function $xF_3(x,Q^2)$ with the results of other neutrino experiments.

Fig. 42 Comparison of the structure function $F_2(x,Q^2)$ extracted under the assumption that $R = 0$ and corrected for slow rescaling, with the results of muon experiments multiplied by 18/5.

Fig. 43 Logarithmic derivatives $d \ln F_2(x,Q^2)/d \ln Q^2$ as a function of x. The slopes are calculated for $Q^2 > 2$ GeV^2, $\nu > 5$ GeV (full circles) and for $Q^2 > 5$ GeV^2, $\nu > 23$ GeV (full squares). Published data from the CCFRR [17], BCDMS [48] and EMC [47] experiments are shown for comparison.

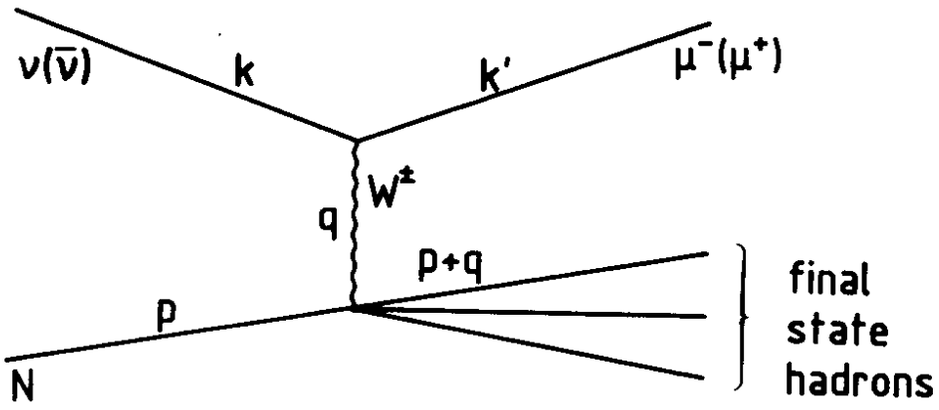

Fig. 1

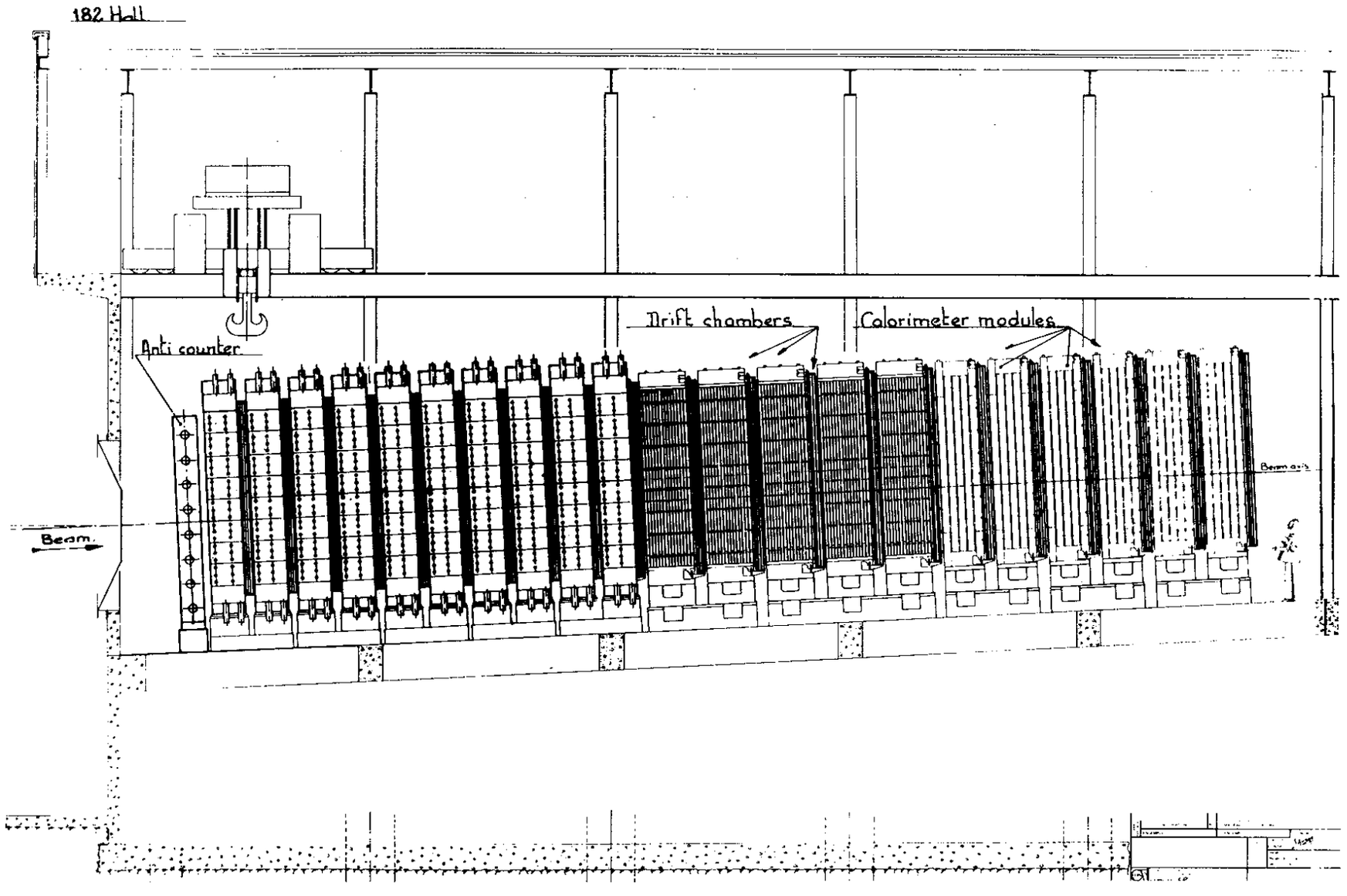
182 Hall
Drift chambers
Colorimeter modules
Anti counter
Beam
Beam axis

Fig. 2

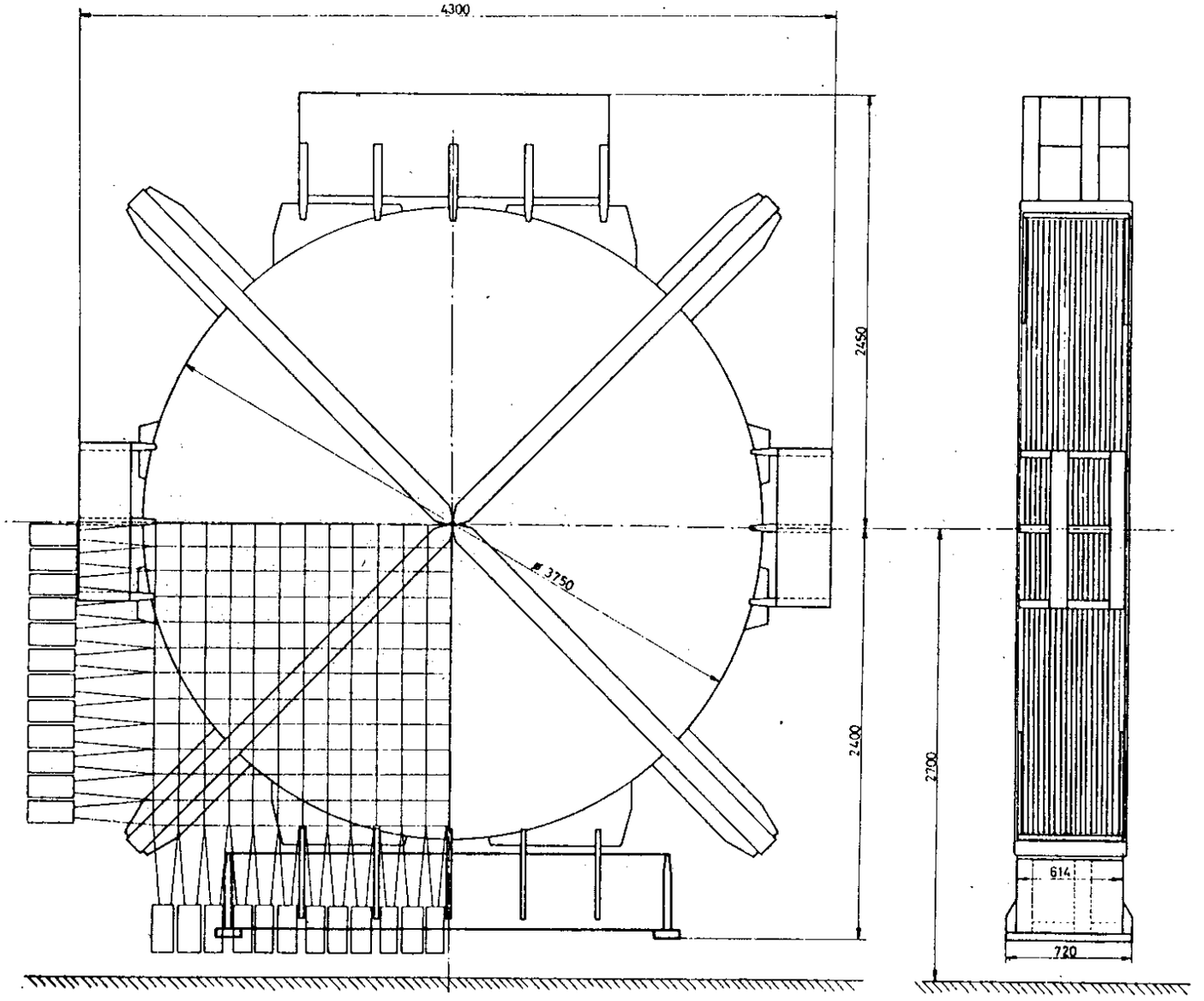

Fig. 3

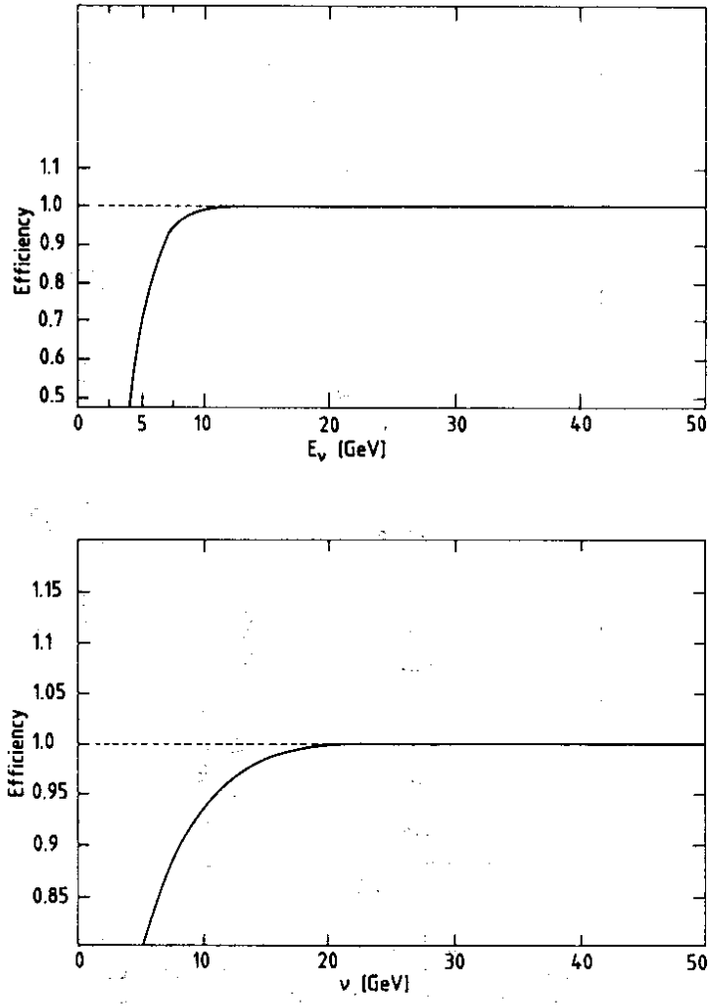
a)
Efficiency
1.1
1.0
0.9
0.8
0.7
0.6
0.5
0
5
10
20
30
40
50
E_ν [GeV]
b)
Efficiency
1.15
1.1
1.05
1.0
0.95
0.9
0.85
0
10
20
30
40
50
ν [GeV]

Fig. 4

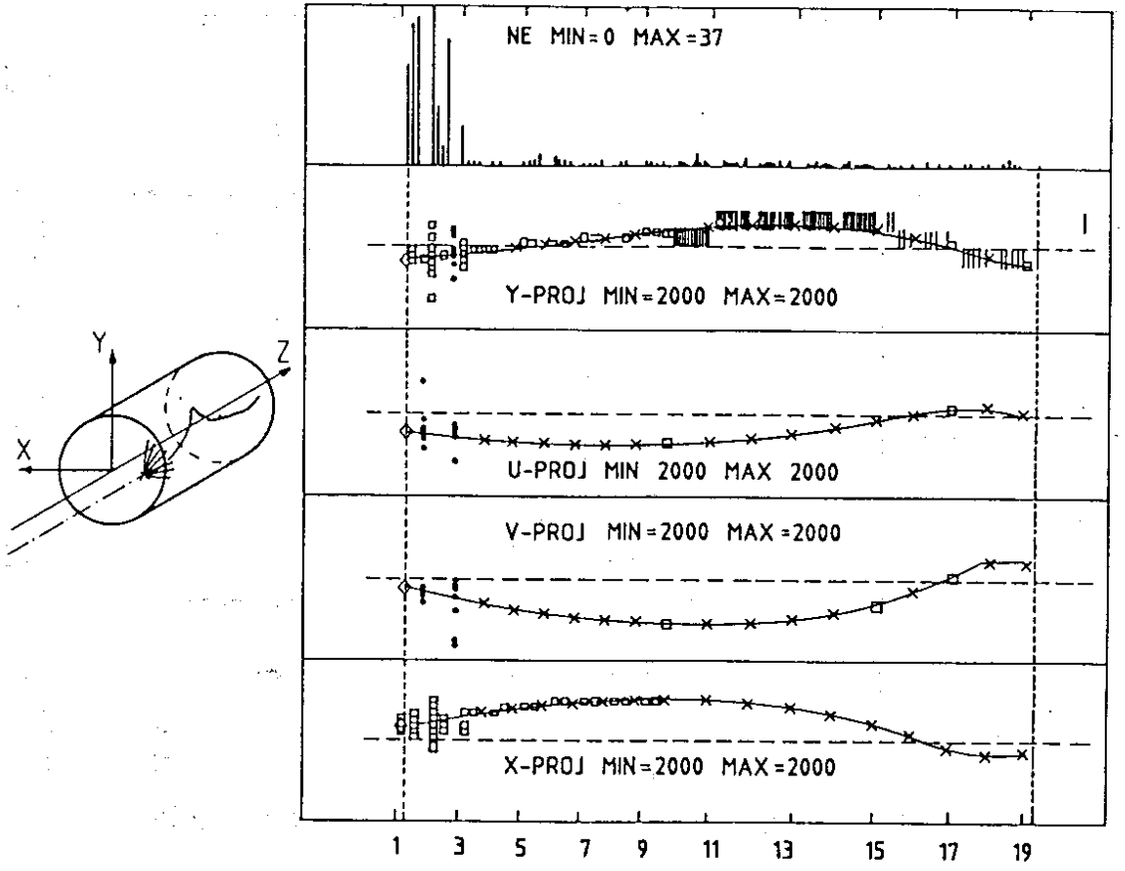
Y
Z
X
NE MIN=0 MAX=37
Y-PROJ MIN=2000 MAX=2000
U-PROJ MIN 2000 MAX 2000
V-PROJ MIN=2000 MAX=2000
X-PROJ MIN=2000 MAX=2000
1
3
5
7
9
11
13
15
17
19

Fig. 5

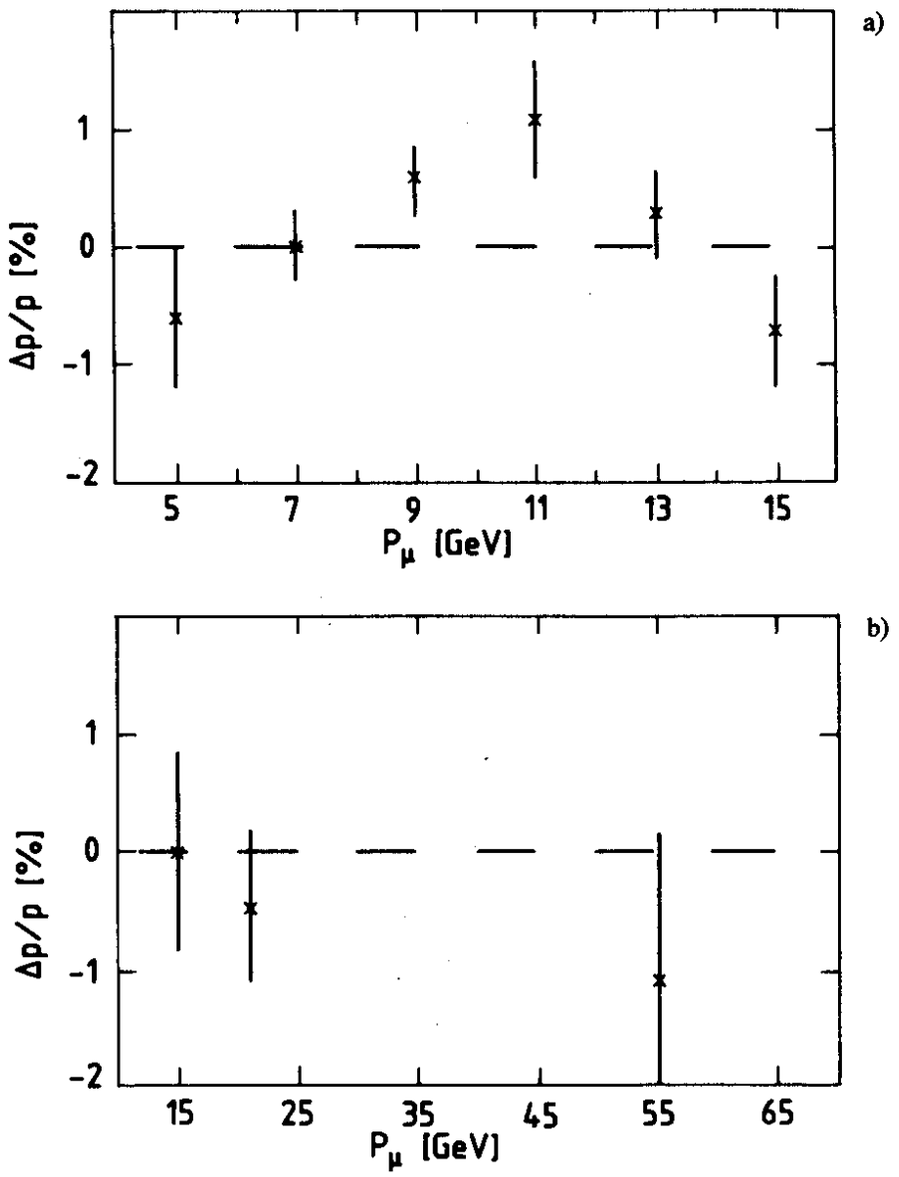
a)
Δp/p [%]
1
0
-1
-2
5
7
9
11
13
15
P_μ [GeV]
b)
Δp/p [%]
1
0
-1
-2
15
25
35
45
55
65
P_μ [GeV]

Fig. 6

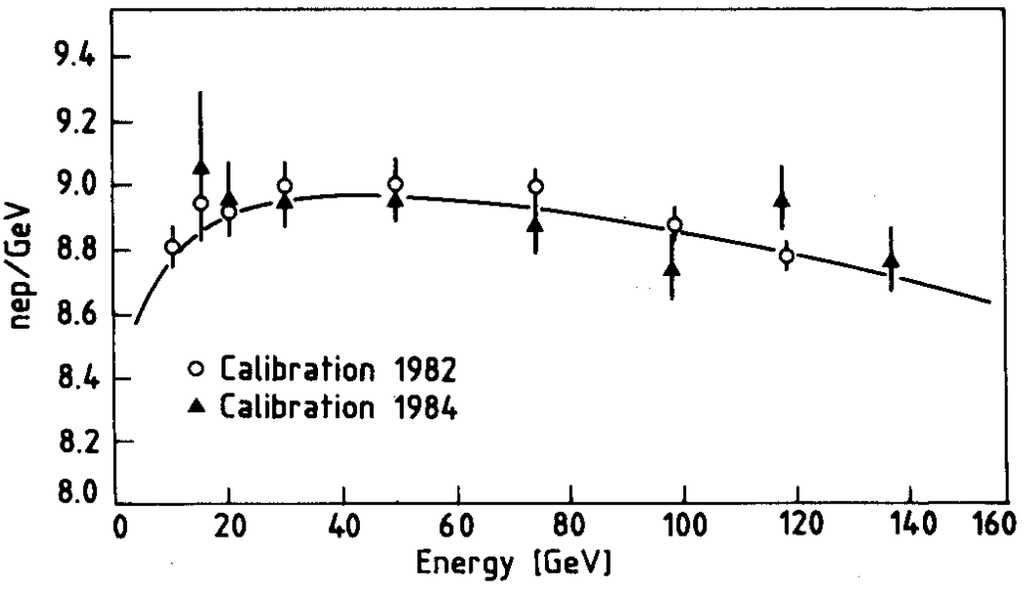
nep/GeV
9.4
9.2
9.0
8.8
8.6
8.4
8.2
8.0
0
20
40
60
80
100
120
140
160
Energy [GeV]
Calibration 1982
Calibration 1984

Fig. 7

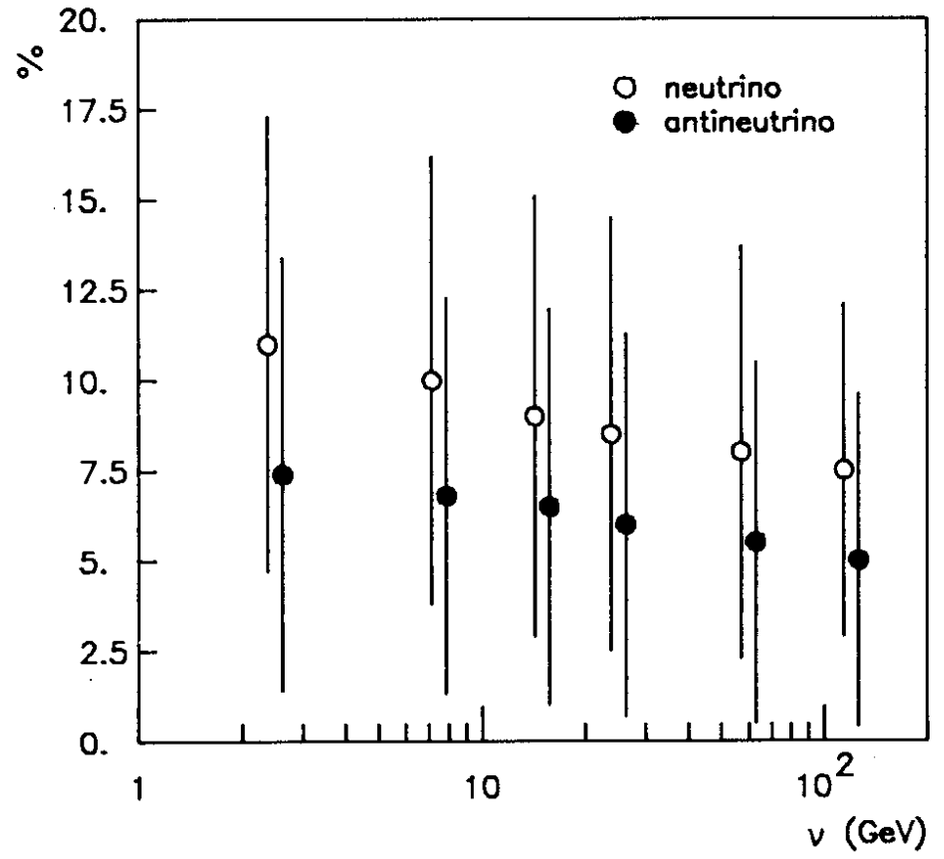
%
20.
17.5
15.
12.5
10.
7.5
5.
2.5
0.
neutrino
antineutrino
1
10
10^2
ν (GeV)

Fig. 8

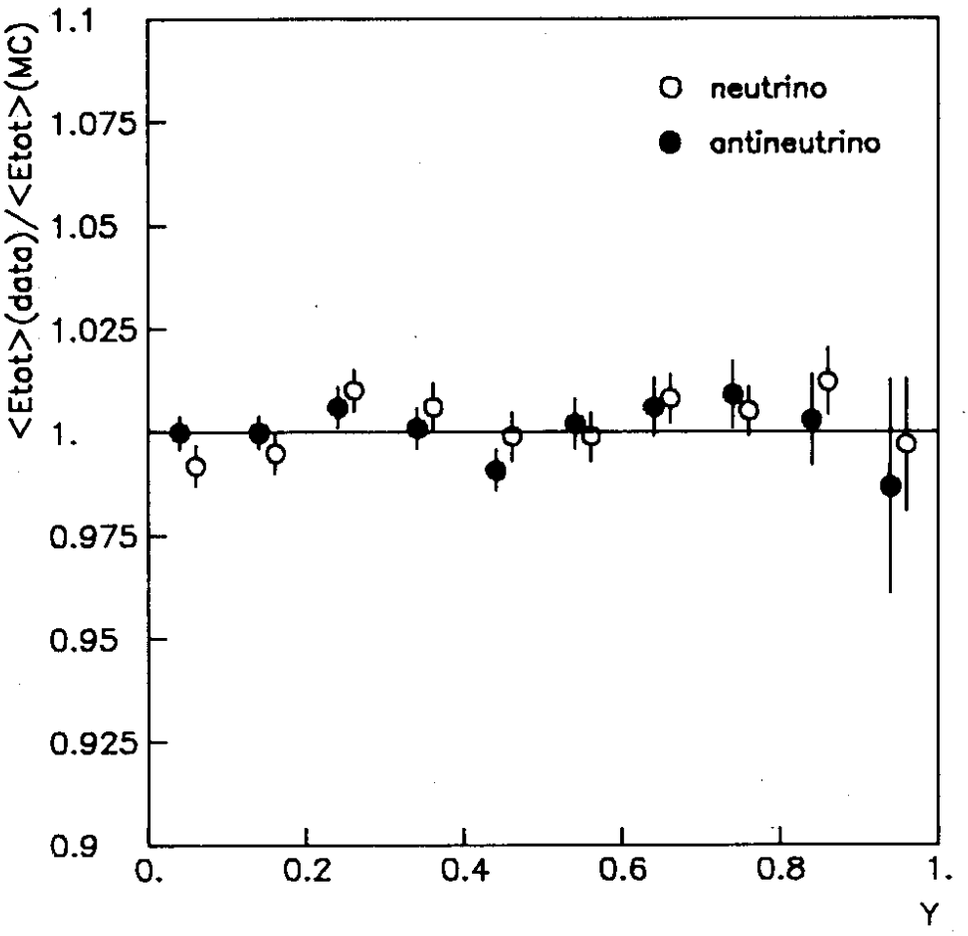
<Etot>(data)/<Etot>(MC)
1.1
1.075
1.05
1.025
1.
0.975
0.95
0.925
0.9
neutrino
antineutrino
0.
0.2
0.4
0.6
0.8
1.
Y

Fig. 9

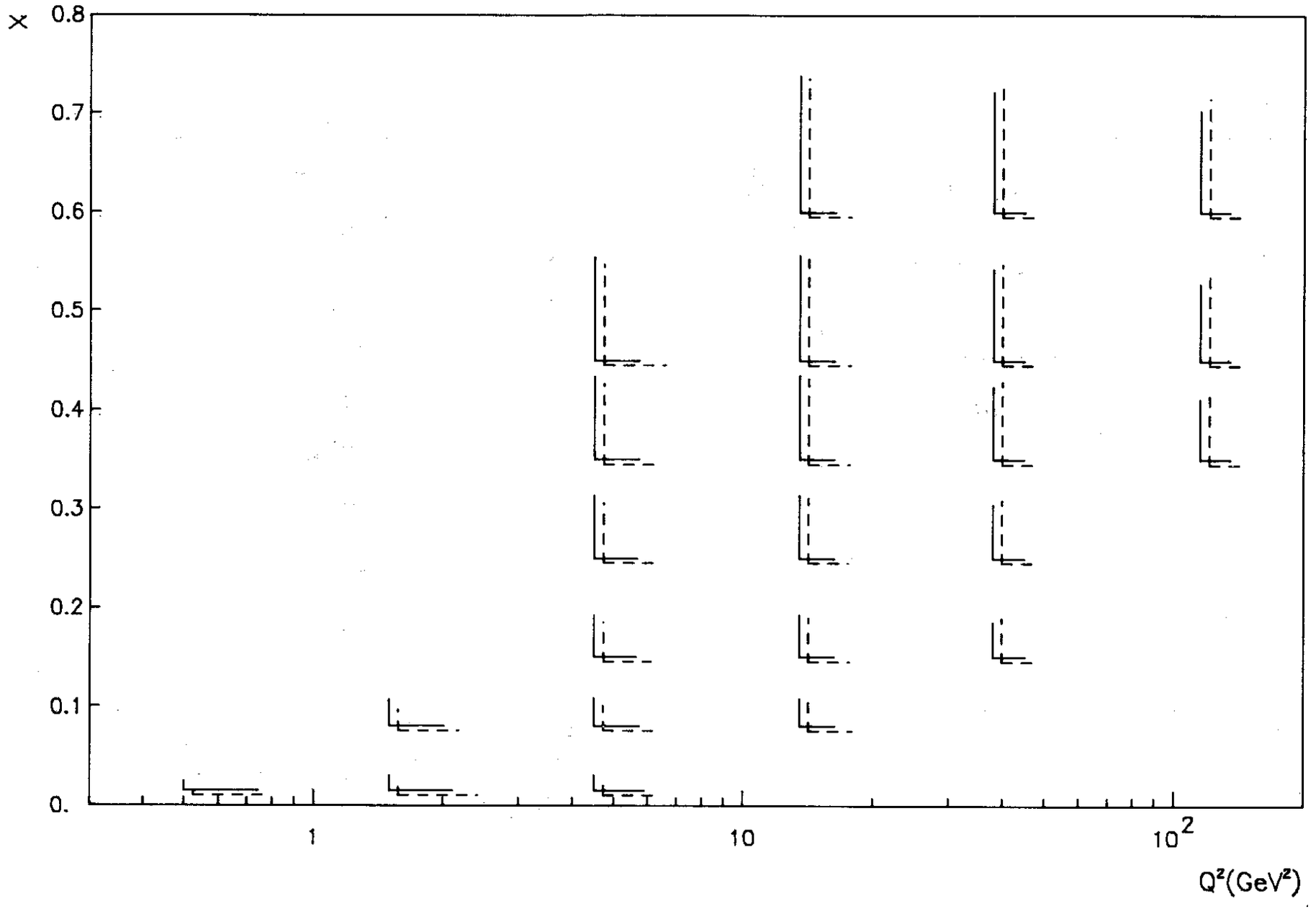

Fig. 10

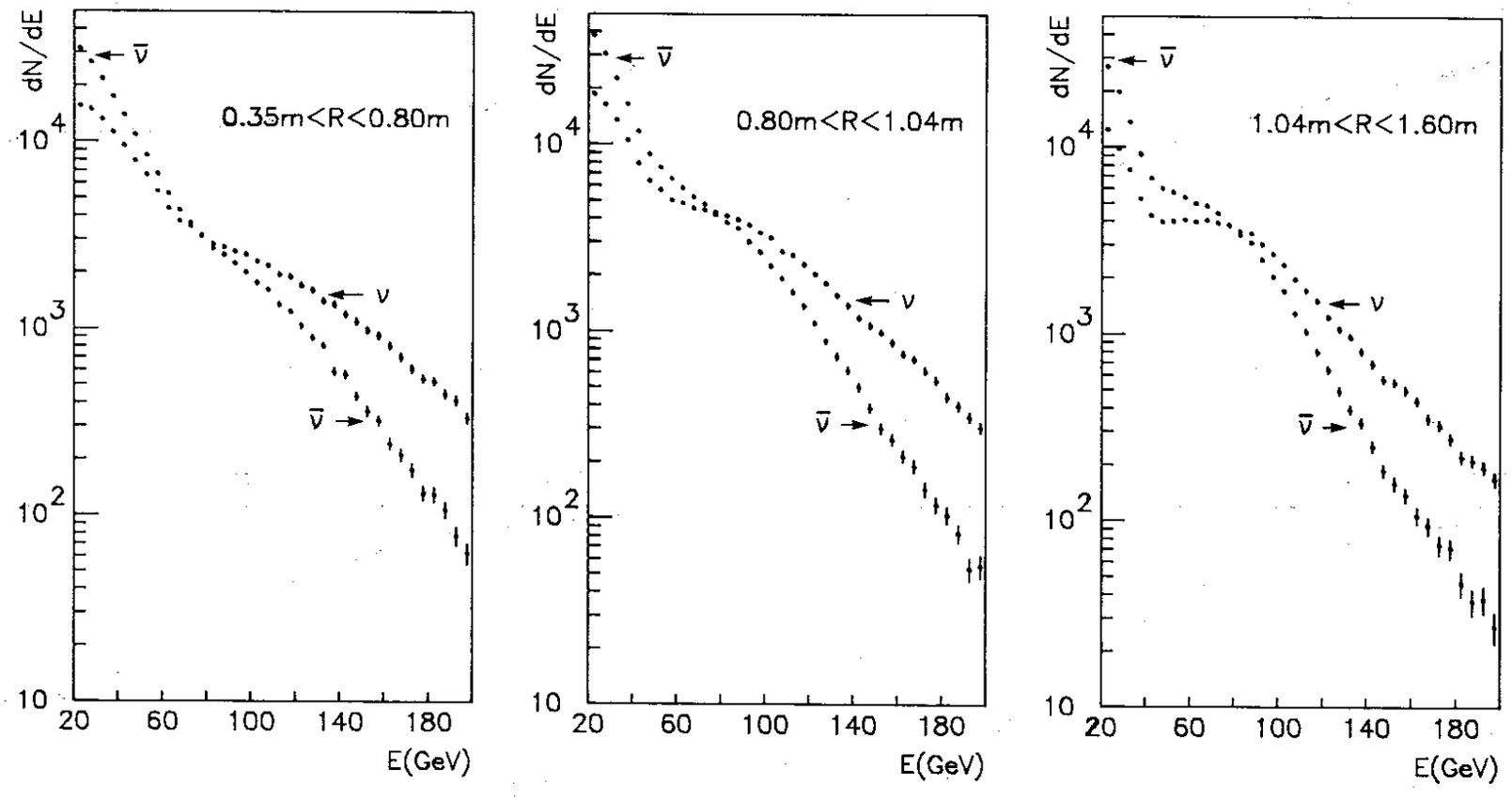
dN/dE
$\bar{\nu}$
0.35m<R<0.80m
ν
$\bar{\nu}$
10^4
10^3
10^2
10
20
60
100
140
180
E(GeV)
dN/dE
$\bar{\nu}$
0.80m<R<1.04m
ν
$\bar{\nu}$
10^4
10^3
10^2
10
20
60
100
140
180
E(GeV)
dN/dE
$\bar{\nu}$
1.04m<R<1.60m
ν
$\bar{\nu}$
10^4
10^3
10^2
10
20
60
100
140
180
E(GeV)

Fig. 11

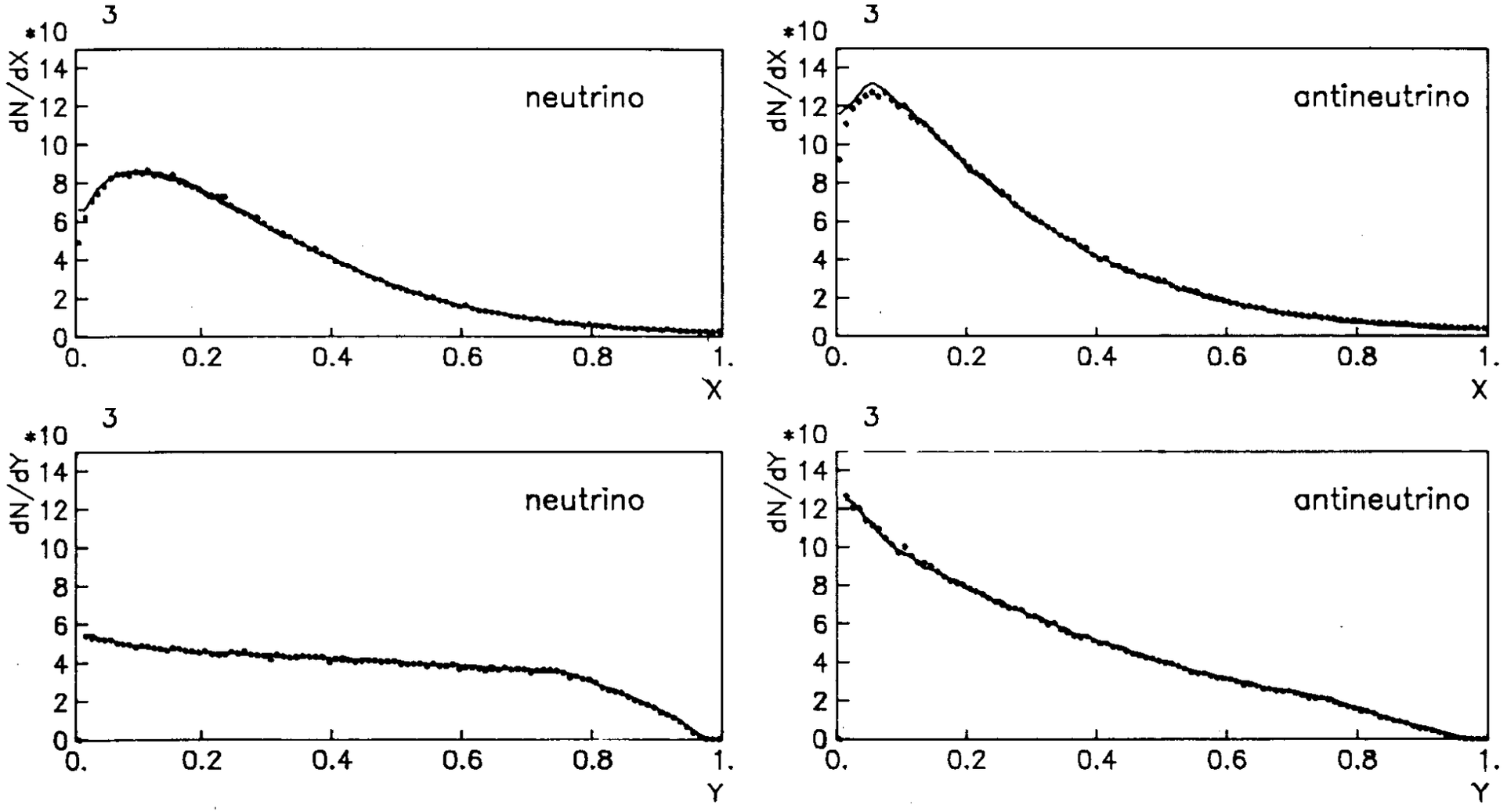
3
*10
dN/dX
neutrino
antineutrino
dN/dY
X
Y
0.
0.2
0.4
0.6
0.8
1.
0
2
4
6
8
10
12
14

Fig. 12

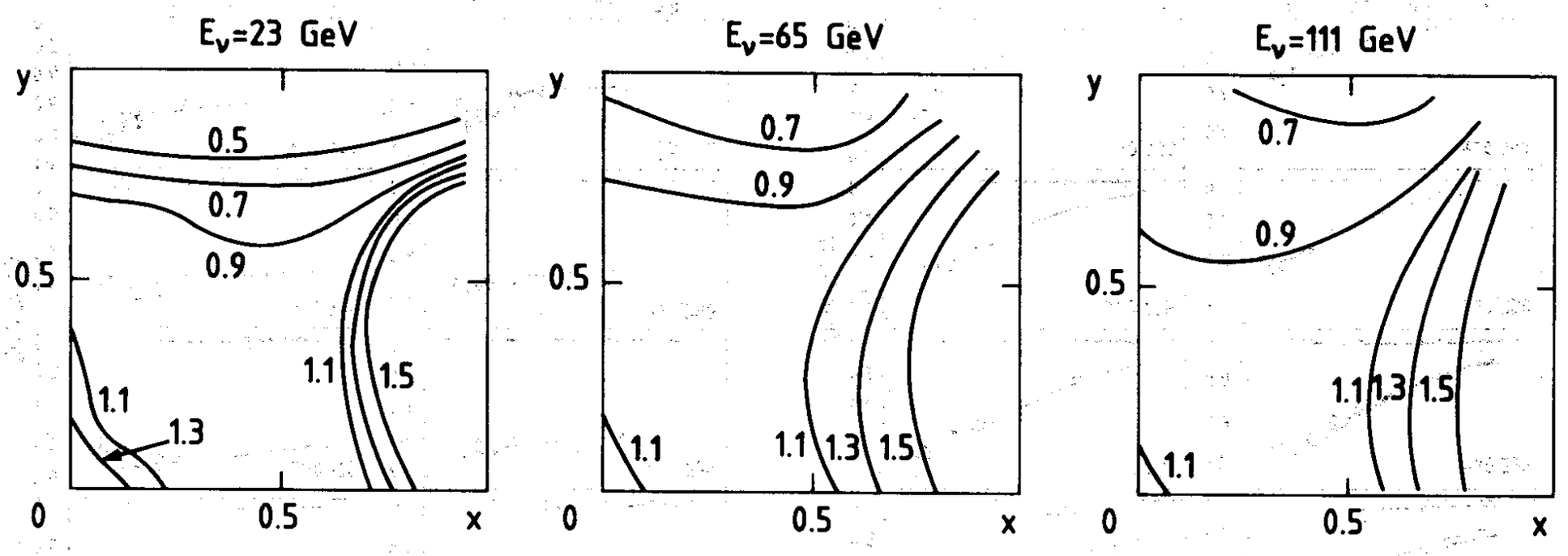

Fig. 13

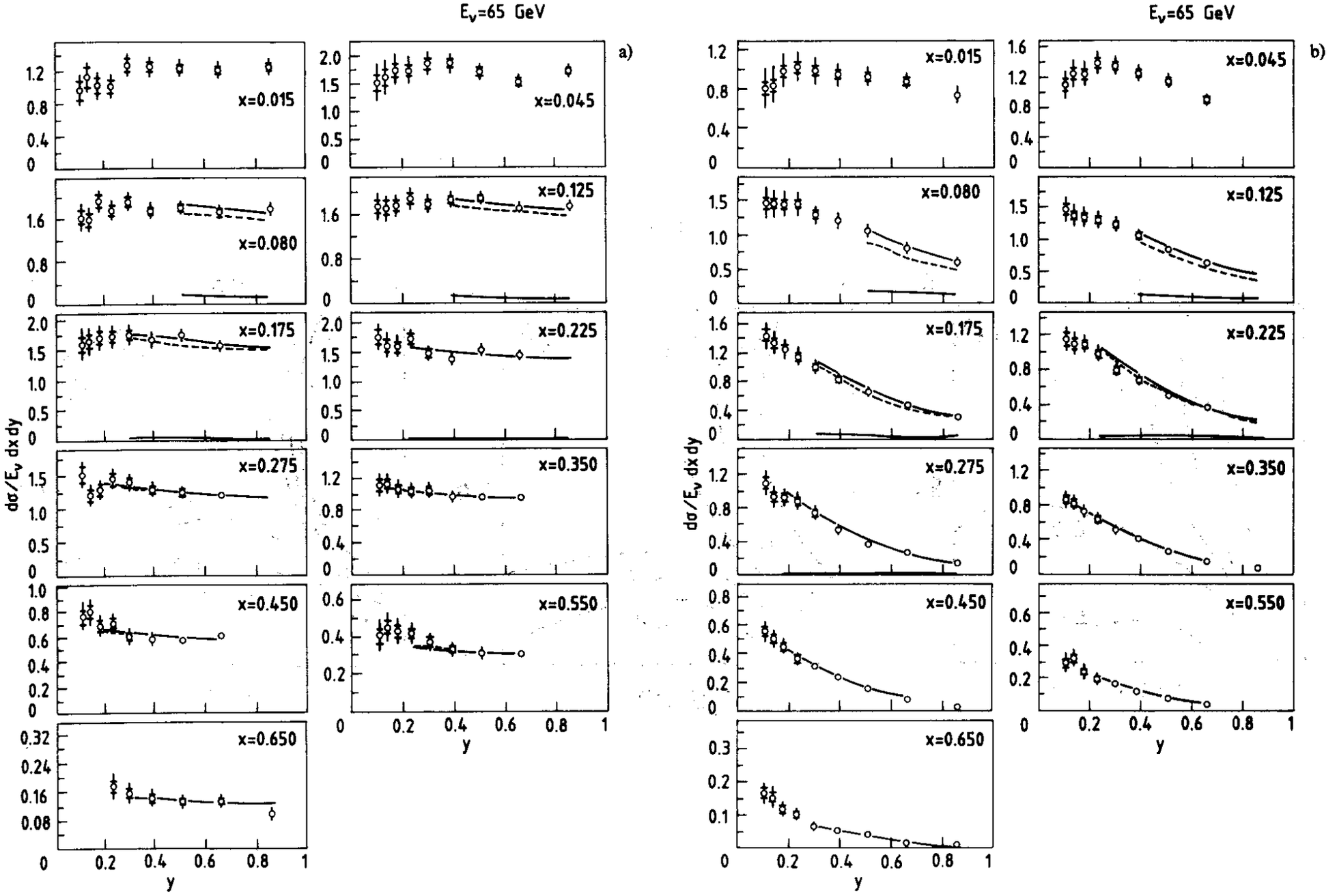
E_ν=65 GeV
a)
x=0.015
x=0.045
x=0.080
x=0.125
x=0.175
x=0.225
x=0.275
x=0.350
x=0.450
x=0.550
x=0.650
$d\sigma/E_\nu\, dx\, dy$
y
E_ν=65 GeV
b)
x=0.015
x=0.045
x=0.080
x=0.125
x=0.175
x=0.225
x=0.275
x=0.350
x=0.450
x=0.550
x=0.650
$d\sigma/E_\nu\, dx\, dy$
y

Fig. 14

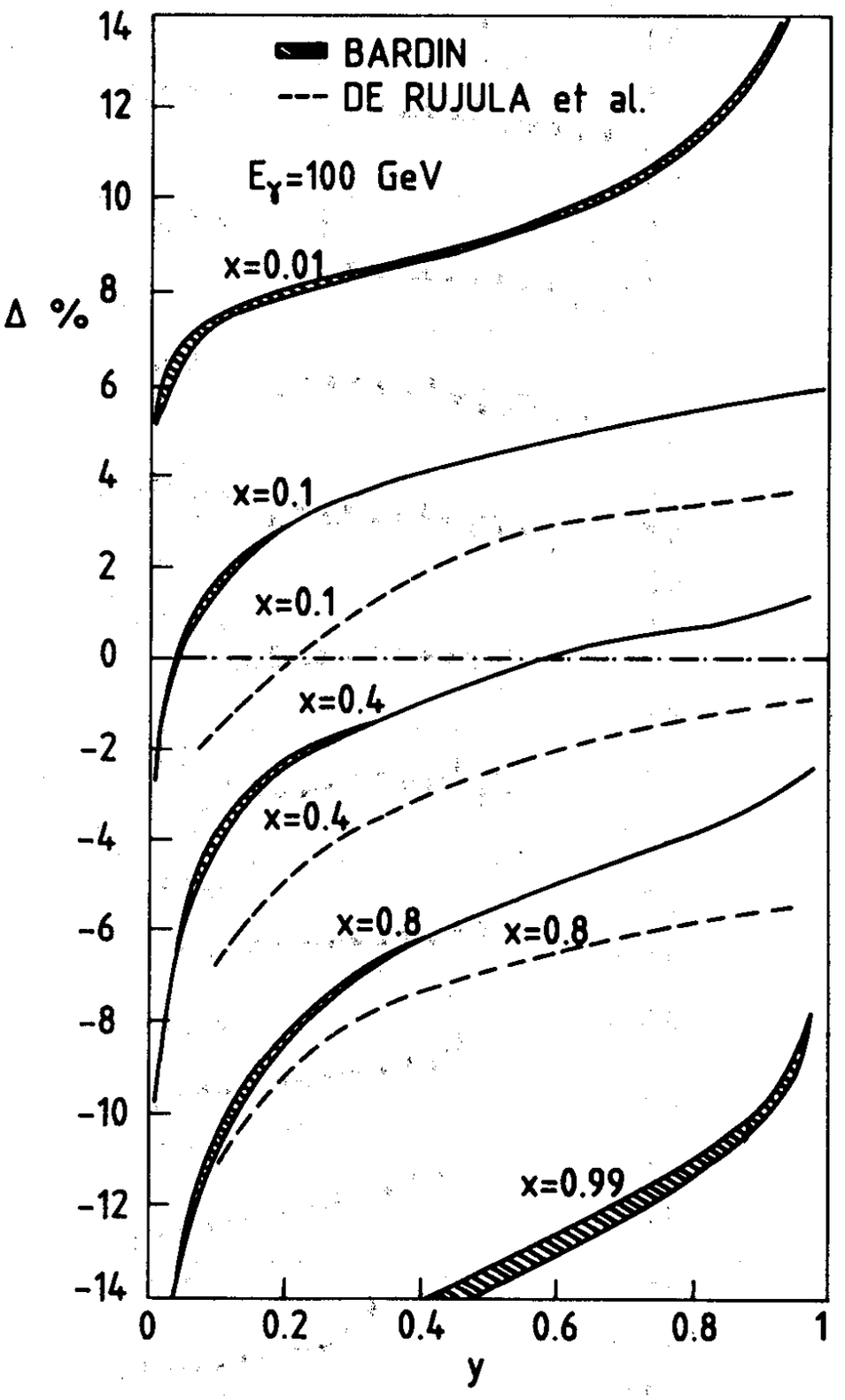
BARDIN
--- DE RUJULA et al.
E_γ=100 GeV
x=0.01
x=0.1
x=0.1
x=0.4
x=0.4
x=0.8
x=0.8
x=0.99
Δ %
y
14
12
10
8
6
4
2
0
-2
-4
-6
-8
-10
-12
-14
0
0.2
0.4
0.6
0.8
1

Fig. 15

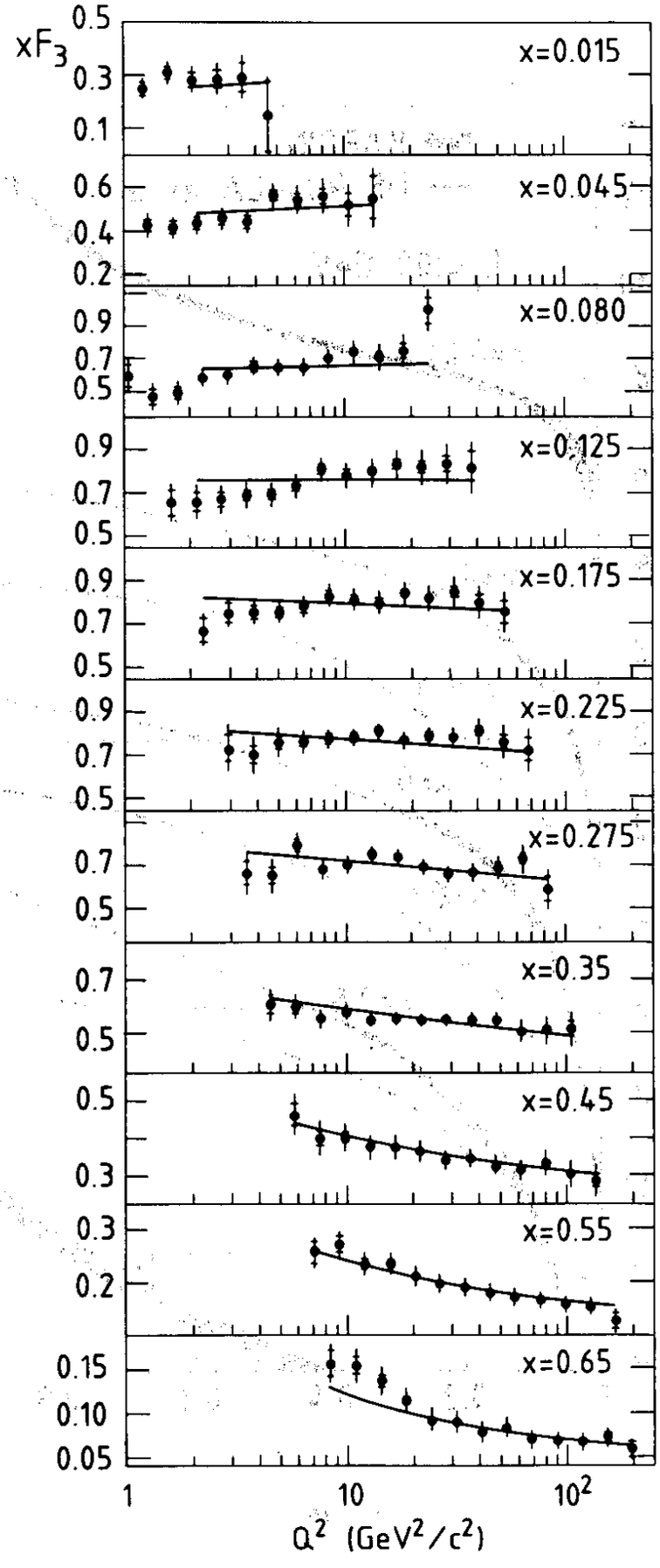
xF3
x=0.015
x=0.045
x=0.080
x=0.125
x=0.175
x=0.225
x=0.275
x=0.35
x=0.45
x=0.55
x=0.65
Q2 (GeV2/c2)

Fig. 16

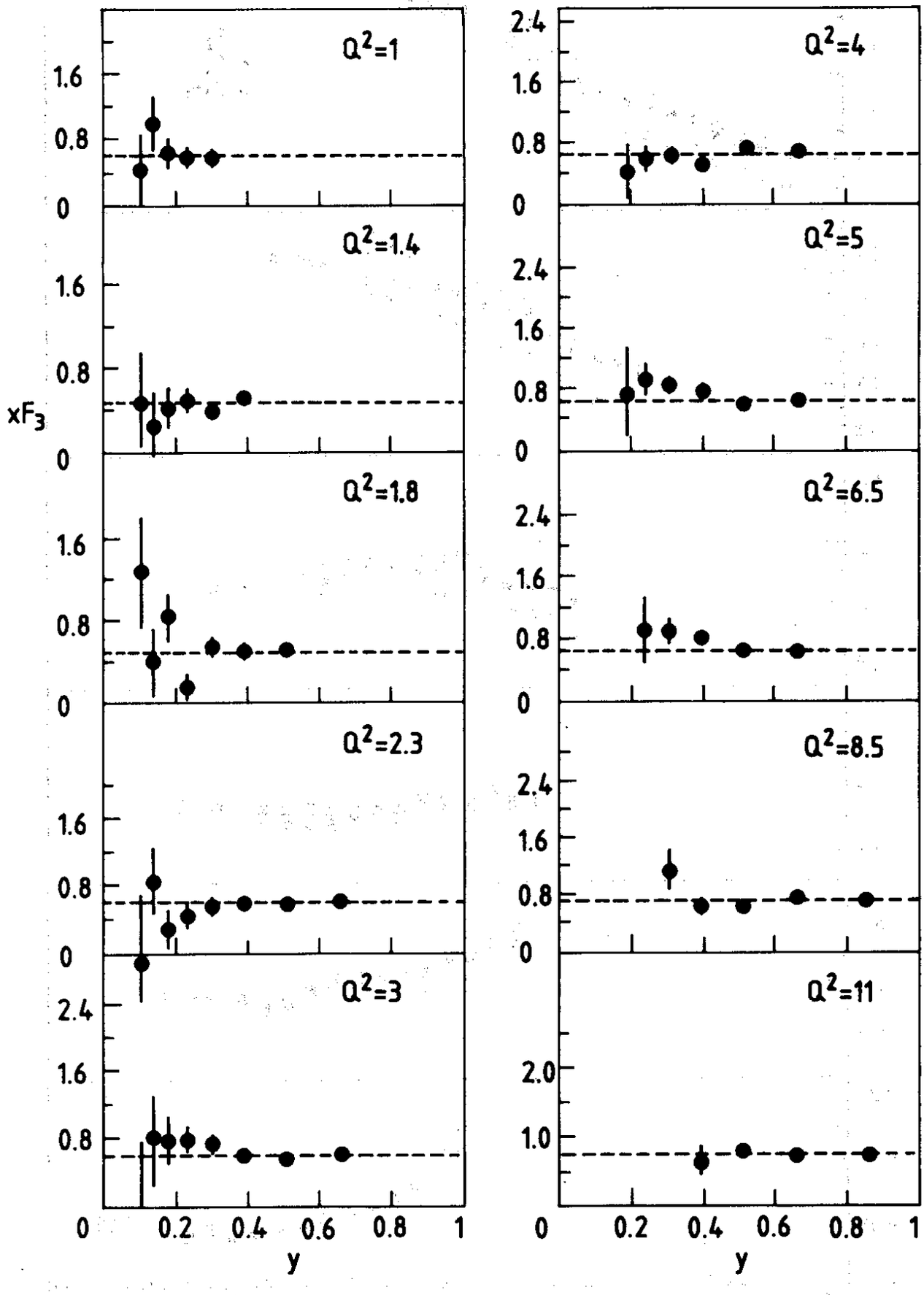

Fig. 17

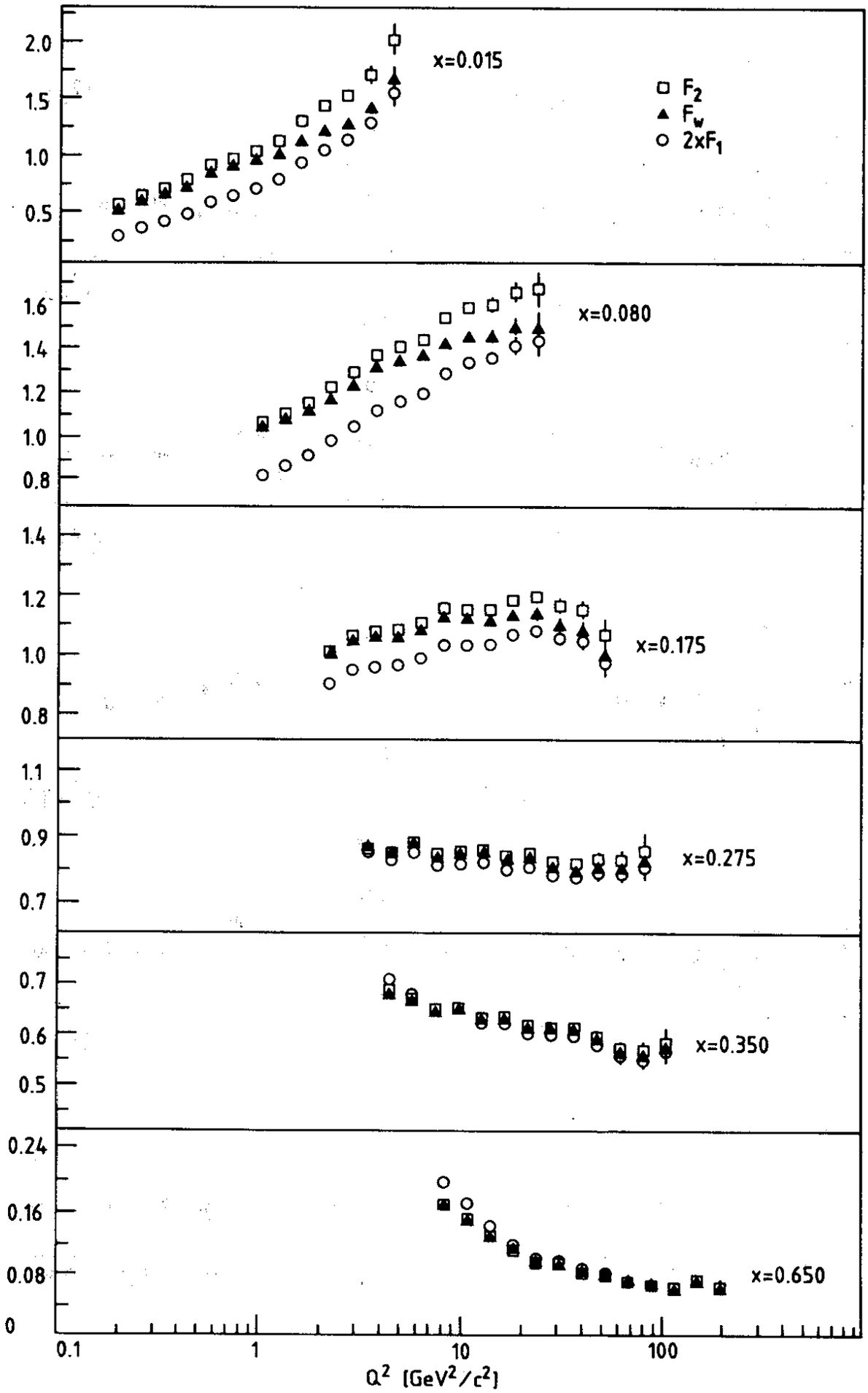

Fig. 18

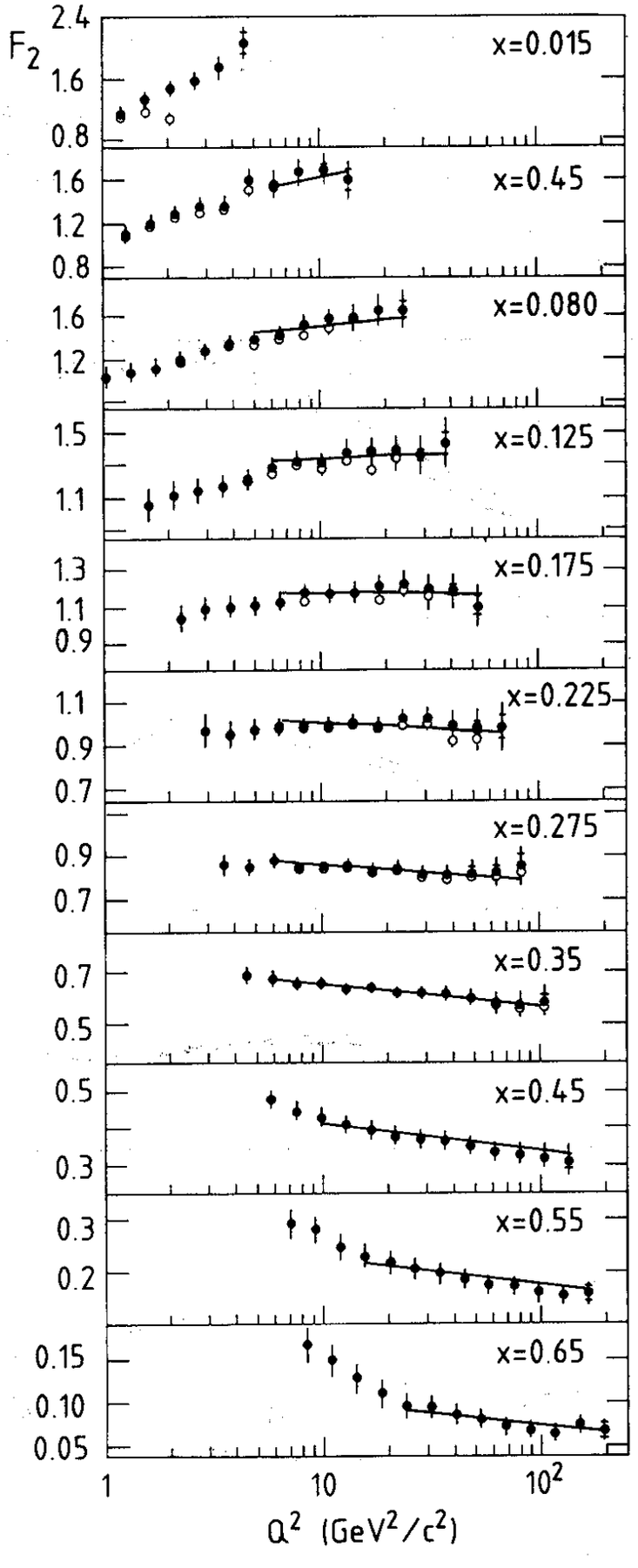
F_2
x=0.015
x=0.45
x=0.080
x=0.125
x=0.175
x=0.225
x=0.275
x=0.35
x=0.45
x=0.55
x=0.65
2.4
1.6
0.8
1.6
1.2
0.8
1.6
1.2
1.5
1.1
1.3
1.1
0.9
1.1
0.9
0.7
0.9
0.7
0.7
0.5
0.5
0.3
0.3
0.2
0.15
0.10
0.05
1
10
10^2
Q^2 (GeV^2/c^2)

Fig. 19

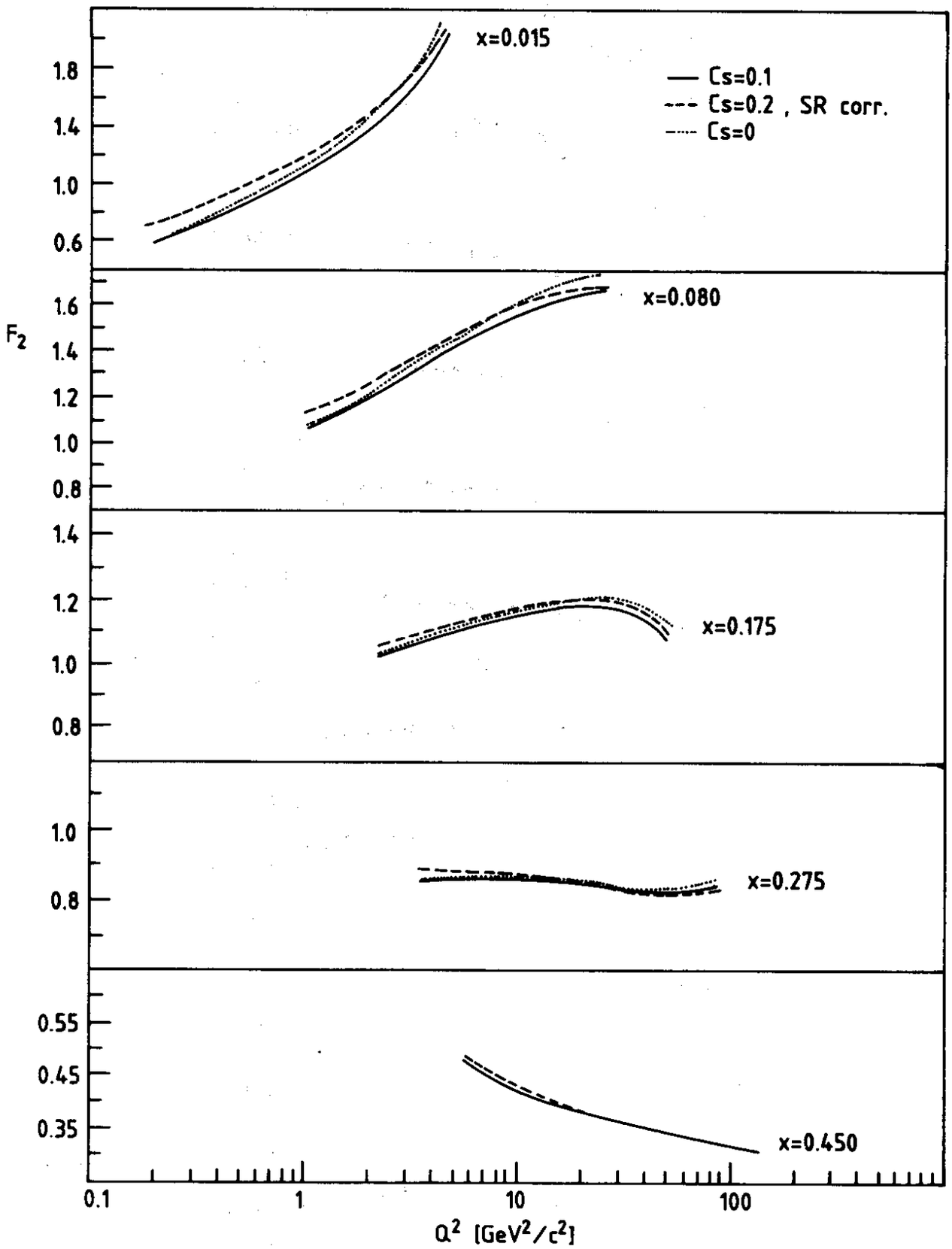
x=0.015
Cs=0.1
Cs=0.2 , SR corr.
Cs=0
x=0.080
x=0.175
x=0.275
x=0.450
F2
Q2 [GeV2/c2]
0.1
1
10
100

Fig. 20

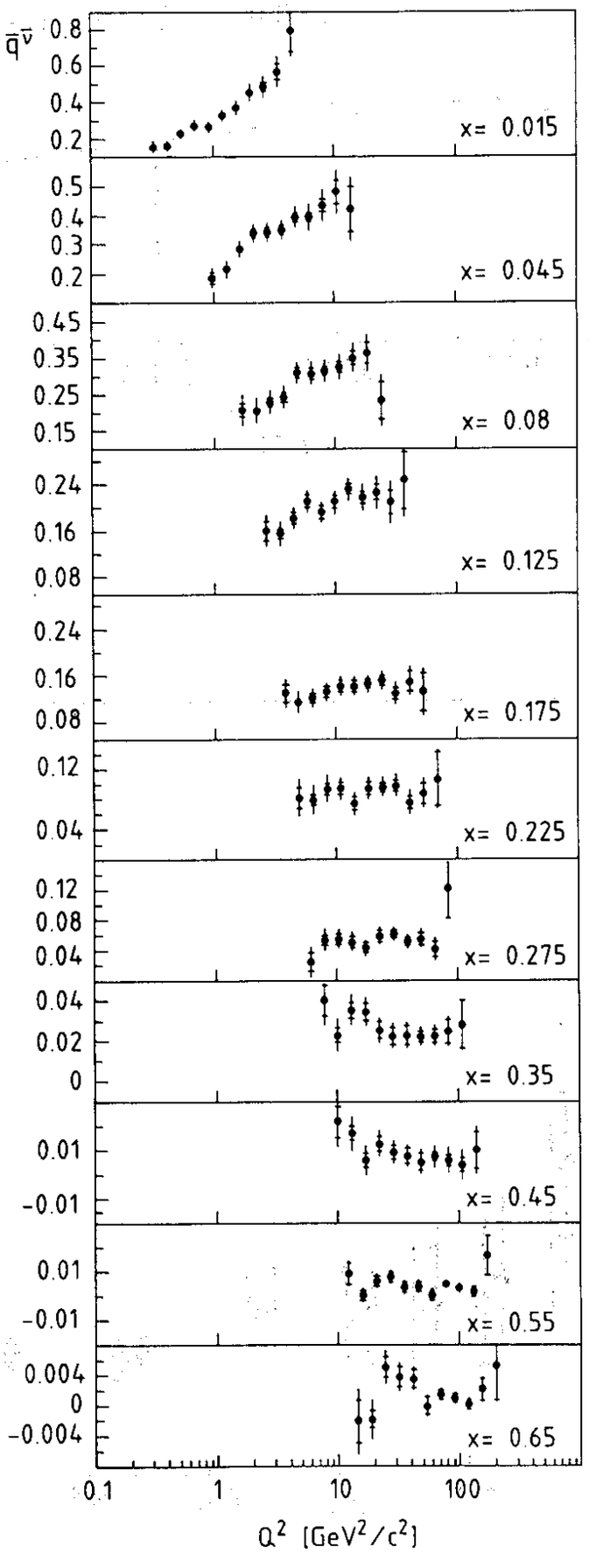
$\bar{q}^{\bar{\nu}}$
x= 0.015
x= 0.045
x= 0.08
x= 0.125
x= 0.175
x= 0.225
x= 0.275
x= 0.35
x= 0.45
x= 0.55
x= 0.65
0.1
1
10
100
Q^2 [GeV^2/c^2]

Fig. 21

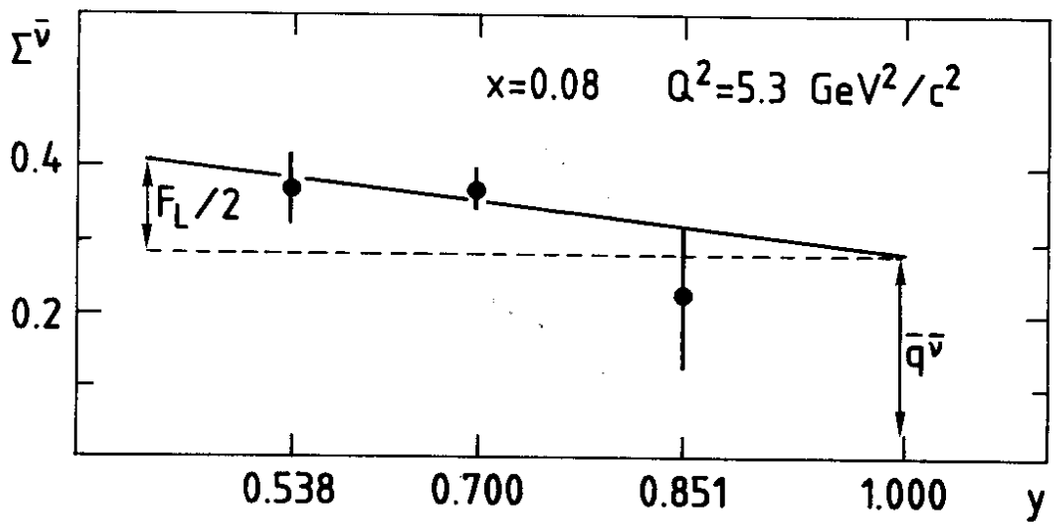
$\Sigma^{\bar{\nu}}$
x=0.08 Q^2=5.3 GeV^2/c^2
0.4
0.2
$F_L/2$
$\bar{q}^{\bar{\nu}}$
0.538
0.700
0.851
1.000
y

Fig. 22

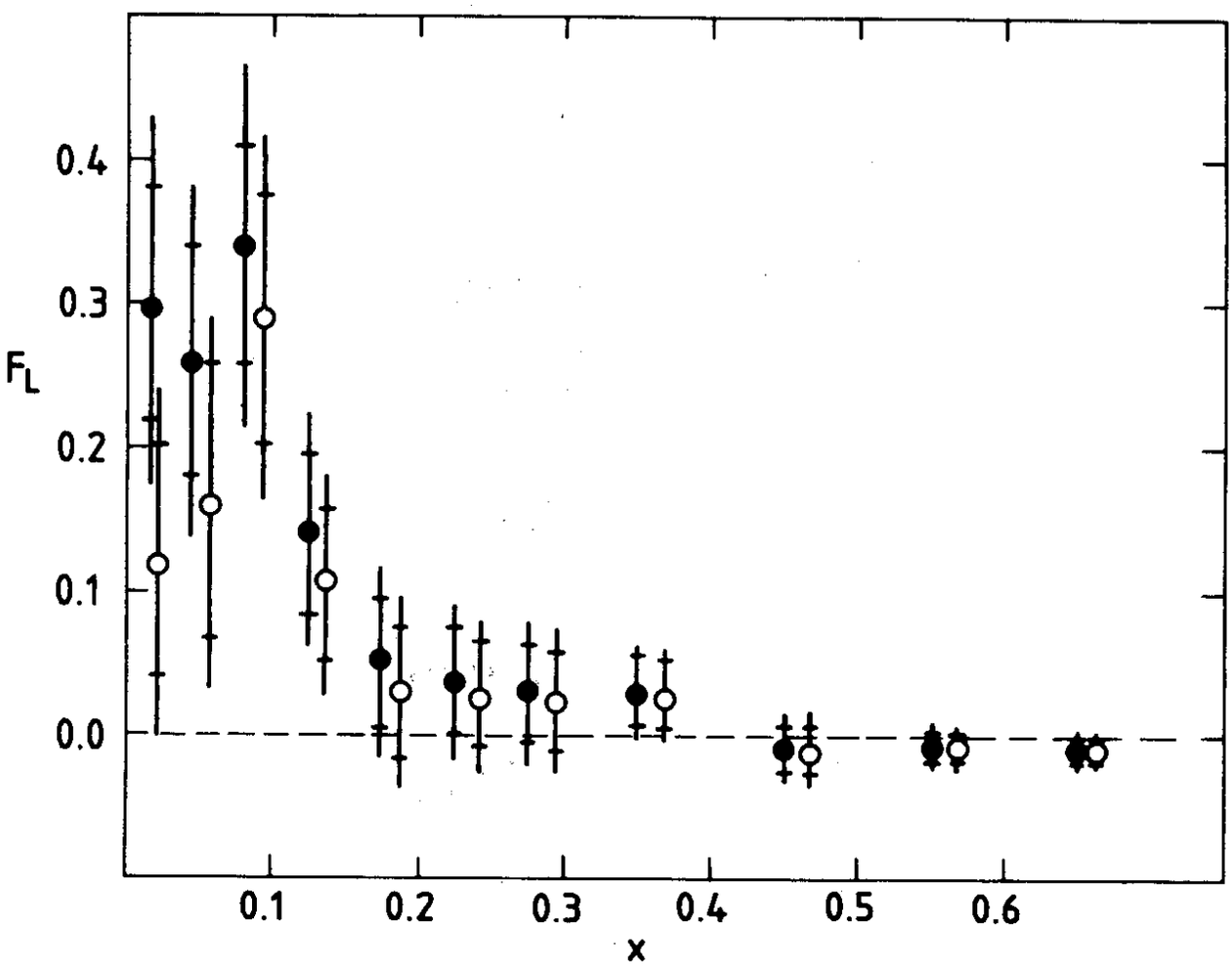
F_L
0.4
0.3
0.2
0.1
0.0
0.1
0.2
0.3
0.4
0.5
0.6
x

Fig. 23

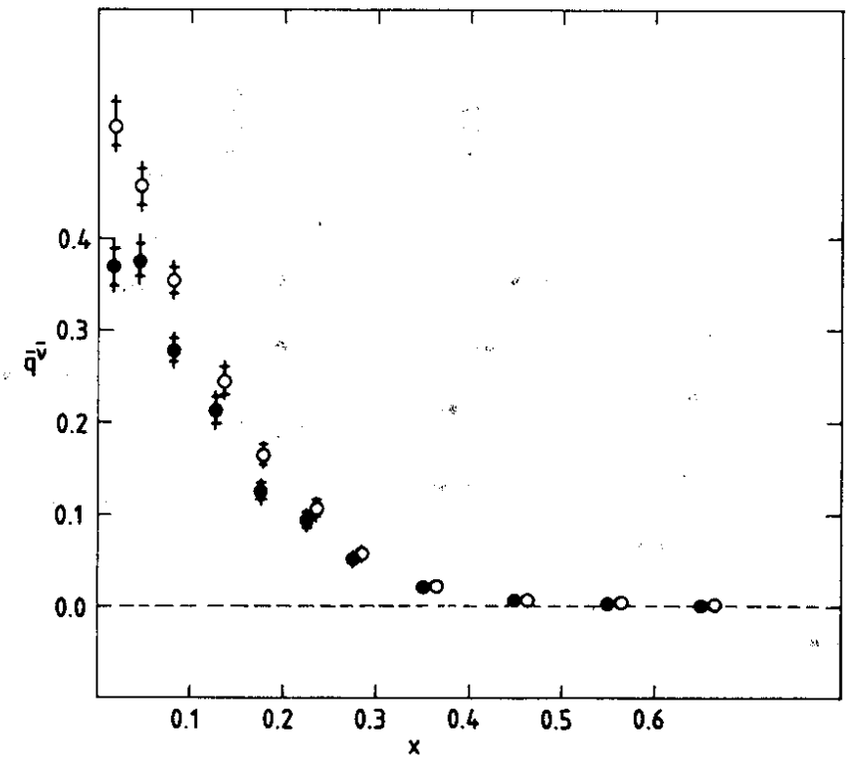
0.4
0.3
$\bar{q}\bar{v}$
0.2
0.1
0.0
0.1
0.2
0.3
0.4
0.5
0.6
x

Fig. 24

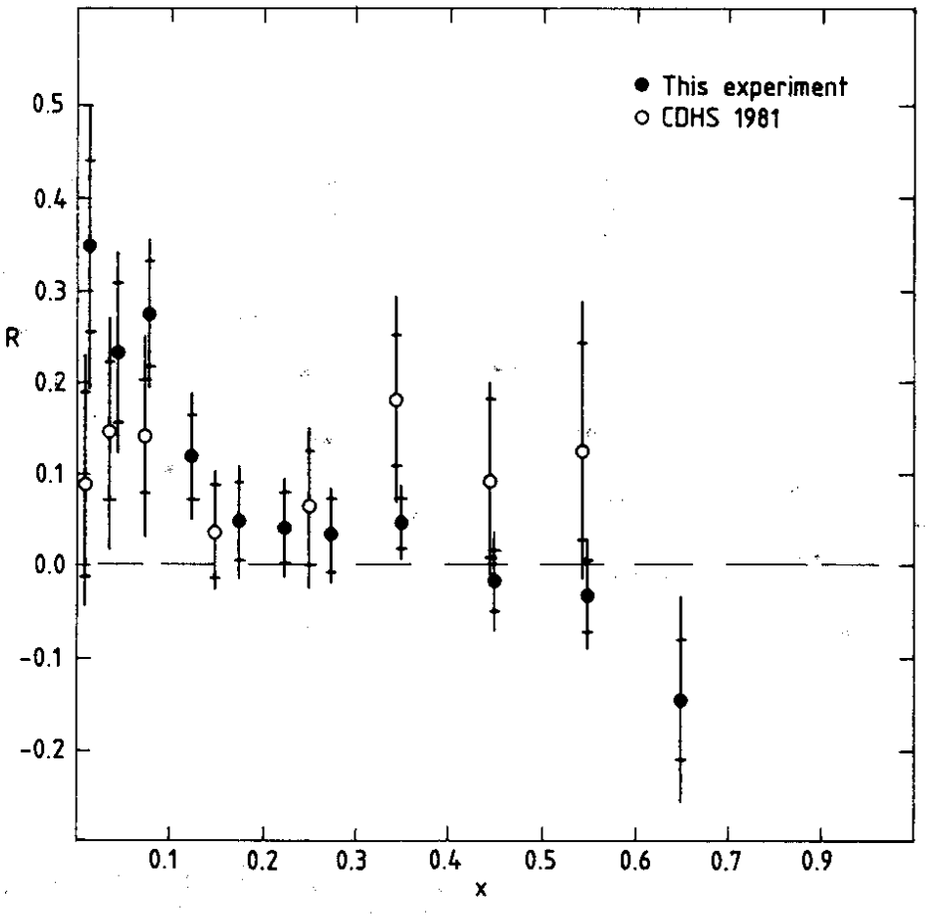
● This experiment
○ CDHS 1981
0.5
0.4
0.3
R
0.2
0.1
0.0
-0.1
-0.2
0.1
0.2
0.3
0.4
0.5
0.6
0.7
0.9
x

Fig. 25

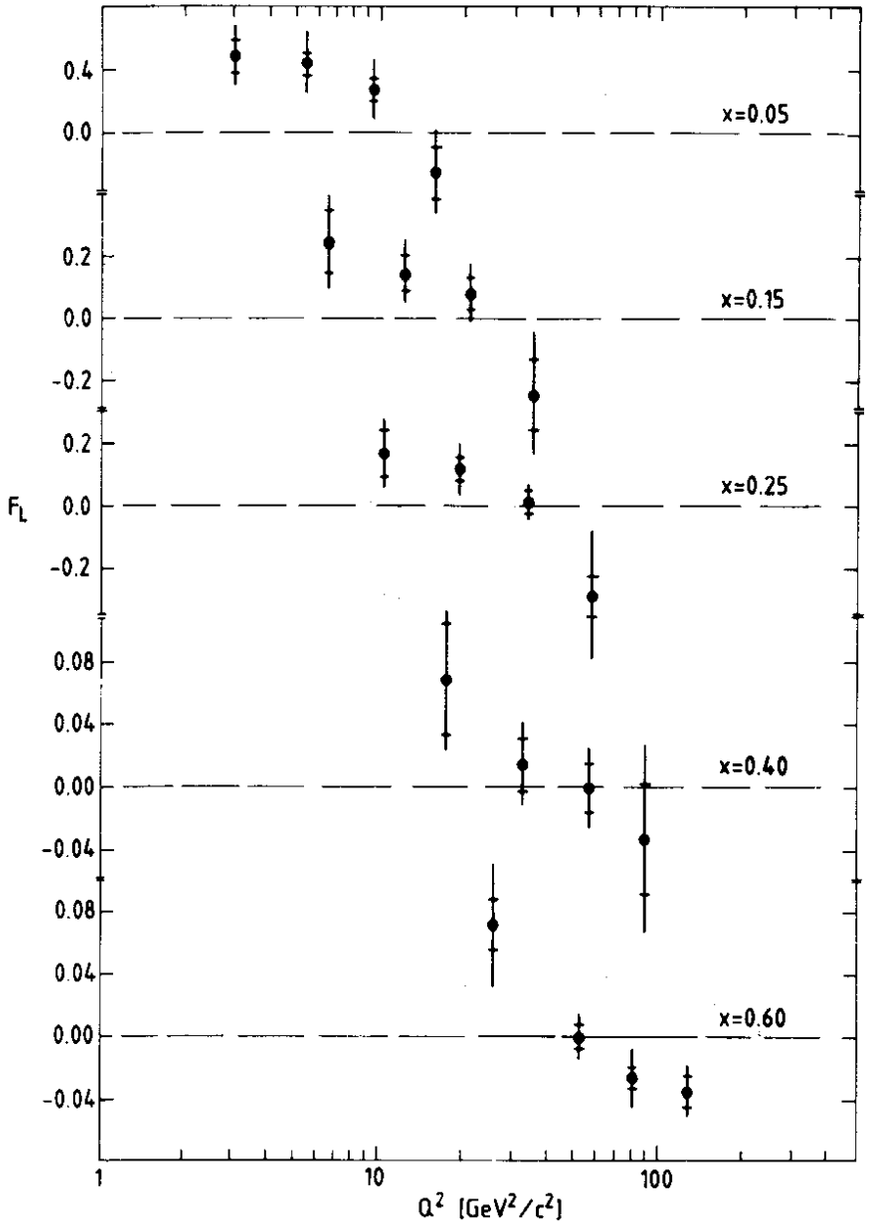
x=0.05
x=0.15
x=0.25
x=0.40
x=0.60
F_L
Q^2 [GeV^2/c^2]

Fig. 26

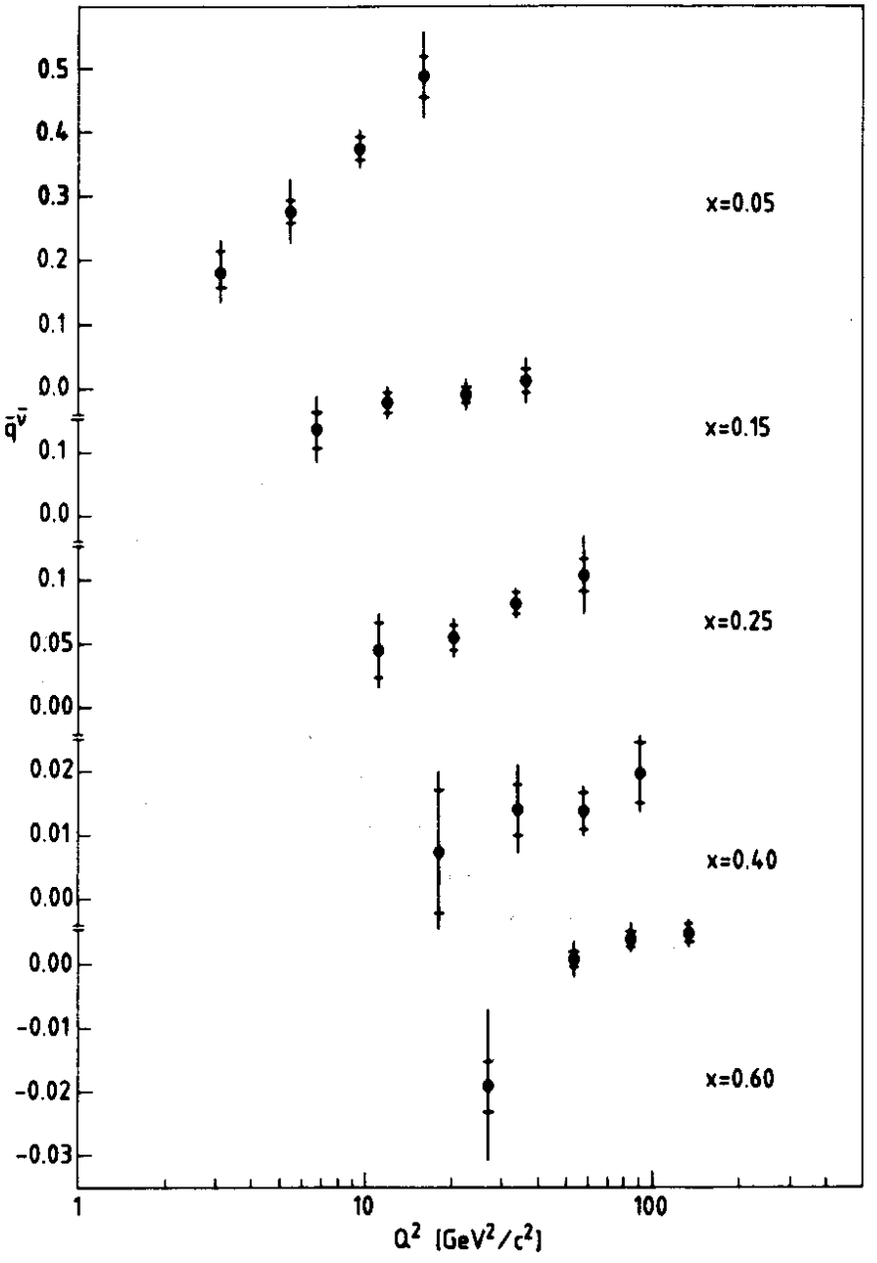
x=0.05
x=0.15
x=0.25
x=0.40
x=0.60
$\tilde{q}^{\nu_l}$
Q^2 [GeV^2/c^2]

Fig. 27

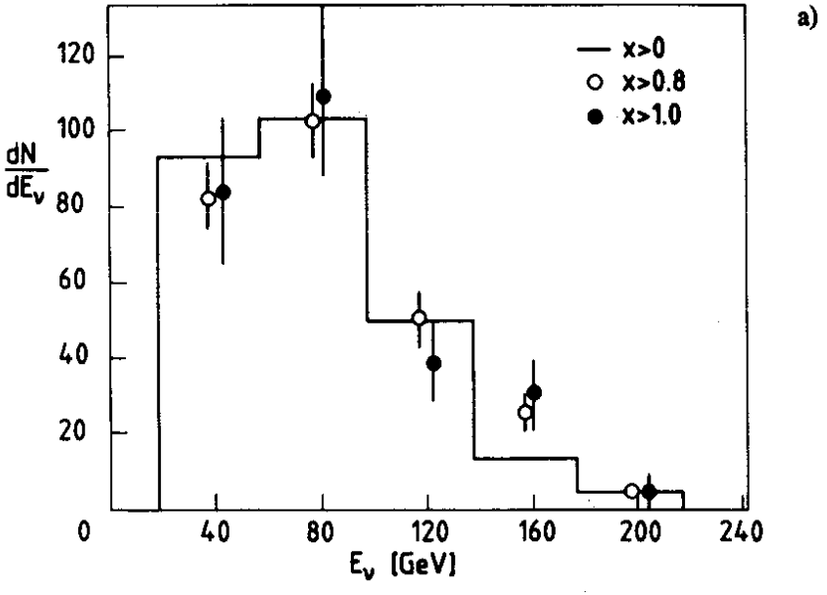
a)
x>0
x>0.8
x>1.0
dN/dE_ν
E_ν [GeV]
b)
x>0.45
x>0.8
x>1.0
dN/dE_ν̄
E_ν̄ [GeV]

Fig. 28

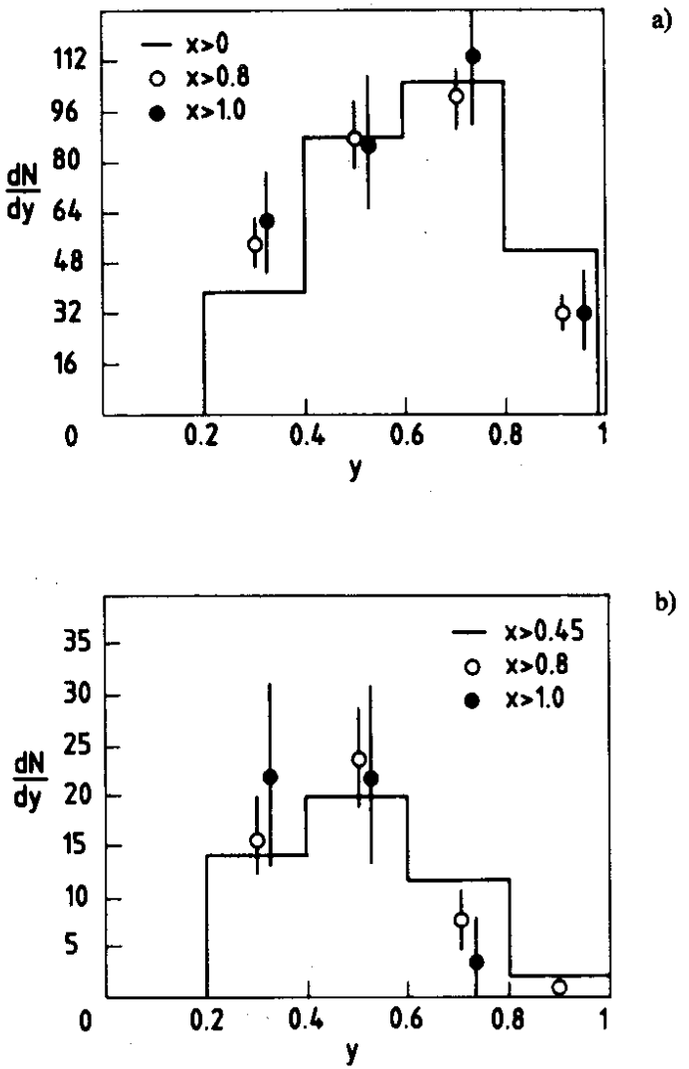
a)
x>0
x>0.8
x>1.0
dN/dy
y
b)
x>0.45
x>0.8
x>1.0
dN/dy
y

Fig. 29

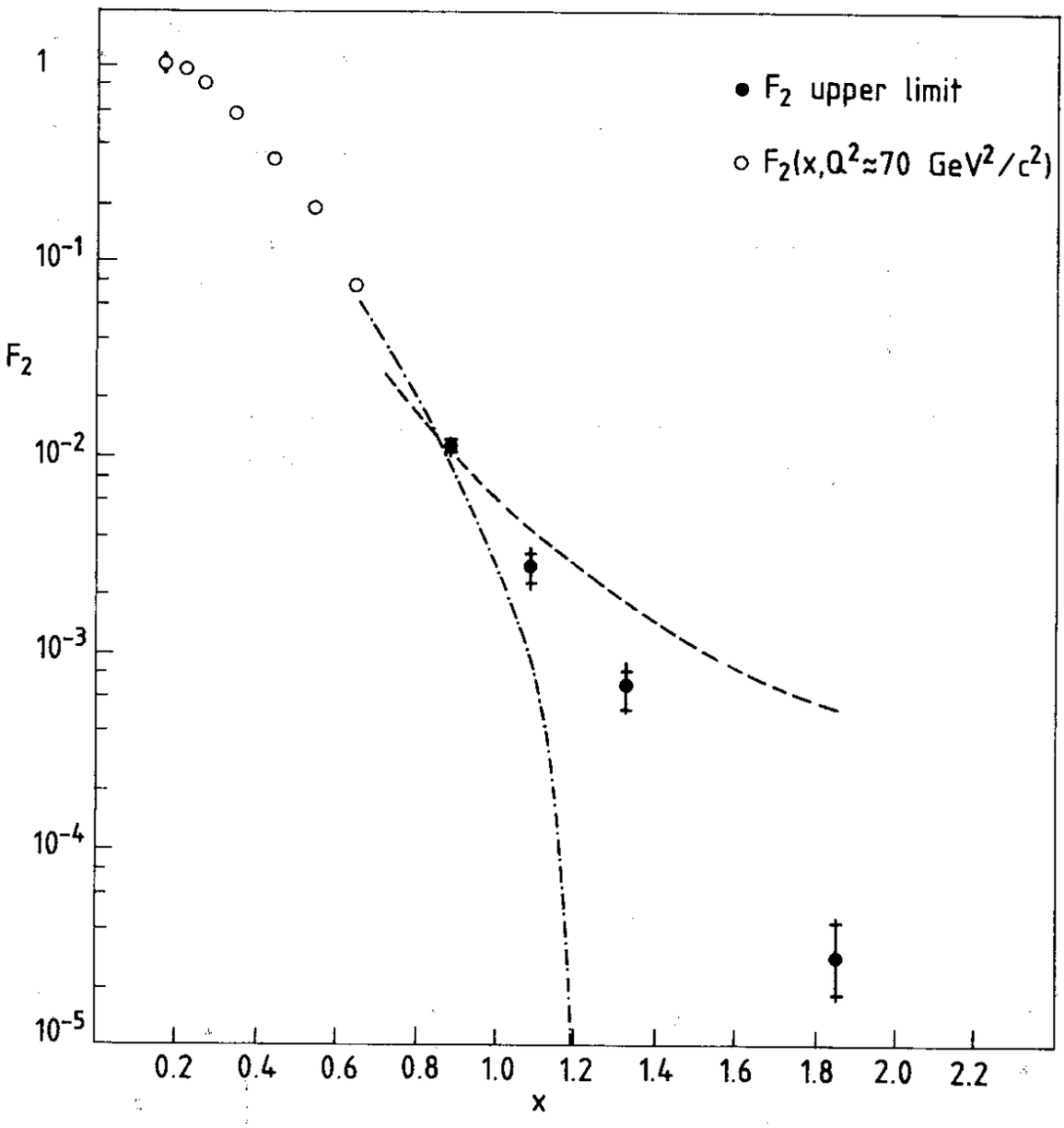
• F_2 upper limit
○ $F_2(x, Q^2 \approx 70\ GeV^2/c^2)$
F_2
1
10^{-1}
10^{-2}
10^{-3}
10^{-4}
10^{-5}
0.2
0.4
0.6
0.8
1.0
1.2
1.4
1.6
1.8
2.0
2.2
x

Fig. 30

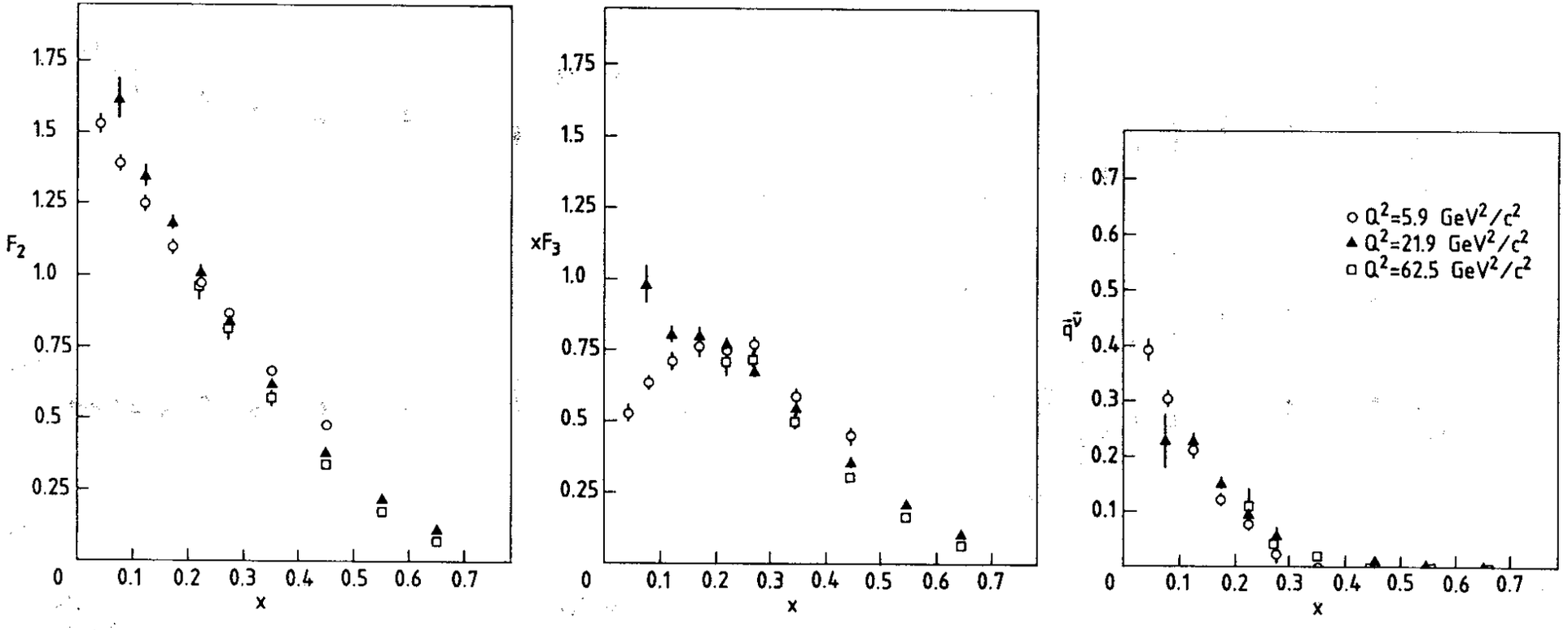
F2
xF3
x
1.75
1.5
1.25
1.0
0.75
0.5
0.25
0
0.1
0.2
0.3
0.4
0.5
0.6
0.7
q̄ν̄
0.7
0.6
0.5
0.4
0.3
0.2
0.1
○ Q²=5.9 GeV²/c²
▲ Q²=21.9 GeV²/c²
□ Q²=62.5 GeV²/c²

Fig. 31

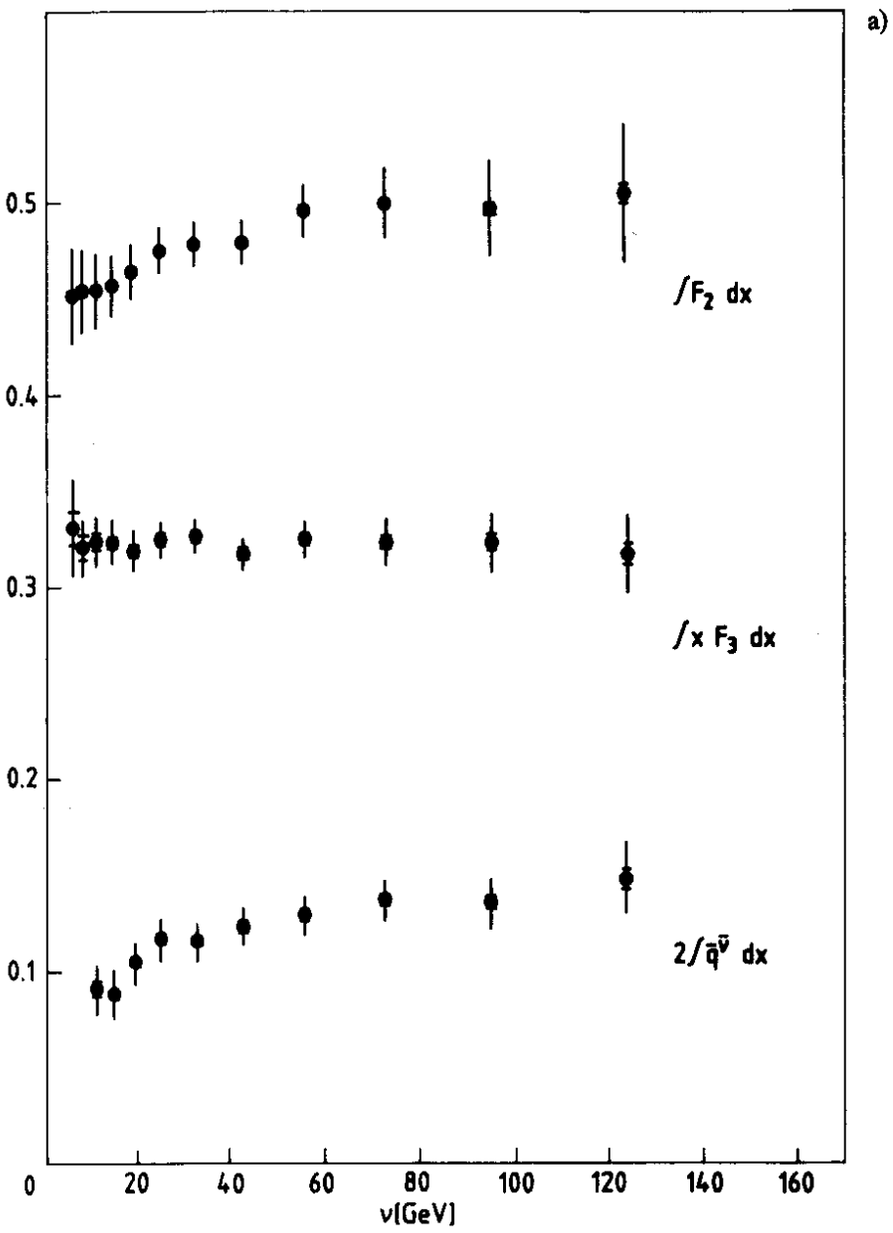
a)
0.5
0.4
0.3
0.2
0.1
0
20
40
60
80
100
120
140
160
ν[GeV]
∫F2 dx
∫x F3 dx
2∫q̄ν dx

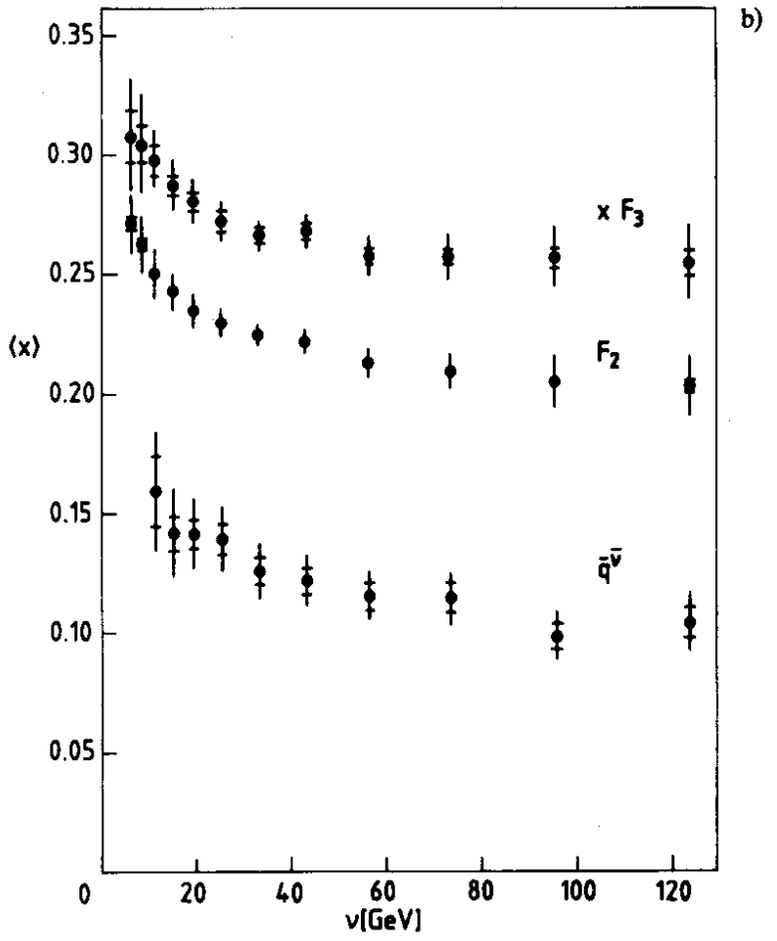
b)
0.35
0.30
0.25
0.20
0.15
0.10
0.05
0
20
40
60
80
100
120
ν[GeV]
⟨x⟩
x F3
F2
q̄ν

Fig. 32

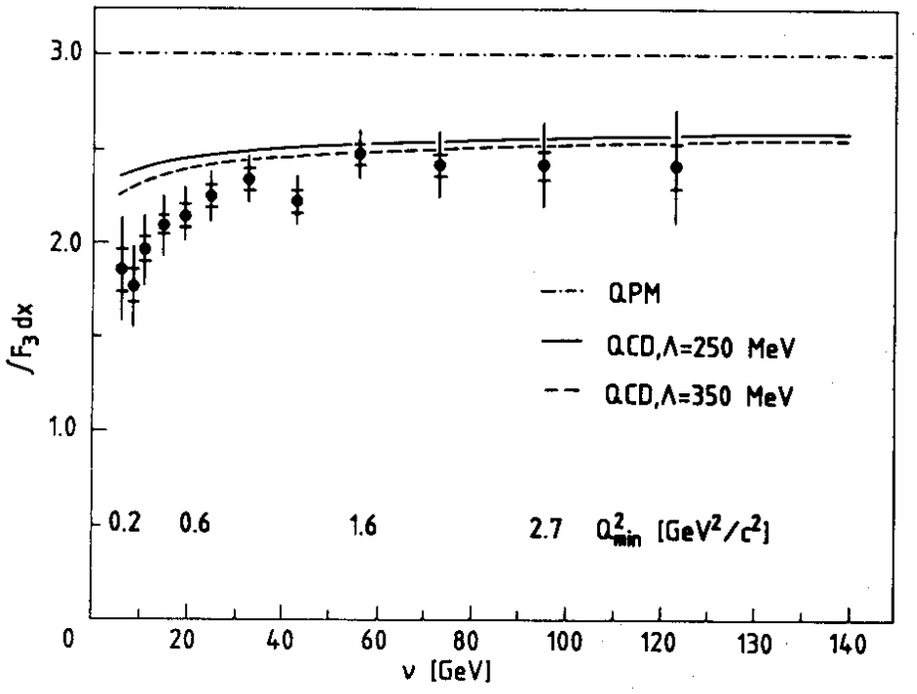
3.0
2.0
1.0
0
$\int F_3\,dx$
QPM
QCD,Λ=250 MeV
QCD,Λ=350 MeV
0.2
0.6
1.6
2.7
Q^2_{min} [GeV²/c²]
20
40
60
80
100
120
130
140
ν [GeV]

Fig. 33

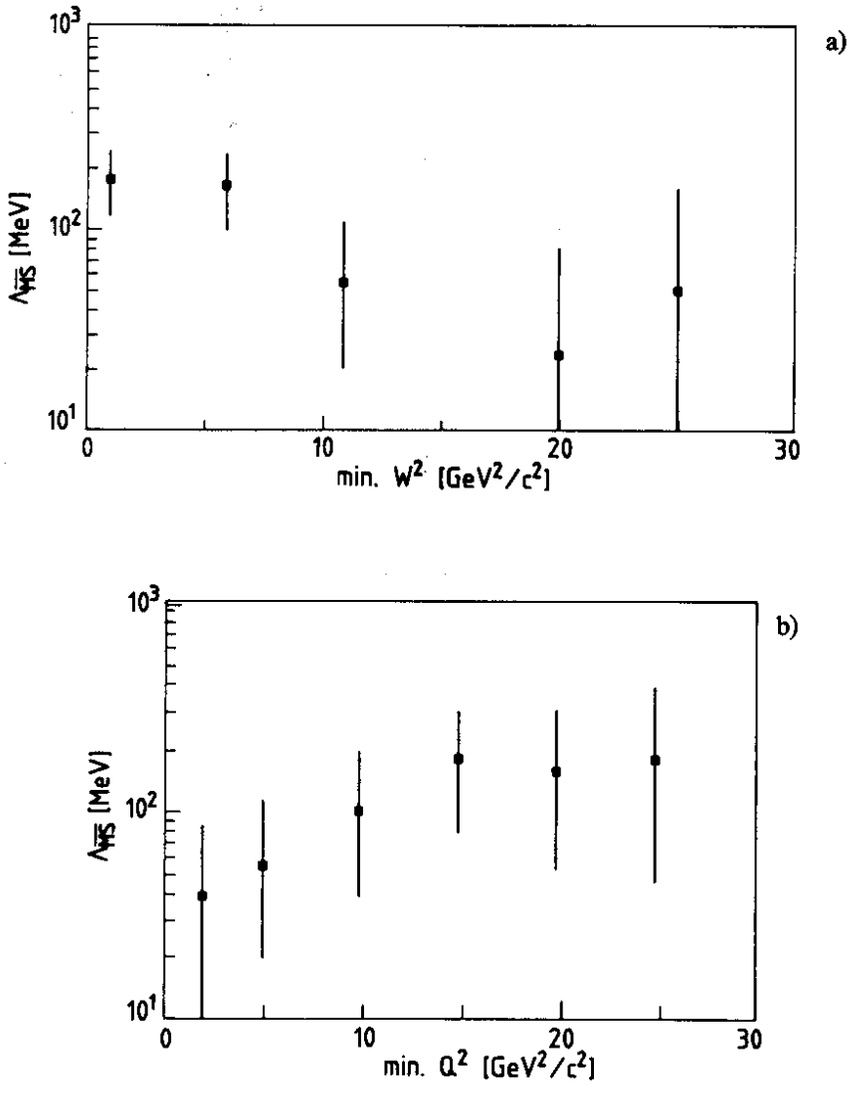
a)
10^3
10^2
10^1
$\Lambda_{\overline{MS}}$ [MeV]
0
10
20
30
min. W^2 [GeV²/c²]
b)
10^3
10^2
10^1
$\Lambda_{\overline{MS}}$ [MeV]
0
10
20
30
min. Q^2 [GeV²/c²]

Fig. 34

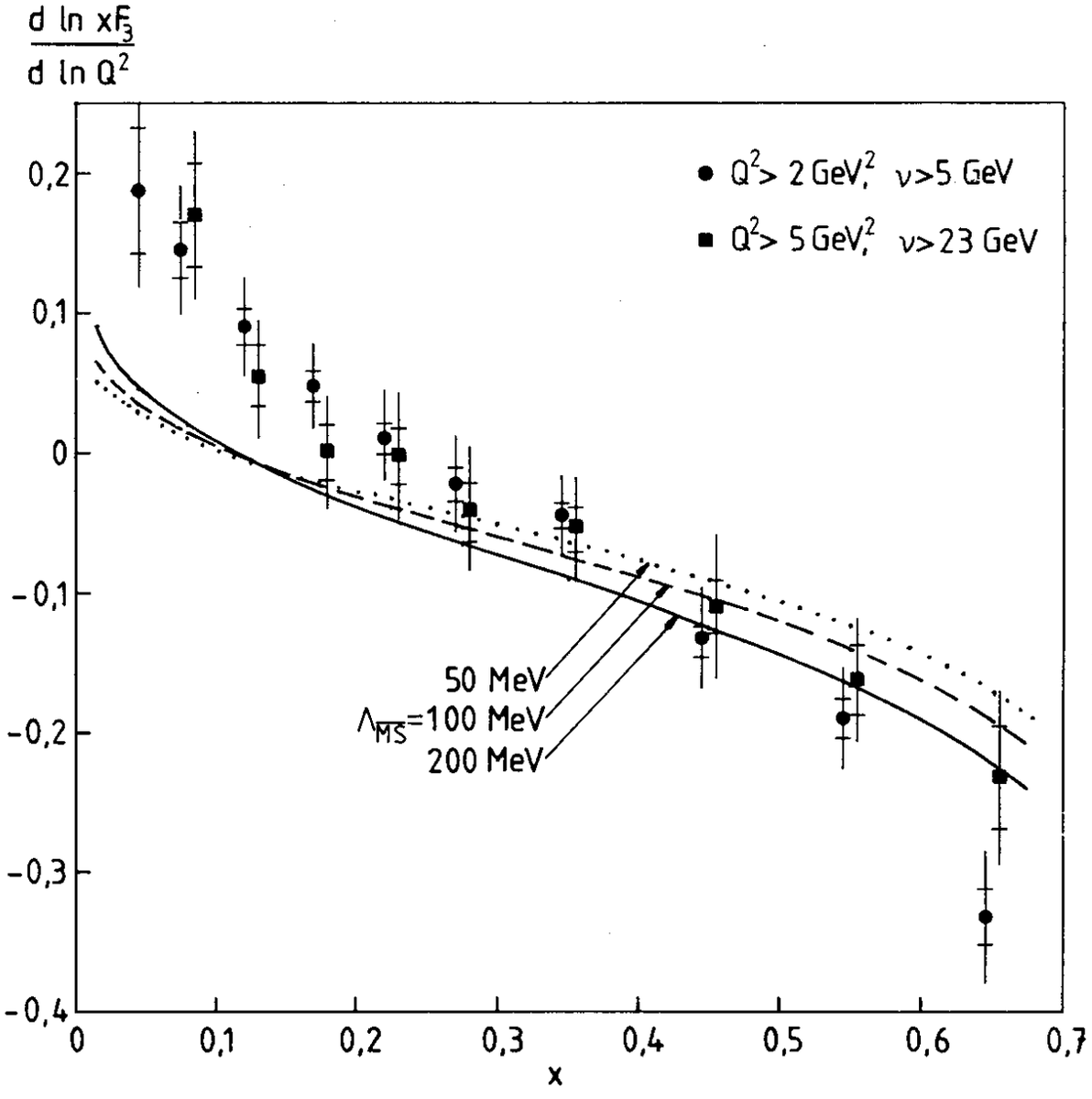
d ln xF3
d ln Q2
Q2> 2 GeV2, ν>5 GeV
Q2> 5 GeV2, ν>23 GeV
50 MeV
ΛMS=100 MeV
200 MeV
0,2
0,1
0
-0,1
-0,2
-0,3
-0,4
0
0,1
0,2
0,3
0,4
0,5
0,6
0,7
x

Fig. 35

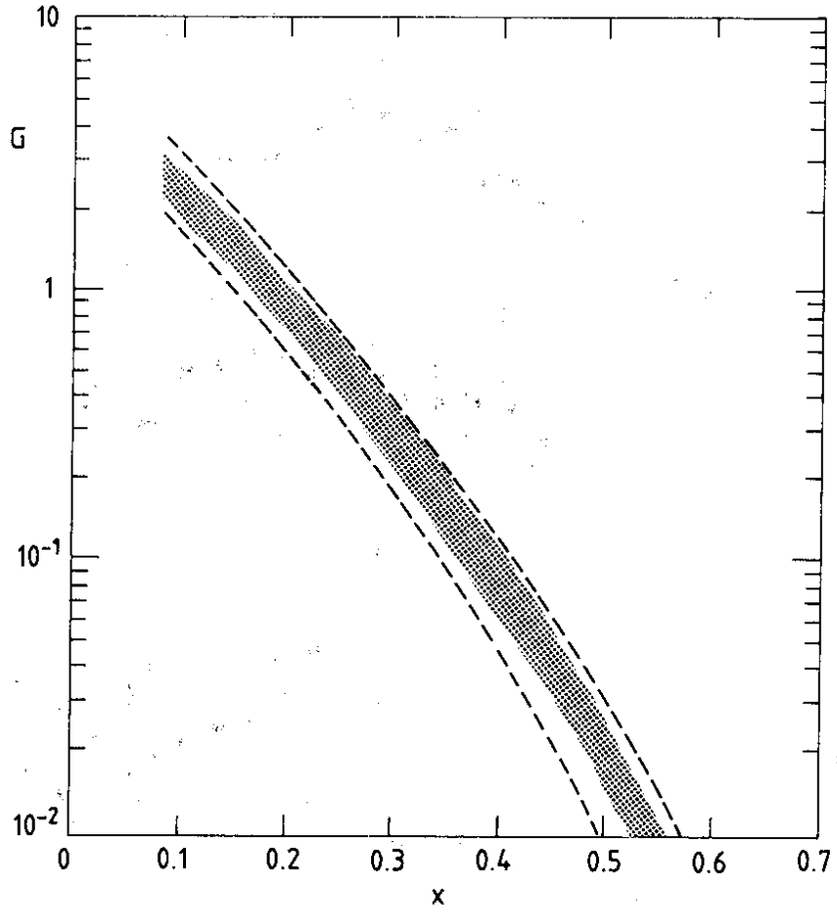
10
G
1
10^{-1}
10^{-2}
0
0.1
0.2
0.3
0.4
0.5
0.6
0.7
x

Fig. 36

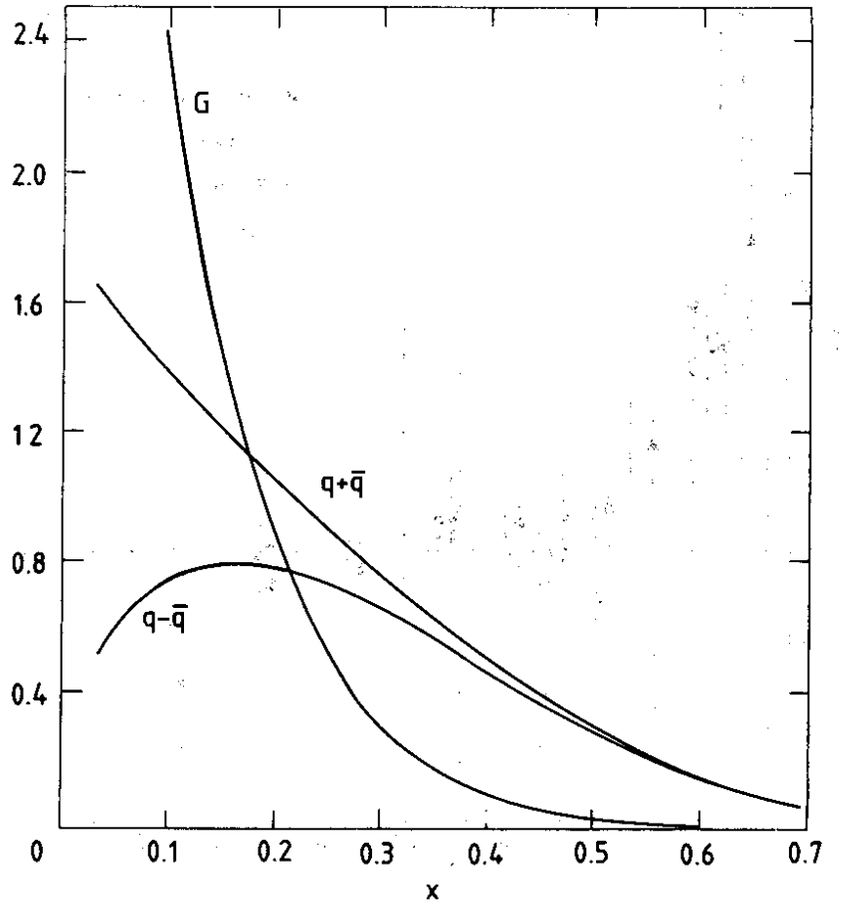
2.4
2.0
1.6
1 2
0.8
0.4
0
G
$q+\bar{q}$
$q-\bar{q}$
0.1
0.2
0.3
0.4
0.5
0.6
0.7
x

Fig. 37

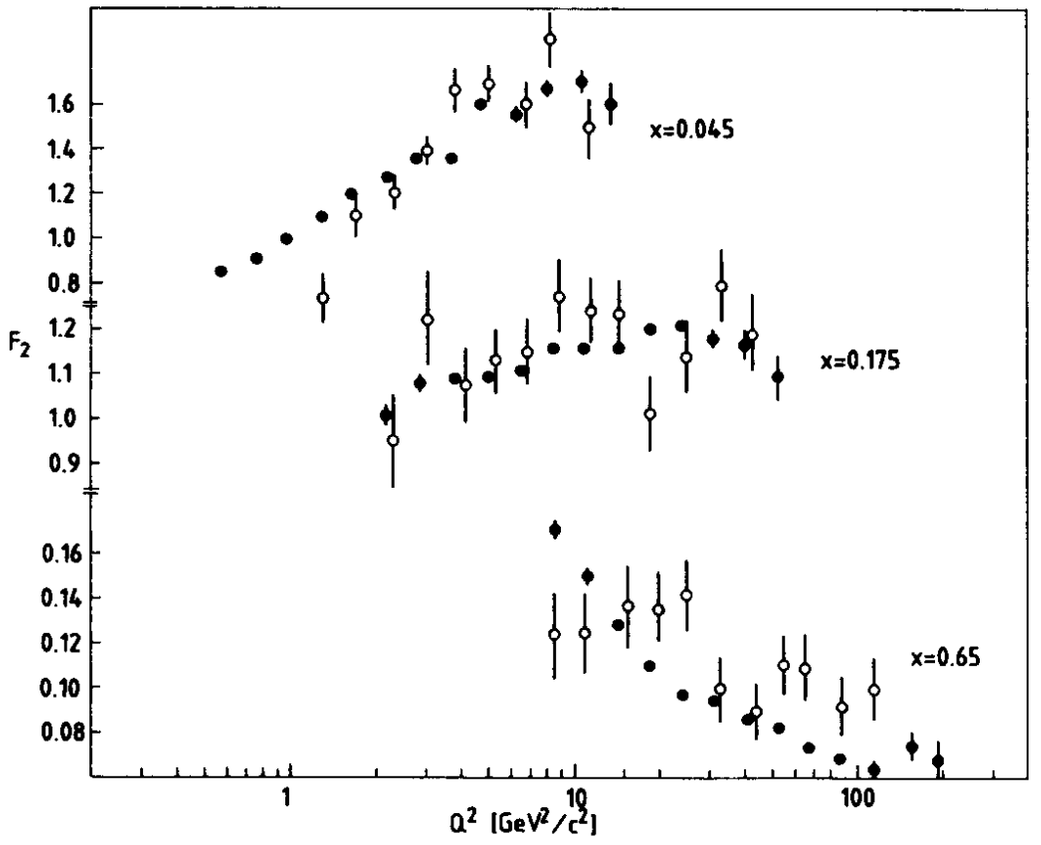
x=0.045
x=0.175
x=0.65
F_2
Q^2 [GeV^2/c^2]

Fig. 38

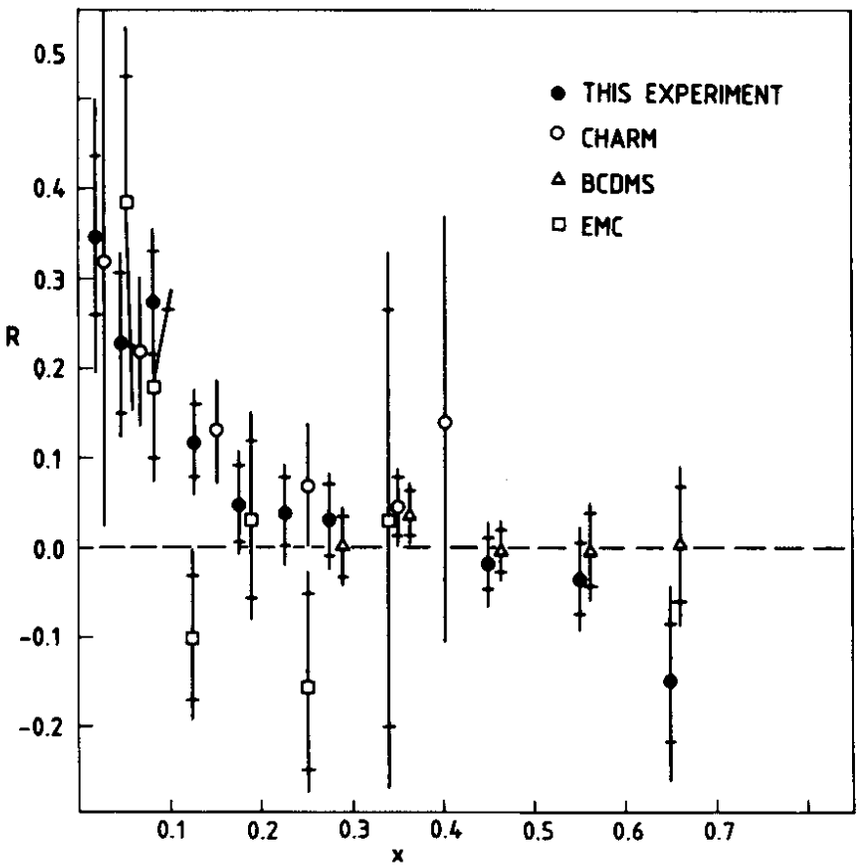
THIS EXPERIMENT
CHARM
BCDMS
EMC
R
x

Fig. 39

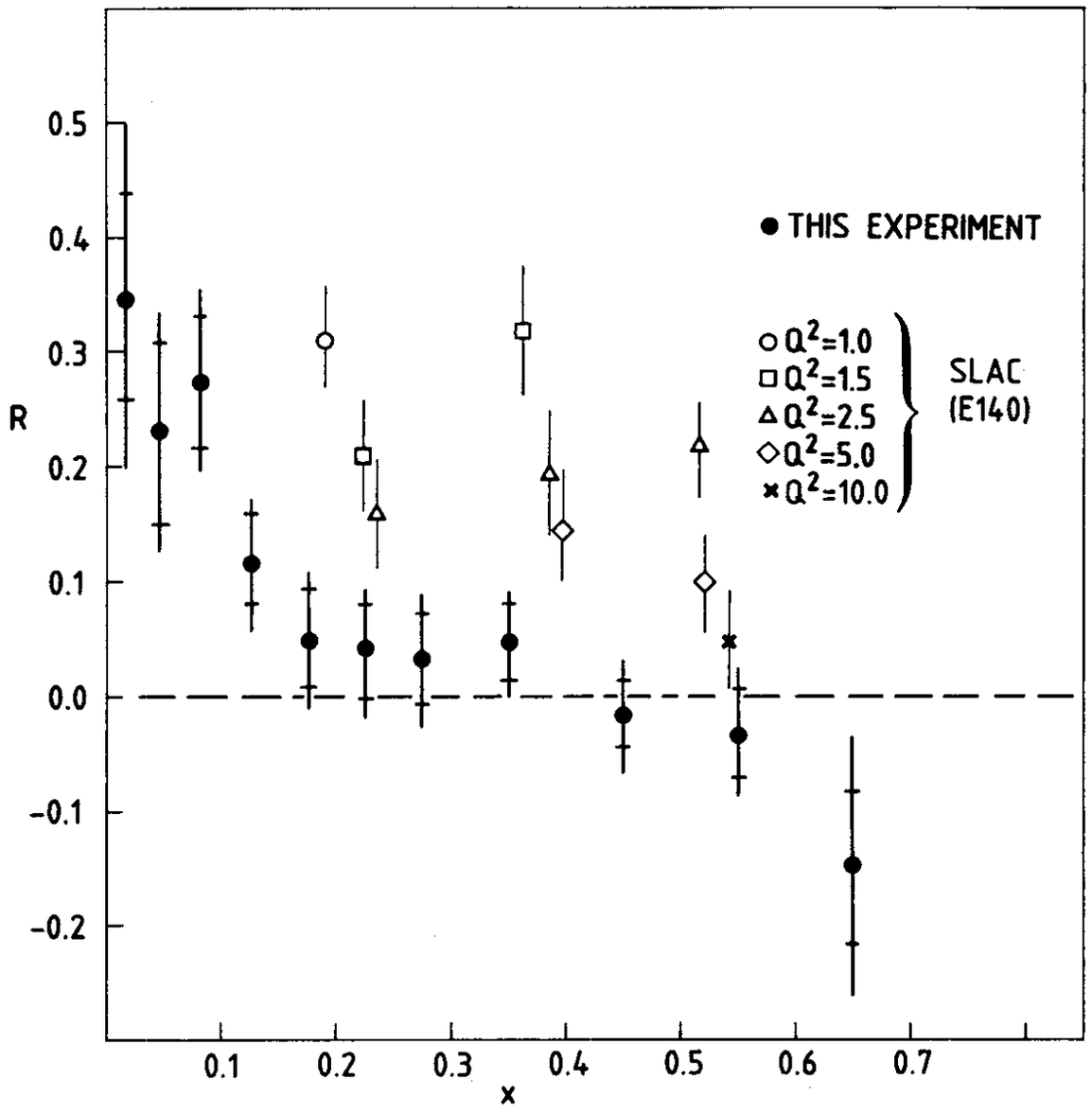
R
x
0.5
0.4
0.3
0.2
0.1
0.0
-0.1
-0.2
0.1
0.2
0.3
0.4
0.5
0.6
0.7
● THIS EXPERIMENT
○ Q²=1.0
□ Q²=1.5
△ Q²=2.5
◇ Q²=5.0
× Q²=10.0
SLAC
(E140)

Fig. 40

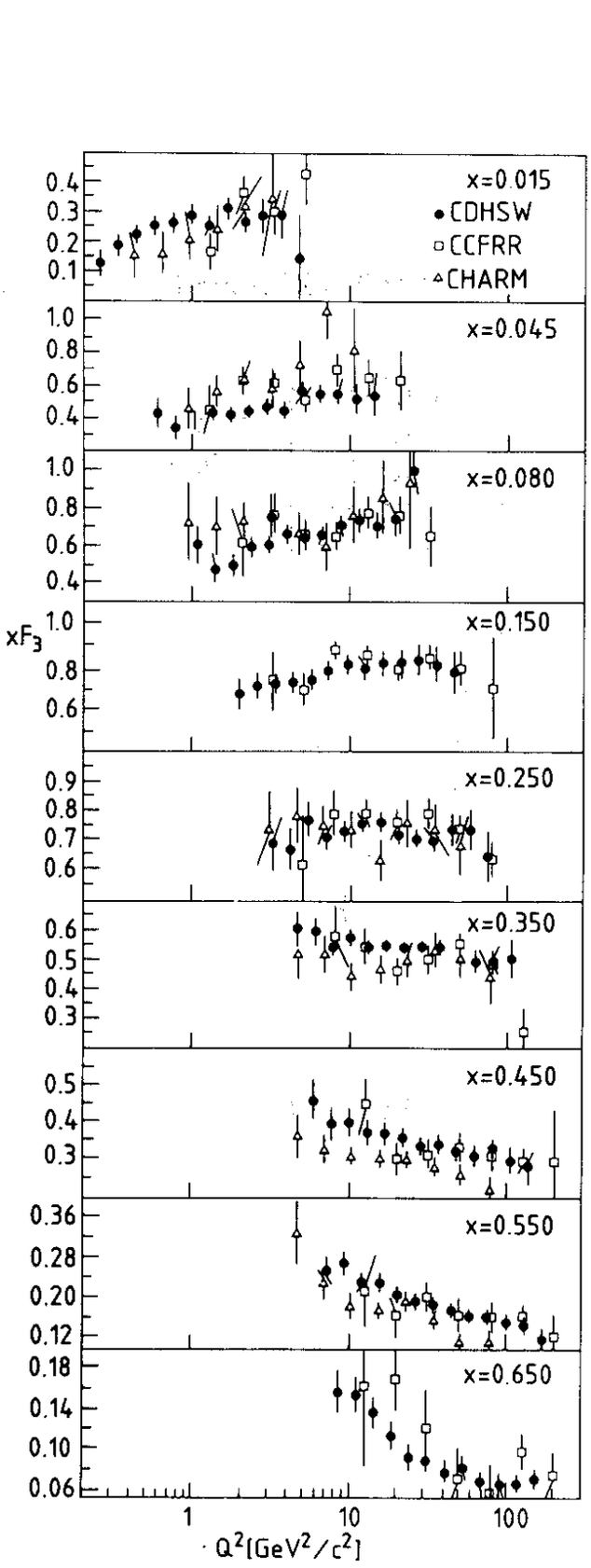
x=0.015
CDHSW
CCFRR
CHARM
x=0.045
x=0.080
x=0.150
x=0.250
x=0.350
x=0.450
x=0.550
x=0.650
xF3
Q2[GeV2/c2]

Fig. 41

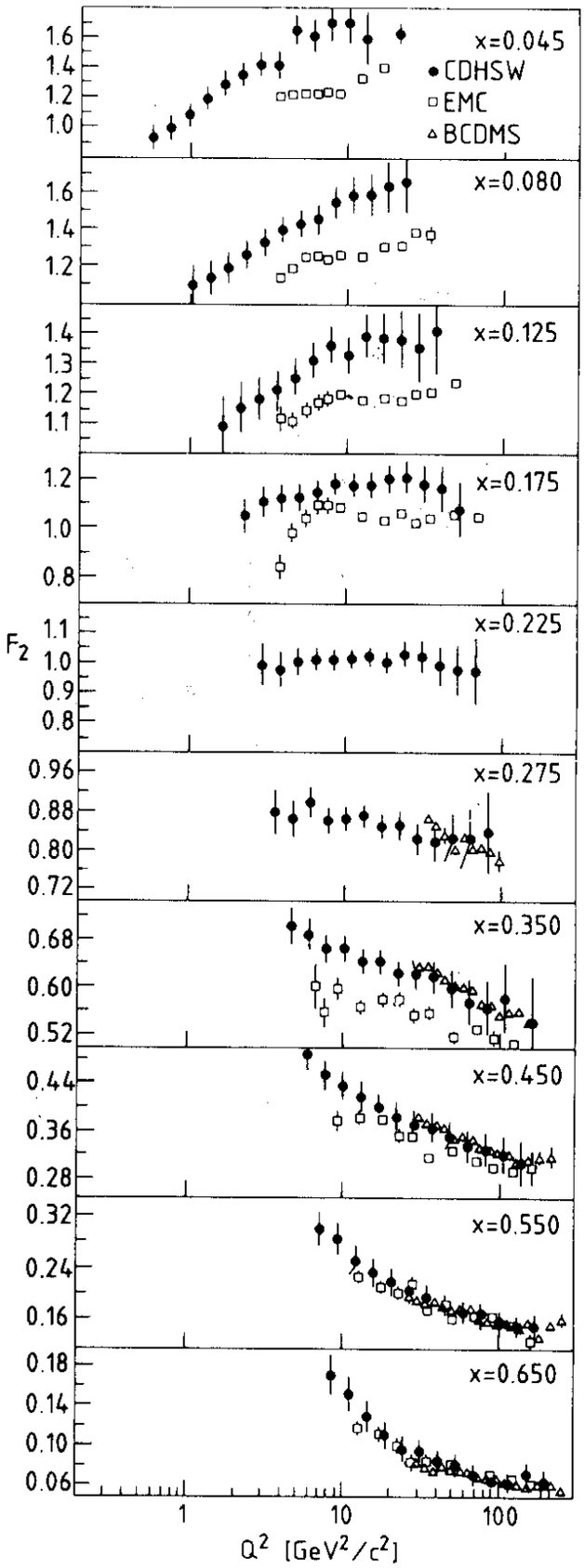
x=0.045
CDHSW
EMC
BCDMS
x=0.080
x=0.125
x=0.175
x=0.225
x=0.275
x=0.350
x=0.450
x=0.550
x=0.650
F2
Q2 [GeV2/c2]

Fig. 42

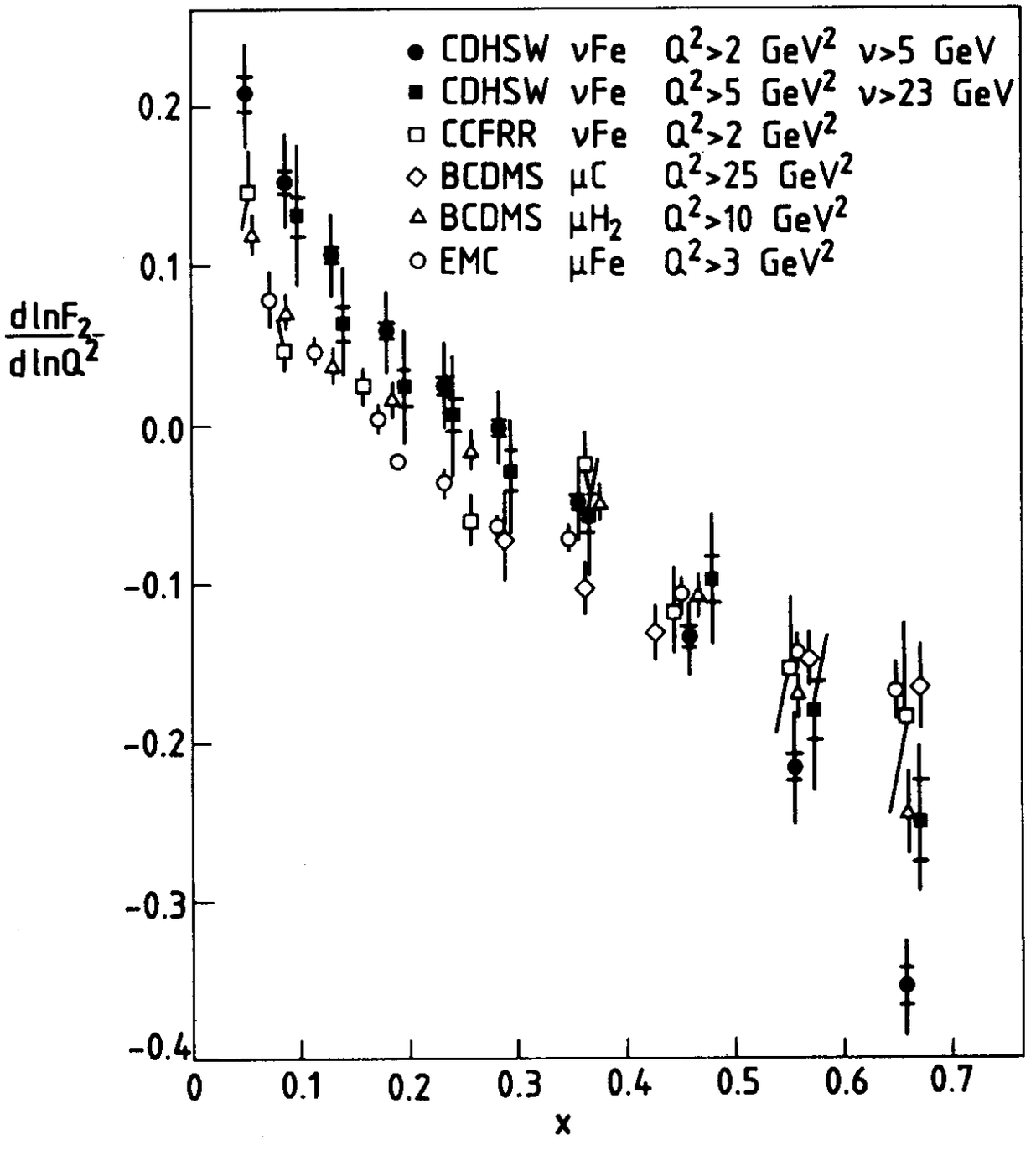
● CDHSW νFe Q²>2 GeV² ν>5 GeV
■ CDHSW νFe Q²>5 GeV² ν>23 GeV
□ CCFRR νFe Q²>2 GeV²
◇ BCDMS μC Q²>25 GeV²
△ BCDMS μH₂ Q²>10 GeV²
○ EMC μFe Q²>3 GeV²
dlnF₂/dlnQ²
0.2
0.1
0.0
-0.1
-0.2
-0.3
-0.4
0
0.1
0.2
0.3
0.4
0.5
0.6
0.7
x

Fig. 43